NASA

CONSTITUTIVE MODELING FOR ISOTROPIC MATERIALS (HOST)

By
U. S. Lindholm
K. S. Chan
S. R. Bodner
R. M. Weber
K. P. Walker
B. N. Cassenti

Southwest Research Institute
P.O. Drawer 28510
San Antonio, TX 78284

Prepared for
NATIONAL AERONAUTICS AND SPACE ADMINISTRATION
NASA-Lewis Research Center
Contract NAS3-23925
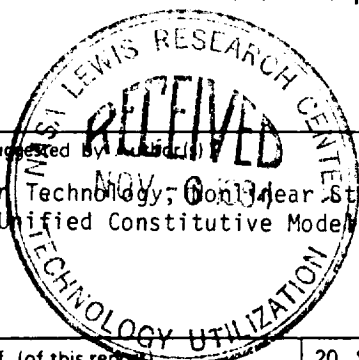
SOUTHWEST RESEARCH INSTITUTE

SAN ANTONIO   HOUSTON

1. Report No. NASA CR 174718	2. Government Accession No.	3. Recipient's Catalog No.
4. Title and Subtitle Constitutive Modeling for Isotropic Materials		5. Report Date May 1984
		6. Performing Organization Code
7. Author(s) U. S. Lindholm, K. S. Chan, S. R. Bodner, R. M. Weber, K. P. Walker, B. N. Cassenti		8. Performing Organization Report No. SwRI Project No. 06-7576
		10. Work Unit No.
9. Performing Organization Name and Address Southwest Research Institute Department of Materials Sciences P.O. Drawer 28510 San Antonio, TX 78284		11. Contract or Grant No. NAS3-23925
		13. Type of Report and Period Covered First Annual Report
12. Sponsoring Agency Name and Address National Aeronautics & Space Administration Washington, DC 20546		14. Sponsoring Agency Code RTOP 533-04-1A

16. Abstract

This report presents the results of the first year of work on a program to validate unified constitutive models for isotropic materials utilized in high temperature regions of gas turbine engines and to demonstrate their usefulness in computing stress-strain-time-temperature histories in complex 3-dimensional structural components. The "unified" theories combine all inelastic strain-rate components in a single term avoiding, for example, treating plasticity and creep as separate response phenomena. An extensive review of existing unified theories is given and numerical methods for integrating these stiff time-temperature-dependent constitutive equations are discussed.

Two particular models, those developed by Bodner and Partom and by Walker, were selected for more detailed development and evaluation against experimental tensile, creep and cyclic strain tests on specimens of a cast nickel base alloy, B1900+Hf. Initial results comparing computed and test results for tensile and cyclic straining for temperature from ambient to 982°C and strain rates from 10^{-7} to 10^{-3} s^{-1} are given. Some preliminary data correlations are presented also for highly non-proportional biaxial loading which demonstrate an increase in biaxial cyclic hardening rate over uniaxial or proportional loading conditions.

Initial work has begun on the implementation of both constitutive models in the MARC finite element computer code.

17. Key Words (Suggested by Author(s)) Hot Section Technology, Nonlinear Structural Analysis, Unified Constitutive Model	18. Distribution Statement Unclassified Unlimited

19. Security Classif. (of this report) Unclassified	20. Security Classif. (of this page) Unclassified	21. No. of Pages	22. Price*

* For sale by the National Technical Information Service, Springfield, Virginia 22161

NASA-C-168 (Rev. 10-75)

PREFACE

This first Annual Report covers the initial effort on the NASA HOST program titled "Constitutive Modeling for Isotropic Materials" conducted under Contract NAS3-23925. The NASA program manager for this project is Mr. Albert Kaufman. The program manager at Southwest Research Institute is Dr. Ulric Lindholm. Contributors to this report are Dr. Kwai Chan and Mr. Andrew Nagy of SwRI, Messrs. Jeff Hill and R. M. Weber of Pratt & Whitney Aircraft, and Dr. Kevin Walker and Prof. Sol R. Bodner, consultants.

TABLE OF CONTENTS

LIST OF FIGURES

LIST OF FIGURES (Continued)

APPENDIX A

LIST OF TABLES

1.0 INTRODUCTION

The objective of the present program is to develop a unified constitutive model for finite-element structural analysis of turbine engine hot section components. This effort constitutes a different approach for non-linear finite-element computer codes which have heretofore been based on classical inelastic methods. The unified constitutive theory to be developed will avoid the simplifying assumptions of classical theory and should more accurately represent the behavior of superalloy materials under cyclic loading conditions and high temperature environments. This class of constitutive theory is characterized by the use of kinetic equations and internal variables with appropriate evolutionary equations for treating all aspects of inelastic deformation including plasticity, creep and stress relaxation. Model development is directed toward isotropic, cast nickel-base alloys used for air-cooled turbine blades and vanes. Recent studies have shown that this approach is particularly suited for determining the cyclic behavior of superalloy type blade and vane materials and is entirely compatible with three dimensional inelastic finite-element formulations. More efficient and accurate inelastic analysis of hot section components--turbine blades, turbine vanes, combustor liners and seals--fabricated from "age hardenable" isotropic superalloy materials will be realized as the result of these developments.

The program is being conducted in two phases. A basic program (Tasks A through I) and an optional follow-on program (Tasks J through M). In the Basic Program of twenty six months' duration, a unified constitutive model will be developed for the prediction of the structural response of isotropic materials for temperatures and strain range characteristics of cooled turbine vanes in advanced gas turbine engines (Task A). A data base of uniaxial and multiaxial material properties required for the constitutive model development will be obtained for the base material (Tasks C and E). The constitutive model will then be incorporated into a finite-element computer code (Task D). An evaluation will be made of the capability of the analytical method to predict the structural response for multiaxial stress states (Task E) and nonisothermal conditions by conducting thermomechanical loading and benchmark notch verification experiments and analysis (Task F). As a final evaluation of the analytical model, a structural analysis will be performed for a hot section component fabricated from the base material for simulated engine operating conditions (Task G). In the optional program material property test procedures will be further developed to minimize the amount of testing required, and to study the possibility for estimating the material model constants from conventional property data (Task J). Further development of the model will be undertaken to consider thermal history effects and to correct any deficiencies indicated in the model or the computational algorithms in the code (Task K). In addition, the constitutive model development will be verified for an alternate material (Task L).

The work under this program is being conducted as a joint effort between Pratt & Whitney Aircraft (PWA) and Southwest Research Institute (SwRI) with technical assistance from Prof. Sol R. Bodner and Dr. Kevin Walker in the area of constitutive model development. The work and data base generated is being coordinated closely with another NASA funded HOST program at PWA (NAS3-23288) to develop advanced life prediction techniques for isotropic superalloy vane and blade materials.

Progress to date on this program has included completion of the review of unified constitutive models (Task A), substantial effort on specimen fabrication (Task B), uniaxial testing (Task C), initiation of effort on the implementation of models in MARC finite-element code (Task D), and multiaxial testing (Task E). A report on technical progress and future plans is given in the following sections.

2.0 TASK A. REVIEW AND SCREENING OF CANDIDATE CONSTITUTIVE MODELS

2.1 Literature Survey

A literature survey has been conducted to assess the state-of-the-art of time-temperature dependent elastic-viscoplastic constitutive theories which are based on the unified approach. This class of constitutive theories is characterized by the use of kinetic equations and internal variables with appropriate evolutionary equations for treating all aspects of inelastic deformation including plasticity, creep, and stress relaxation. The review identifies more than ten such unified theories which are shown to satisfy the uniqueness and stability criteria imposed by Drucker's postulate and Ponter's inequalities. These theories are compared on the basis of the types of flow law, kinetic equation, evolutionary equation of the internal variables, and treatment of temperature dependence. The similarities and differences of these theories are first outlined in terms of mathematical formulations and then illustrated by comparisons of theoretical calculations with experimental results which include monotonic stress-strain curves, cyclic hysteresis loops, creep and stress relaxation rates, as well as thermomechanical loops. Numerical methods used for integrating these stiff time-temperature dependent constitutive equations are also reviewed.

Because of its length, this review has been included as Appendix A of this report.

2.2 Model Selection for Subsequent Study

As a result of the literature survey and based upon SwRI recommendations, two constitutive models have been selected and approved for further study. These are the models of Bodner and Partom [1] and of Walker [2]. These two models are both representative of the class of unified models considered in the review process but differ significantly in the choice of particular functional forms for the basic flow law, the kinetic relationship, the parameter used as a measure of hardening and the evolutionary equations for the internal variables describing strain hardening. Thus, a direct comparison between these two models and the experiments should illustrate well the consequences of a wide range in constitutive modeling approach. It is also significant that both models have already found significant application to analysis of gas turbine materials and to hot section components. Therefore, they are further along in their development and evaluation than most of the other comparable models.

2.3 Identification of Model Modifications

As a result of the literature survey and of direct experience in working with existing models, three specific areas have been identified which will potentially require modification to the models as they currently exist. These areas are listed and discussed below.

1. <u>Multiaxial, non-proportional load or strain histories.</u> There is existing data which indicates that the rate of strain hardening varies with a change in direction of the strain rate vector; i.e., when the ratio of the plastic strain increments is not held constant as in a uniaxial or proportional loading history. This has been demonstrated for both monotonically increasing and cyclic loading. This poses potential problems in formulation of the evolutionary equations for the hardening variables which will require some measure of the rate of change in direction of the strain increments and the functional inclusion of this measure in the hardening relations. Additional practical difficulties will accrue if the material constants associated with the non-proportional hardening cannot be obtained from uniaxial tests, since the availability of multiaxial test facilities is low and the generation of such data is quite expensive relative to uniaxial testing.

2. <u>Non-isothermal strain cycles.</u> It is not evident at this time that isothermal test data will be sufficient input for a model adequate to handle non-isothermal problems. At elevated temperatures, metallurgical processes affecting strength may be occurring which depend not only on the current temperature but upon time at temperature or rate of change of temperature. Such effects are generally not incorporated in current models. Again, a requirement for non-isothermal testing in order to determine constitutive model constants would be a practical limitation.

3. <u>Description of hardening over a wide strain range.</u> Some current experience indicates a difficulty in developing hardening behavior which is accurate for both small (near yield) and large (saturation) plastic strain values. Multiple functions may be required for a general model. The corresponding increase in number of material constants required is the penalty incurred.

2.4   References

1.   S. R. Bodner and Y. Partom, ASME J. of Applied Mechanics, Vol. 42, p. 385, 1975.

2.   K. P. Walker, NASA Contract Report NASA CR 165533, 1981.

3.0 TASK B. SPECIMEN FABRICATION

3.1 Material Selection

A B1900+Hf was selected as the model material for study in the base program and MAR-M247 the material for consideration in the optional tasks. Both materials are extensively utilized in the gas turbine industry and considerable benefit will derive from their characterization. A major factor in the selection of B1900+Hf is the availability of cyclic and monotonic constitutive data from a concurrent NASA HOST program, NAS3-23288, conducted by PWA to develop life prediction analysis methodology for isotropic blades and vanes. Selection of the same material, material processing, and specimen configurations in both efforts significantly enhances the data base available for life prediction and constitutive model development.

Sufficent material of each type was procured to satisfy specimen requirements in the program.

The B1900+Hf material was part of a single heat, designated W-0098, obtained from Certified Alloy Products Inc., Long Beach, California. The chemical composition of this heat is compared to nominal specification in Table 3.I.

TABLE 3.I

CHEMICAL COMPOSITION OF B1900+Hf (HEAT W-0098)

Element	Nominal (%)	Heat W-0098
C	0.11	0.09
Cr	8.0	7.72
Co	10.0	9.91
Mo	6.0	5.97
Al	6.0	6.07
Ta	4.3	4.21
Ti	1.0	0.99
B	0.015	0.016
Zr	0.08	0.04
Fe	0.35*	0.17
W	0.1*	0.04
Cb	0.1*	0.08
Bi	0.5 ppm	0.1
Pb	10.0 ppm	0.1
Hf	1.5	1.19
Ni	Remainder	Remainder

*Maximum

Casting configurations, pour and mold temperatures for the B1900+Hf specimens were selected to assure that grain size, material structure and integrity match, as closely as possible, those in the PWA test specimens. Goals for this phase of the fabrication effort were:

1. A grain size of ASTM No. 1 to 2 in the Gage section when measured using standard procedures.

2. A porosity-free casting, see Figure 3.1.

3. A γ' size of .9 μm in the fully heat treated condition.

Following casting, all B1900+Hf test bars were fully heat treated according to the following schedule:

Solution: $1079\pm14°C$ ($1975\pm25°F$) for 4 hours; air cool
Precipitation: $899\pm14°C$ ($1659\pm25°F$) for 10 hours; air cool.

3.2   Specimen Fabrication

The gage section geometries of the monotonic tensile/creep, isothermal cyclic, thermomechanical cyclic, and isothermal biaxial test specimens were chosen to correspond to the gage section geometries of the corresponding specimens in the concurrent life prediction contract. Major differences, however, in the specimen gripping systems between SwRI and PWA resulted in different overall specimen and casting configurations, Figure 3.2. The use of colletted grips at SwRI considerably simplified the specimen design, but added to the length and diameter of each casting. A number of casting trials and specimen design changes were evaluated before suitable specimen and casting configurations were chosen to satisfy grain size and integrity goals. Additional details on the fabrication are provided below for each specimen type:

- Tensile and Creep Specimens - The increase in cast bar length from a standard configuration of 4 inches to 7.2 inches did not appreaciably alter specimen integrity or grain size. Twenty-two test specimens were prepared from the cast bars by centerless grinding. All specimens were subsequently electro-polished prior to shipment to SwRI for testing.

- Thermomechanical Constitutive Specimen - A common, constant OD 2.74 cm (1.08 inch) cast bar configuration of 20 cm (8 inch) length was proposed from which each type of uniaxial constitutive specimen could be machined. Grain size and porosity goals could not be satisfied simultaneously with a casting of this configuration. Casting of "net shape" bars of two lengths was then attempted. Microstructural evaluation indicated that an adequate casting could be obtained if the
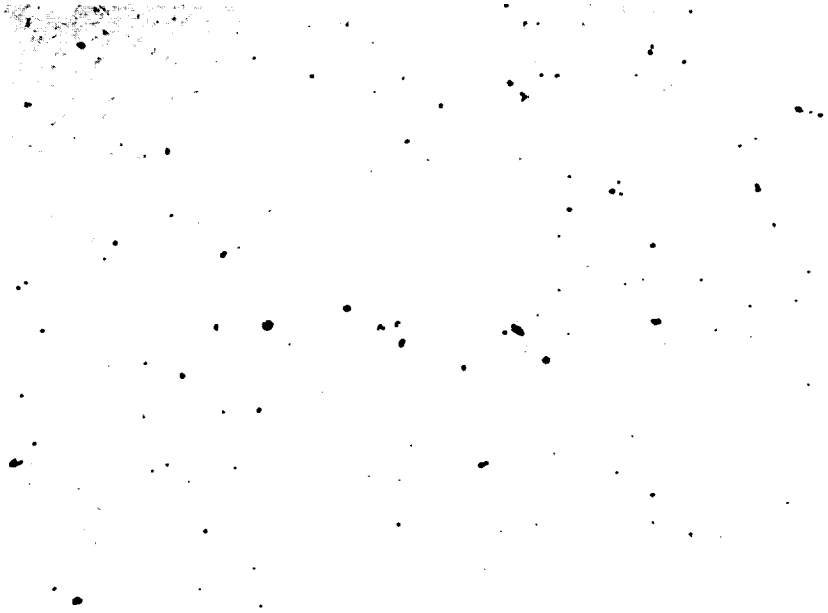
Original casting procedure   12X

Modified casting procedure   12X

FIGURE 3.1.   COMPARISON OF CAST BAR POROSITY.

(a) Monotonic tensile/creep specimen

(b) Isothermal cyclic specimen

(c) Thermomechanical cyclic specimen

(d) Isothermal biaxial test specimen
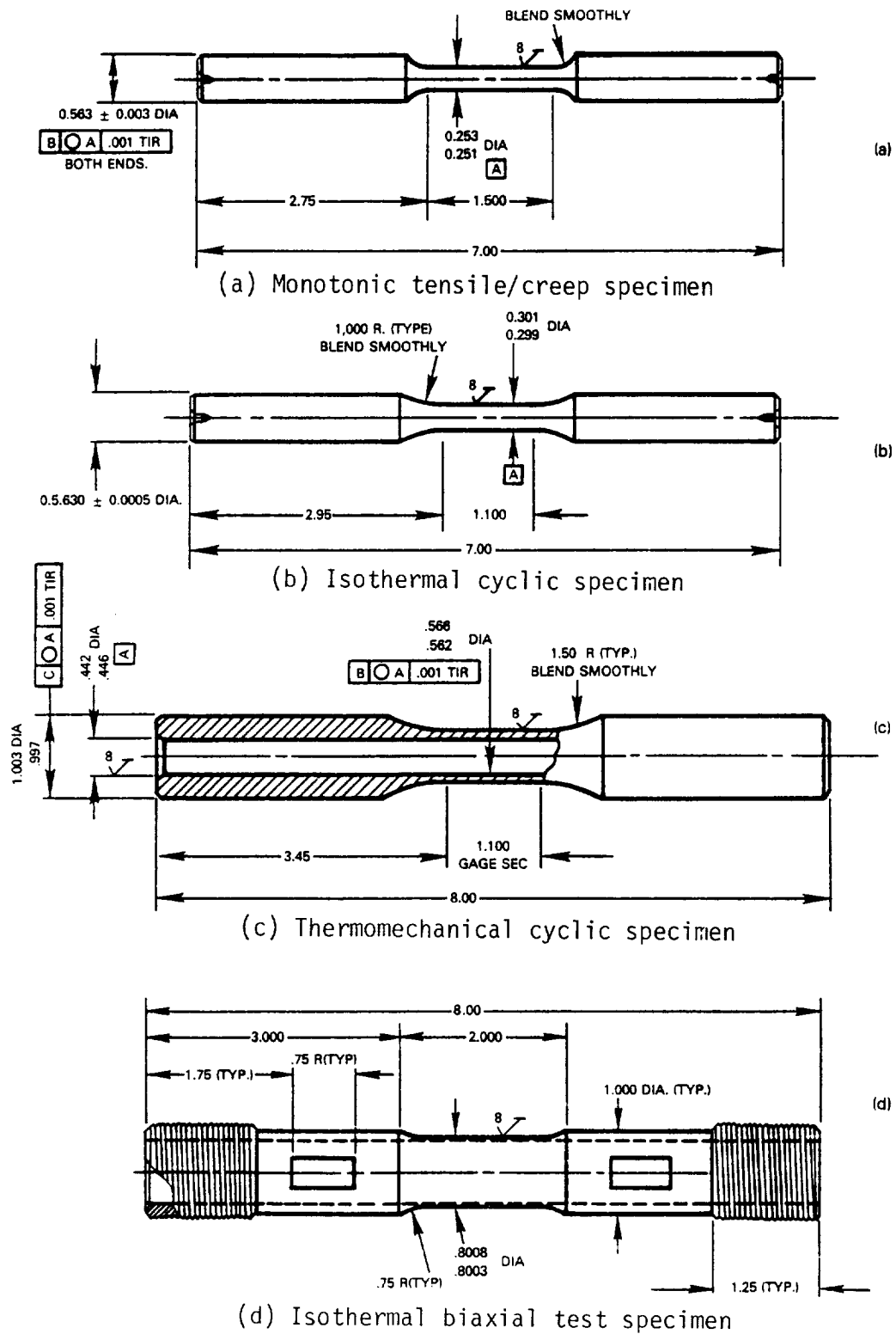
FIGURE 3.2.   SPECIMEN DESIGNS UTILIZED IN VARIOUS CONSTITUTIVE TESTS.

total cast bar length were limited to 6-1/2 inches.
Figure 3.3 indicates the acceptable level of micro-
porosity in the gage section of the 6-1/2 inch speci-
men. Twenty-five castings of this configuration are
available. Cylindrical buttons of .8 inch length are
being electron beam welded to the ends of each speci-
men to increase the stock length to the required
8 inches.

- Isothermal Constitutive Specimen - Difficulties in
  casting the 2.74 cm OD x 20 cm L (1.08 inch x 8.25 inch L)
  solid bars prompted a reappraisal of the recommended speci-
  men configuration. A reduction in specimen length to
  17.78 cm (7.0 inches) and diameter to 1.43 cm (.563 inches)
  was agreed upon. This change permitted use of the tensile/
  creep specimen casting configuration. Twenty-eight cast-
  ings have been obtained and are being machined.

- Multiaxial Tension-Torsion Specimen - A constant OD 30.2 cm
  (1.19 inch) cast bar configuration of 20.3 cm (8 inch)
  length was initially evaluated. Grain size and porosity
  levels could not be satisfied simultaneously. A second
  casting attempt was made with a revised gating scheme, but
  microporosity and grain size results were equally unsatis-
  factory. A decision was reached to cast these specimens
  with a hollow core. Hitchiner Mfg. of Milford, N.H, has
  been contracted to provide the castings.
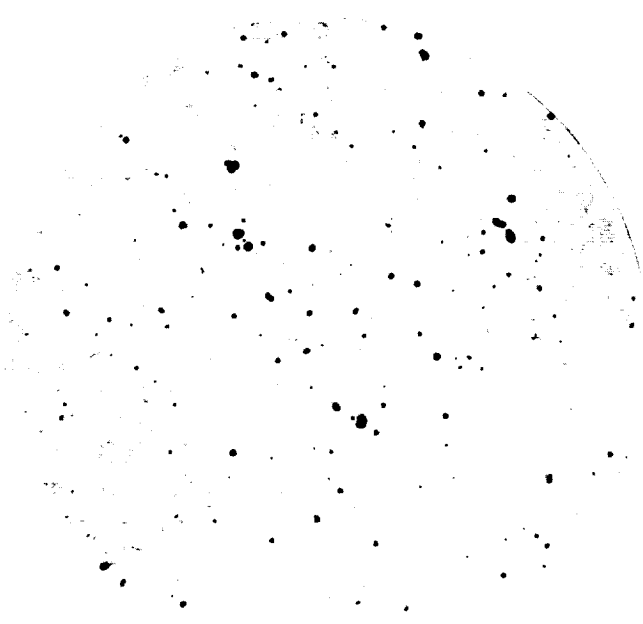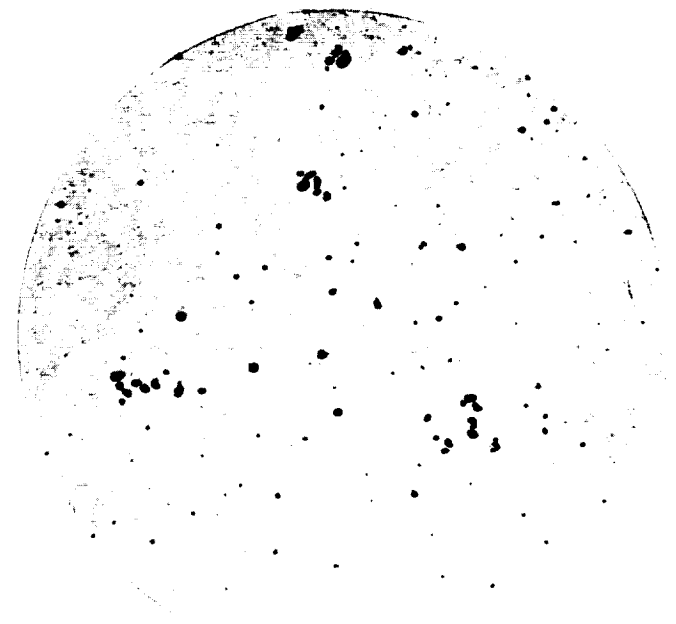
(a) Gage section　　　　　　　　　　　(b) Shoulder section

(c) Grip section
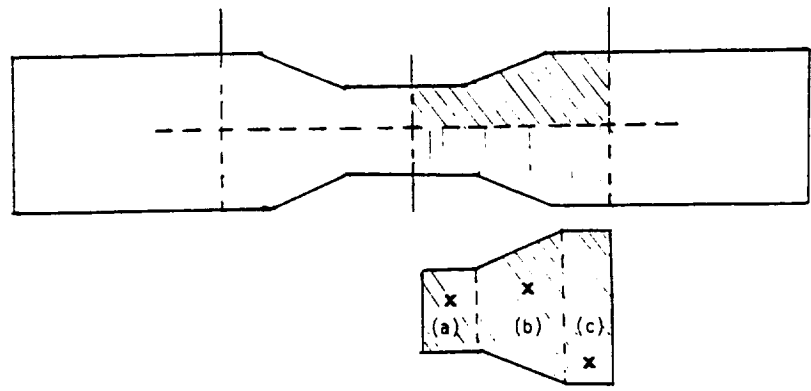
FIGURE 3.3.　THE LEVEL OF MICROPOROSITY AT VARIOUS POSITIONS OF A TYPICAL SPECIMEN.

3-6

4.0 TASK C. UNIAXIAL EVALUATION OF CONSTITUTIVE MODELS

4.1 Tensile, Creep and Cyclic Property Testing

The B1900+Hf specimen requirement for the base program is presented in Table 4-I. A total of 39 smooth uniaxial bar specimens will be fabricated to provide constitutive response data for the loading conditions in Task C. A total of 20 biaxial specimens will be prepared for response data under multiaxial stress states for the effort under Task E. Ten notched benchmark specimens will be available for the work in Task F. All testing is being performed at SwRI. The specimens are being fabricated by PWA as described in the preceding Section 3.

The matrices for tensile and isothermal cyclic testing are given in Tables 4.II and 4.III, respectively. All the tensile and five creep tests have been completed. The cyclic testing is just being initiated. Correlations with cyclic data given below are based on results from PWA Contract NAS3-23288.

All the uniaxial tests are being conducted in a closed-loop, servo-hydraulic test machine under strain control. Figure 4.1 shows the configuration of the test specimen, the hydraulic collet grips, the induction heating coil and the externally mounted extensometer with quartz reach-rods attached to the specimen. The plastic tubing carries cooling water to the hydraulic collets and copper face plates. Temperature variations over the specimen gage section are within ASTM specifications for short term tests.

4.2 Comparison of Experiment and Bodner-Partom Model

The material constants in the Bodner-Partom elastic-viscoplastic constitutive theory were evaluated for B1900+Hf. Most of the constants were evaluated from uniaxial tensile and isothermal cyclic data. Creep data were occasionally used for evaluating the constants in the thermal recovery terms when slow strain rate ($\dot{\varepsilon} \leq 4 \times 10^{-6} \sec^{-1}$) tensile data were not available. A summary of the Bodner-Partom theory and an outline of a systematic procedure for evaluating the Bodner-Partom model constants analytically are shown in Figures 4.2 and 4.3, respectively, while the various material constants are shown as a function of temperature in Figures 4.4(a) and 4.4(b). It is worthy to note that for B1900+Hf most of the material constants in the Bodner-Partom theory are independent of temperature; in the temperature range of 25-1093°C, only three parameters (n, Z_0, and A) vary with temperature. Another material input to the Bodner-Partom theory is the elastic modulus which was determined from uniaxial tensile data and found to decrease with temperature also, as shown in Figure 4.5.

TABLE 4.I

B1900+Hf SPECIMEN FABRICATION REQUIREMENTS FOR THE BASE PROGRAM

Specimen Type	Base Program	Task	Fig. 3.2
Tensile Specimens	11	C	(a)
Creep Specimens	5	C	(a)
Isothermal Cyclic Constitutive Specimens	20	C	(b)
Thermomechanical Constitutive Specimens	3	C	(c)
Multiaxial Cyclic Constitutive Specimens	20	E	(d)
Benchmark Notch Specimens	10	F	*

---

* To be determined.

TABLE 4.II

INTEGRATED TENSILE TEST MATRIX

Strain Rate (sec^{-1})	Temperature (°F)					
	RT	1200	1400	1600	1800	2000
4×10^{-7}			*			*
4×10^{-6}			*	1	1	1
4×10^{-5}	1,*	1	1,*	2	2	2,*
4×10^{-4}			*	1	1	1
4×10^{-3}			*			*
4×10^{-2}			*			*

1,2 = Test requirements, Contract NAS3-23288.

  * = Additional test conditions under this contract.

TABLE 4.III

ISOTHERMAL CYCLIC CONSTITUTIVE TESTS

Test #	Temp(°F)	R	$\dot{\varepsilon}(\text{sec}^{-1})$	$\Delta\varepsilon_1$	$\Delta\varepsilon_2$	$\Delta\varepsilon_3$	$\Delta\varepsilon_4$
o Effect of Temperature and Strain Rate							
1	RT	0	4×10^{-4}	X	X	X	X
2	800	0	4×10^{-4}	X	X	X	X
3	800	0	$4\times10^{-2*}$	X	X	X	X
4	800	0	4×10^{-6}	X	X	X	X
5	1200	0	4×10^{-4}	X	X	X	X
6	1200	0	$4\times10^{-2*}$	X	X	X	X
7	1200	0	4×10^{-6}	X	X	X	X
8	1400	-1	$4\times10^{-2*}$	X	X	X	X
			Thermal memory erasure cycle				
9	1600	-1	4×10^{-4}	X	X	X	X
10	1800	-1	Thermal memory erasure cycle				
11	2000	-1	4×10^{-6}	X	X	X	X
o Effect of Mean Strain							
12	1200	-1	4×10^{-4}	Same as 5 except fully reversed			
13	1400	0	$4\times10^{-2*}$	Same as 8 except one way tension			
14	1400	-∞	$4\times10^{-2*}$	Same as 8 except one way compression			
15	1600	-∞	4×10^{-4}	Same as 9 except one way compression			
16	2000	-∞	4×10^{-6}	Same as 11 except one way compression			
o Strain Holds to Probe for Back Stress							
17	1200	0	4×10^{-4}	X	X	X	X
18	1400	-1	4×10^{-4}	X	X	X	X
19	1600	-1	4×10^{-4}	X	X	X	X
20	2000	-1	4×10^{-4}	X	X	X	X

*It may be desirable to reduce this upper strain rate (4×10^{-2} S^{-1}) based on actual component rates and on measurement accuracy for small inelastic strains.

FIGURE 4.1. TENSILE SPECIMEN UNDER TEST AT 1600°F.

1. Flow Law:

$$\dot{\epsilon}_{ij} = \dot{\epsilon}_{ij}^{e} + \dot{\epsilon}_{ij}^{p}$$

$$\dot{\epsilon}_{ij}^{p} = \lambda S_{ij} \; ; \; \dot{\epsilon}_{kk}^{p} = 0$$

with $S_{ij} = \sigma_{ij} - \frac{1}{3} \delta_{ij}\sigma_{kk}$

2. Kinetic Equation:

$$D_2^p = D_0^2 \exp\left\{ -\left[\frac{Z^2}{3J_2}\right]^n \right\}$$

with $Z = Z^I + Z^D$

$$D_2^p = \frac{1}{2} \dot{\epsilon}_{ij}^{p} \dot{\epsilon}_{ij}^{p}$$

$$J_2 = \frac{1}{2} S_{ij}S_{ij}$$

$$\lambda^2 = D_2^p/J_2$$

3. Evolution Equations of Internal Variables:

a. Isotropic Hardening

$$\dot{Z}^I = m_1 \left[Z_1 + \alpha Z_3 - Z^I\right] \dot{W}_p - A_1 Z_1 \left[\frac{Z^I - Z_2}{Z_1}\right]^{r_1}$$

where $\dot{\alpha} = m_2 (1 - \alpha) \dot{W}_p \sin\theta$

$\theta = \cos^{-1}(V_{ij}\bar{V}_{ij})$ or $\theta = \cos^{-1}(u_{ij}\bar{u}_{ij})$

$V_{ij} = \beta_{ij}/(\beta_{kl}\beta_{kl})^{1/2}$, $\bar{V}_{ij} = \dot{\beta}_{ij}/(\dot{\beta}_{kl}\dot{\beta}_{kl})^{1/2}$

$u_{ij} = \sigma_{ij}/(\sigma_{kl}\sigma_{kl})^{1/2}$, $\bar{u}_{ij} = \dot{\sigma}_{ij}/(\dot{\sigma}_{kl}\dot{\sigma}_{kl})^{1/2}$

with $Z^I(o) = Z_0$; $\dot{W}_p = \sigma_{ij}\dot{\epsilon}_{ij}^{p}$; $W_p(o) = 0$; $\alpha(0) = 0$

b. Directional Hardening

$$\dot{\beta}_{ij} = m_2 (Z_3 u_{ij} - \beta_{ij}) \dot{W}_p - A_2 Z_1 \left[\frac{(\beta_{kl}\beta_{kl})^{1/2}}{Z_1}\right]^{r_2} V_{ij}$$

with $Z^D = \beta_{ij}u_{ij}$; $Z^D(o) = 0$, $\beta_{ij}(o) = 0$

$$m_2 = \frac{\bar{m}_2}{2}(1+\sin\theta)\left[1 + \exp(-m_3 Z^D)\right]$$

Material Constants: D_0, Z_0, Z_1, Z_2, Z_3, m_1, m_2, m_3

A_1, A_2, r_1, r_2, n, and elastic constants

FIGURE 4.2. A SUMMARY OF BODNER-PARTOM'S MODEL.

```
                         ┌──────────┐
                         │  START   │
                         └────┬─────┘
                              │
                              ▼
   ┌─────────────────────────────────────────────────────┐
   │   fit σ and ε^P to a polynominal and obtain          │
   │                                                      │
   │   γ = (1/σ) (dσ/dε^P)  (tensile data)                │
   └──────────────────────┬──────────────────────────────┘
                          │
                          ▼
   ┌─────────────────────────────────────────────────────┐
   │   obtain m₁, m₂, and r from the slopes               │
   │   of γ vs. σ  (tensile data); set D_0                │
   └──────────────────────┬──────────────────────────────┘
                          │
                          ▼
   ┌─────────────────────────────────────────────────────┐
   │   obtain n from the slope of saturation              │
   │   stress vs. strain rate  (tensile data)             │
   └──────────────────────┬──────────────────────────────┘
                          │
                          ▼
   ┌─────────────────────────────────────────────────────┐
   │   calculate the sum of Z₁ and Z₃ from saturation     │
   │   stress, n and ε̇^P  (tensile data)                 │
   └──────────────────────┬──────────────────────────────┘
                          │
                          ▼
   ┌─────────────────────────────────────────────────────┐
   │   obtain Z₃ from isothermal cyclic data;             │
   │   calculate Z₁                                       │
   └──────────────────────┬──────────────────────────────┘
                          │
                          ▼
   ┌─────────────────────────────────────────────────────┐
   │   obtain Z_0 by fitting to tensile                   │
   │   stress-strain curves; set Z₂ = Z_0                 │
   └──────────────────────┬──────────────────────────────┘
                          │
                          ▼
   ┌─────────────────────────────────────────────────────┐
   │   calculate A from slow rate tensile data            │
   │   or steady state creep rate                         │
   └──────────────────────┬──────────────────────────────┘
                          │
                          ▼
                    ┌──────────┐
                    │   END    │
                    └──────────┘
```

The equations in the flow chart:

First box:
$$\gamma = \frac{1}{\sigma}\frac{d\sigma}{d\epsilon^P} \quad \text{(tensile data)}$$

FIGURE 4.3. A FLOW CHART SHOWING A SYSTEMATIC PROCEDURE FOR
EVALUATING THE MATERIAL CONSTANTS IN THE
BODNER-PARTOM THEORY.
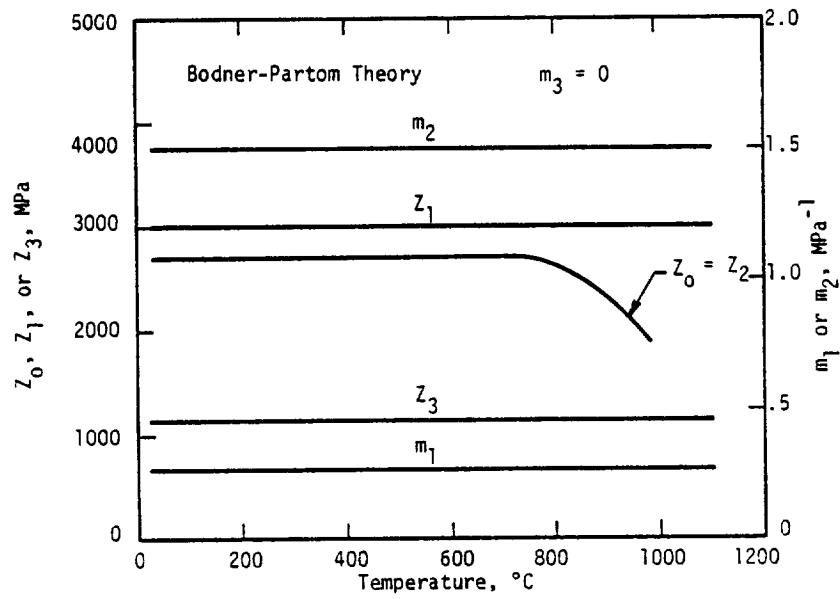
FIGURE 4.4(a).   THE VALUES OF Z_0, Z_1, Z_3, m_1, AND m_2
FOR B1900+Hf AT VARIOUS TEMPERATURES.
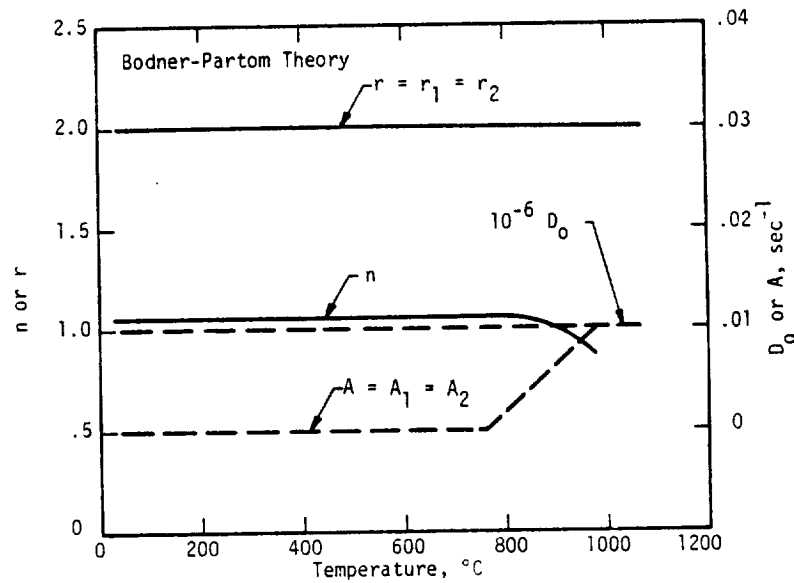
FIGURE 4.4(b).   THE VALUES OF D_0, n, A, AND r FOR
B1900+Hf AT VARIOUS TEMPERATURES.

4-8

The Bodner-Partom model was used to simulate the uniaxial tensile behavior of B1900+Hf as a function of both temperature and strain rate. Stress-strain curves were first calculated and the results were then used to obtain the "yield stress" at .2% plastic strain for various imposed strain rates and temperatures. Figure 4.5 shows that the calculated .2% ε^P yield stresses at $\dot{\varepsilon} = 8.3 \times 10^{-5}$ sec^{-1} at various temperatures are in good agreement with the experimental values. The effects of strain rate on the .2% εP yield stress at 760°C, 871°C, and 982°C are summarized in Figure 4.6. The results indicate that the rate effect is relatively small compared to that of temperature, in good agreement with experimental observations. Figure 4.7 shows the stress-strain curves at $\dot{\varepsilon} = 8.3 \times 10^{-5}$ sec^{-1} at 538, 871, and 982°C. Both the experimental and the calculated curves show that the flow stress at a given strain decreases with temperature while the apparent hardening rate is increased as the temperature is increased.

The Bodner-Partom model was used to calculate the isothermal cyclic hysteresis loops at various strain ranges using the same set of constants shown in Figures 4.4(a) and 4.4(b). The calculated cyclically-saturated hysteresis loops at various strain ranges are compared with experimental data in Figures 4.8 and 4.9 for 538°C and 871°C, respectively. The comparisons indicate reasonably good agreement between theory and experiment for both small (near yield) and large plastic strain hysteresis loops. Cyclic hardening is also predicted by the Bodner-Partom theory. Figure 4.10(a) shows that both the calculated hysteresis loops after 1-2 cycles and at cyclic saturation; these calculated loops are in fair agreement with the experimental loops shown in Figure 4.10(b).

4.3   Comparison of Experiment with Walker Model

A very large quantity of constitutive information has already been generated as part of the data acquisition efforts in the HOST Isotropic Fatigue Contract (NAS3-23288). Much more data will be generated as that contract continues, as well as in the present contract. An important need in the present contract effort and in other related HOST programs is the ability to deal expeditiously with this information while still maintaining a high level of insight into the underlying physical processes. A computer program to do this utilizes the COPES/CONMIN Optimization Code written by L. E. Masden and G. N. Vanderplaats. The COPES/CONMIN deck has been coupled with PWA codes which provide interactive access for real time use of the COPES/CONMIN system and direct access to PWA graphics/file manipulation routines and the data base established for the HOST Isotropic Fatigue Contract data. A flow chart describing these decks and their interrelations is shown in Figure 4.11. A summary of Walker's model is shown in Figure 4.12.

In addition to the motivation to use optimization techniques resulting from the large volume of constitutive data available and the heuristic nature of the current constitutive theories, the limited deformation observed in the
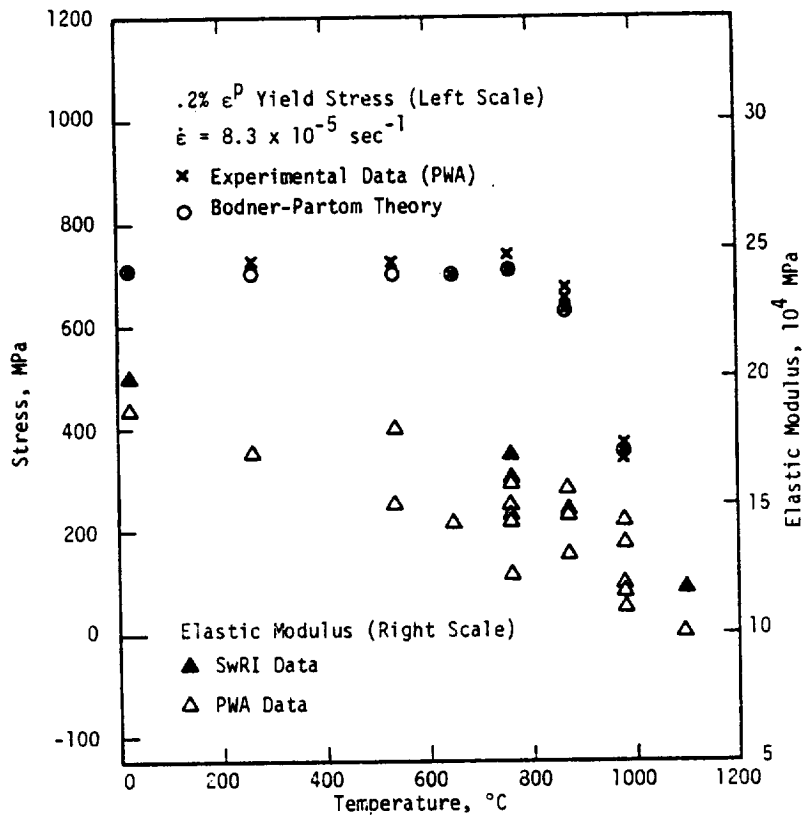
FIGURE 4.5 THE ELASTIC MODULUS AND THE .2% ϵ^p YIELD STRESS AS A
FUNCTION OF TEMPERATURE. The calculated .2% ϵ^p
yield stresses using Bodner-Partom theory are in
good agreement with experimental data.
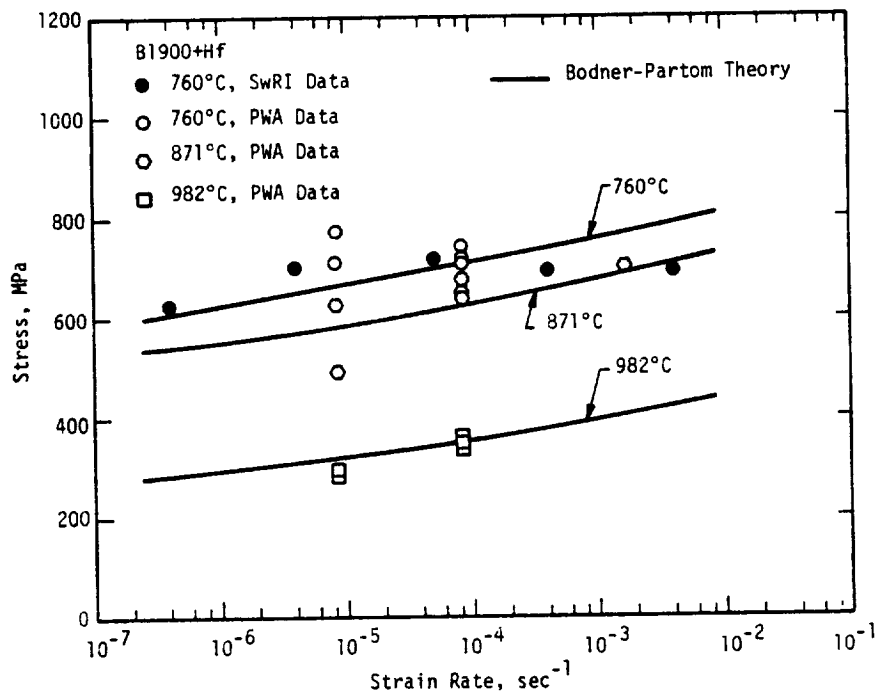
FIGURE 4.6. A COMPARISON OF THE CALCULATED (BODNER-PARTOM THEORY)
AND THE EXPERIMENTAL .2% ϵ^p YIELD STRESS AS A FUNCTION
OF STRAIN RATE FOR B1900+Hf AT 760, 871 and 982°C.
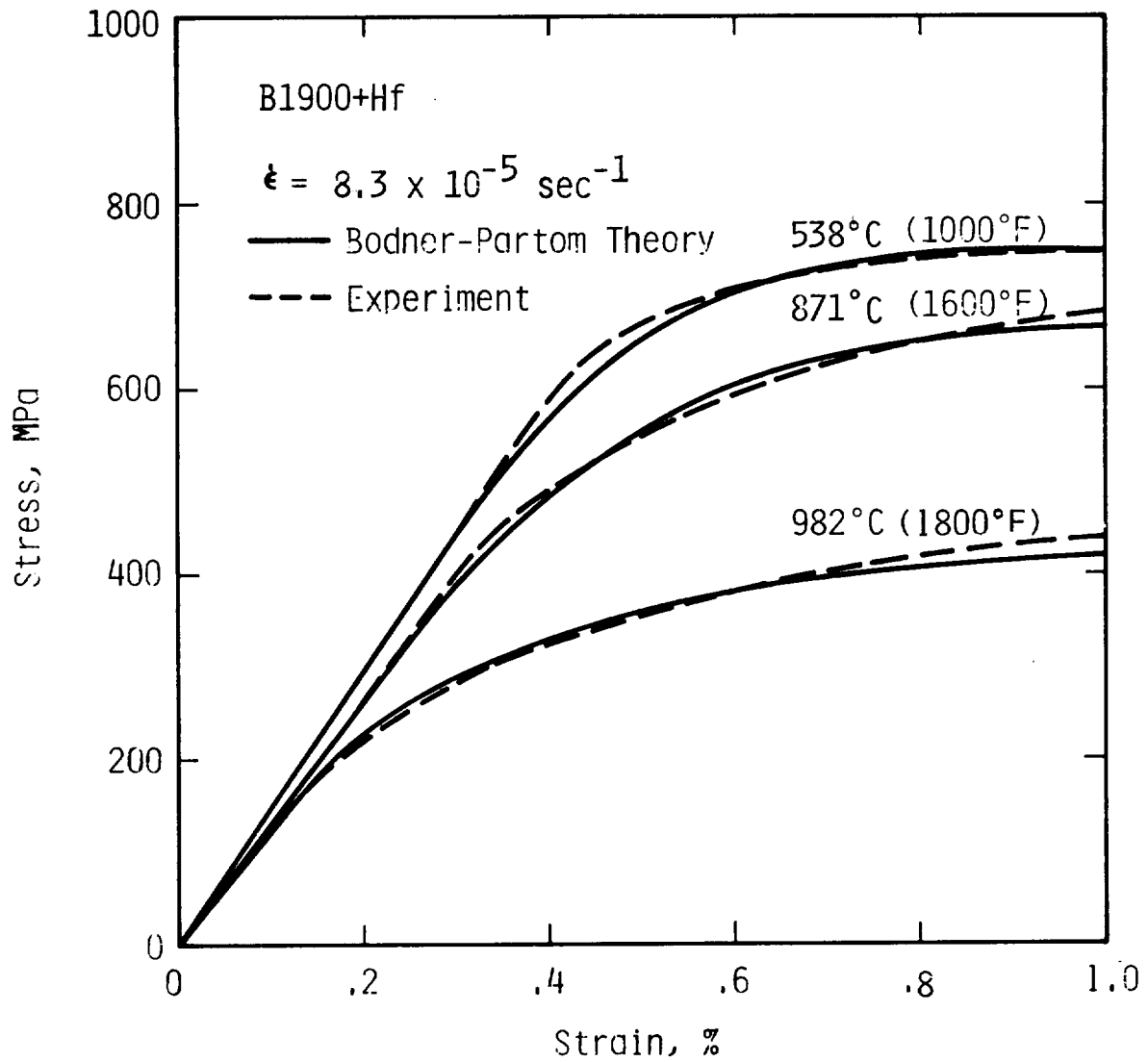
FIGURE 4.7   A COMPARISON OF THE CALCULATED (BODNER-PARTOM THEORY)
AND THE EXPERIMENTAL STRESS-STRAIN CURVES OF
B1900+Hf AT 538, 871 AND 982°C.
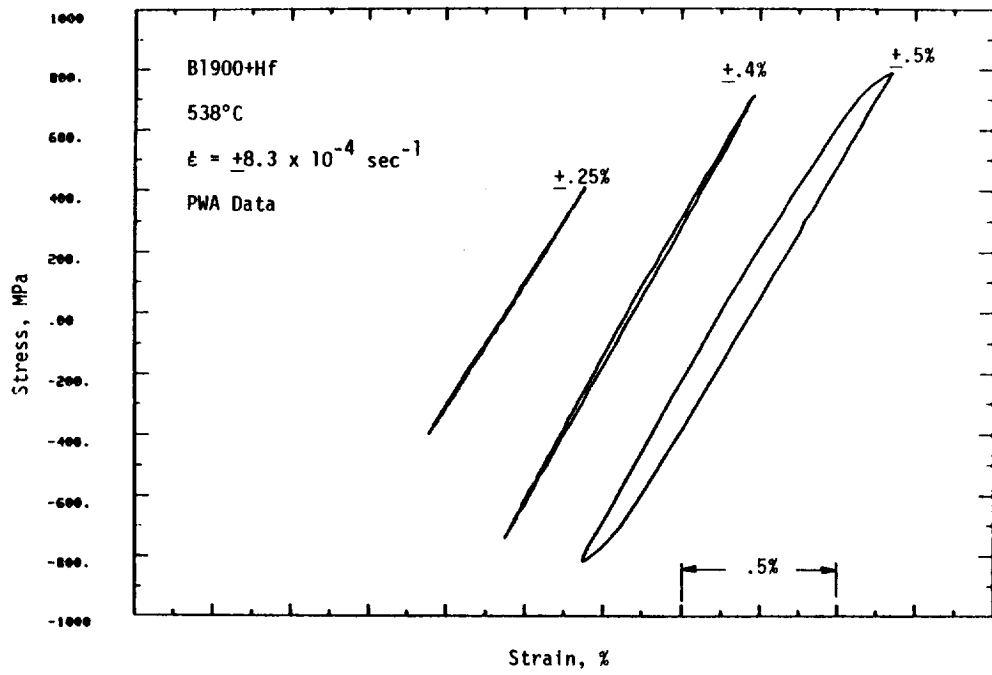
(a) Experiment
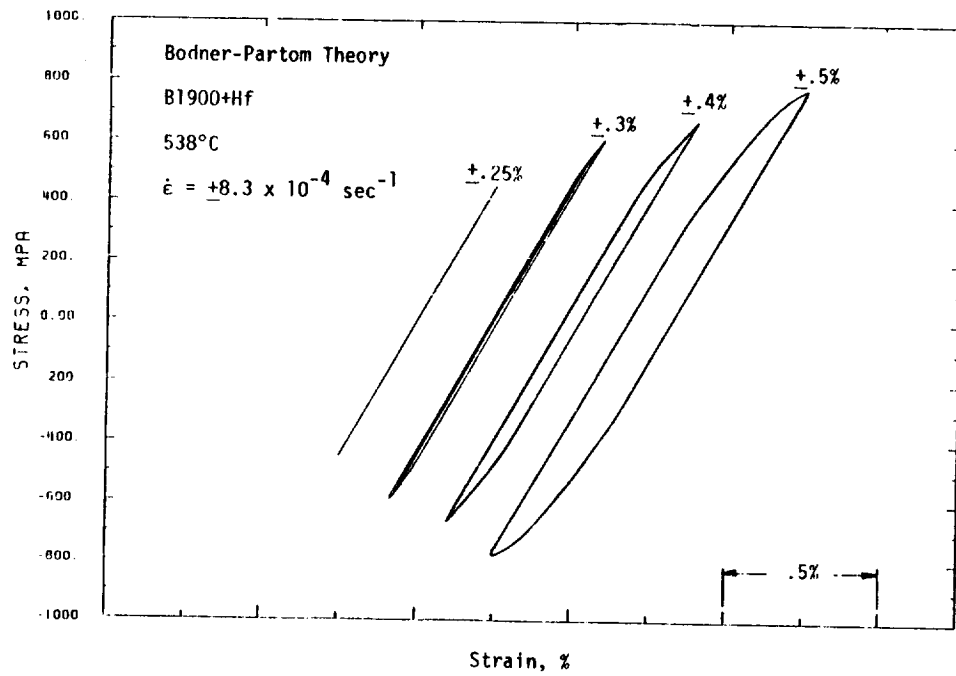
(b) Bodner-Partom Theory

FIGURE 4.8. A COMPARISON OF THE CALCULATED (BODNER-PARTOM THEORY) AND THE EXPERIMENTAL SATURATED HYSTERESIS LOOPS FOR B1900+Hf AT 538°C.

B1900+Hf

871°C

$\dot{\epsilon} = \pm 8.3 \times 10^{-4}$ sec^{-1}

PWA Data

$\pm .2\%$

$\pm .25\%$

$\pm .4\%$

.5%

Stress, MPa

Strain, %

(a) Experiment

Bodner-Partom Theory

B1900+Hf

871°C

$\dot{\epsilon} = \pm 8.3 \times 10^{-4}$ sec^{-1}

$\pm .25\%$

$\pm .3\%$

$\pm .35\%$

$\pm .4\%$

.5%

STRESS, MPA

Strain, %
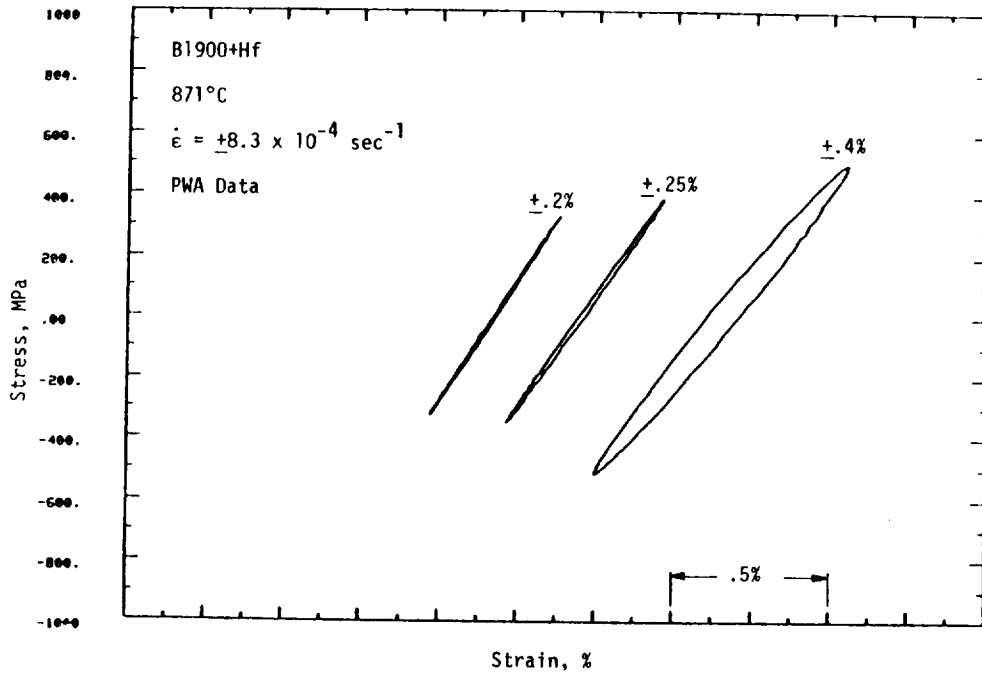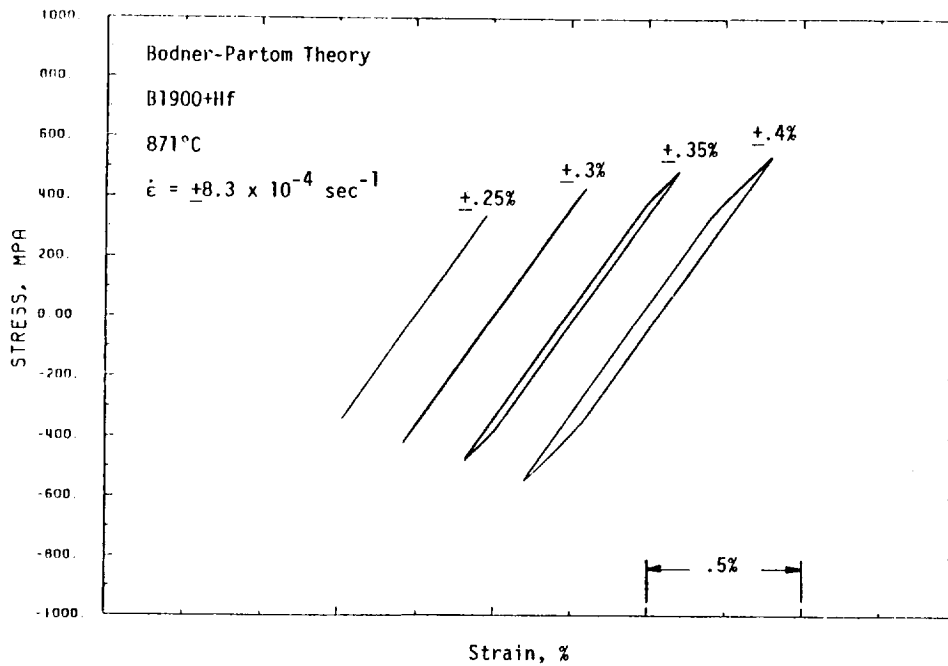
(b) Bodner-Partom Theory

FIGURE 4.9. A COMPARISON OF THE CALCULATED (BODNER-PARTOM THEORY) AND THE EXPERIMENTAL SATURATED HYSTERESIS LOOPS FOR B1900+Hf AT 871°C.

4-13
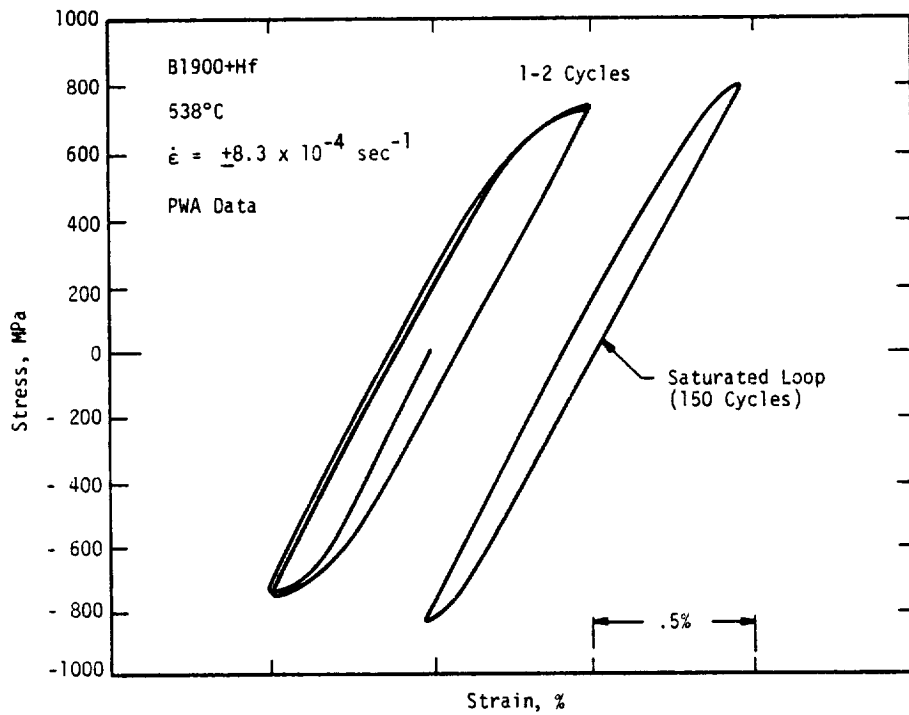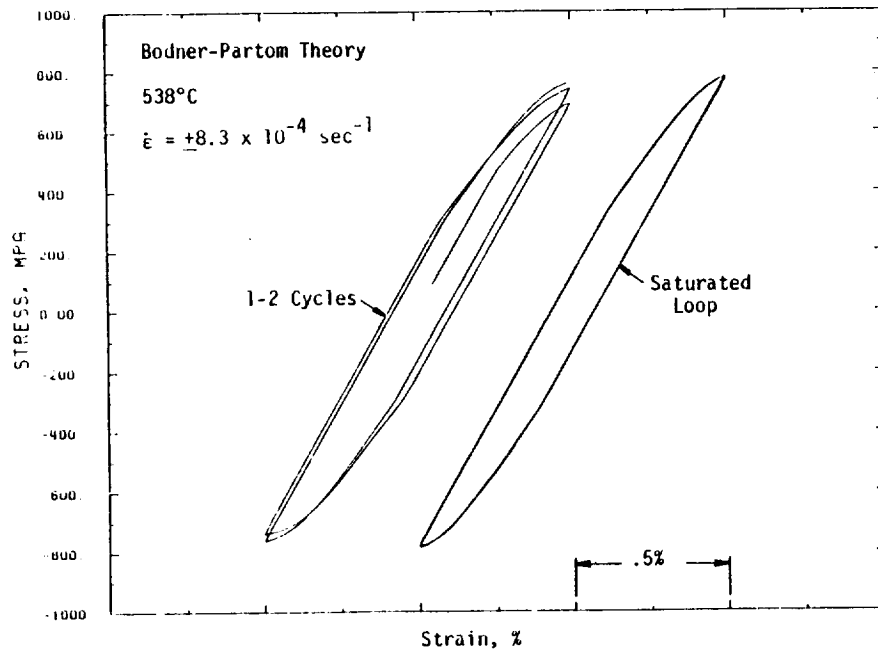
(a) Experiment

(b) Bodner-Partom Theory

FIGURE 4.10. A COMPARISON OF THE CALCULATED (BODNER-PARTOM THEORY)
AND THE EXPERIMENTAL HYSTERESIS LOOPS AFTER 1-2 CYCLES
AND AT CYCLIC SATURATION.

4-14
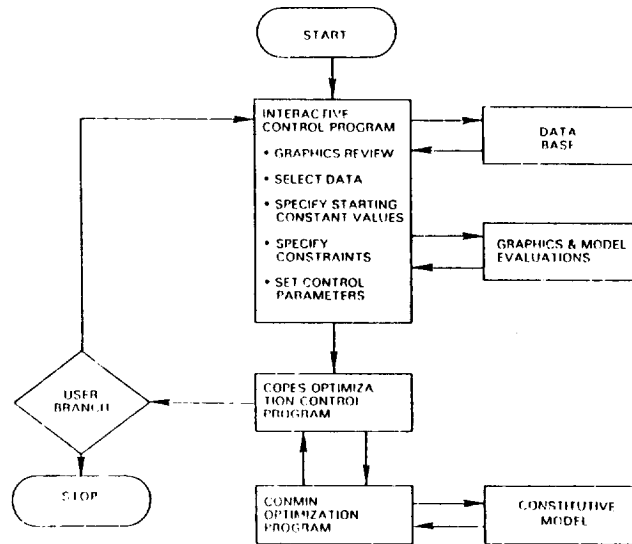
FIGURE 4.11(a). A FLOW CHART SHOWING THE COPES/CONMIN
OPTIMIZATION CODE AND ITS INTERACTIONS
WITH PWA GRAPHICS/FILE MANIPULATION
ROUTINES AND THE DATA BASE.
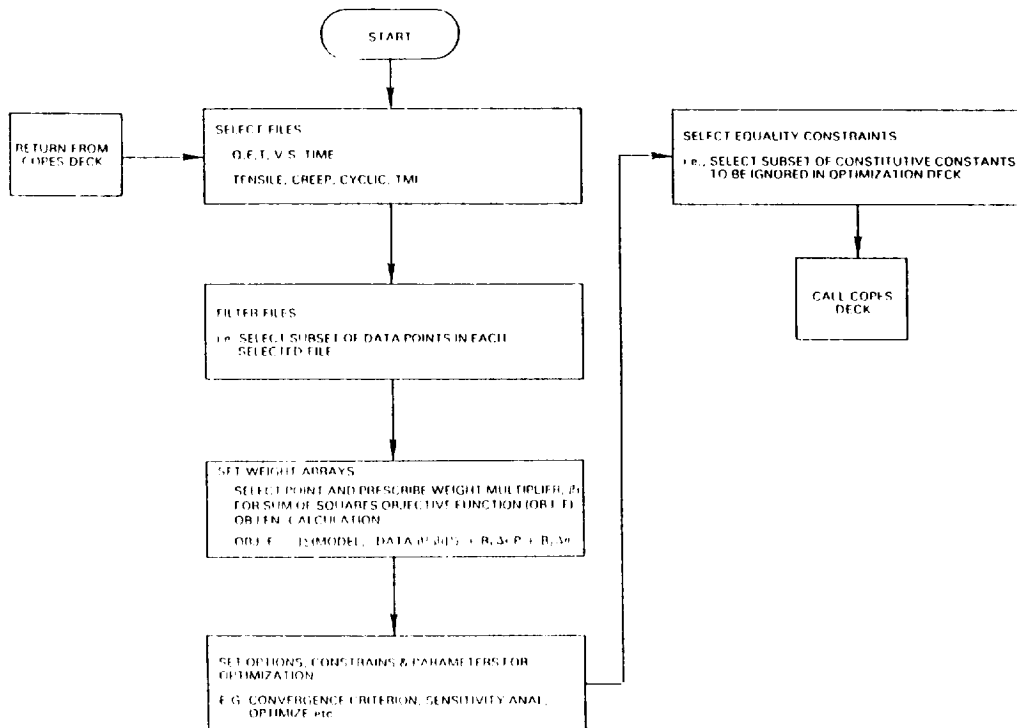
FIGURE 4.11(b). A FLOW CHART SHOWING THE OPTIMIZATION PROCEDURES
UTILIZED IN SELECTING MATERIAL CONSTANTS IN
WALKER'S MODEL.

4-15

$$\dot{\varepsilon}_{ij}^{p} = \left(\frac{\sqrt{\frac{2}{3}\left(\frac{3}{2}S_{ij} - \Omega_{ij}\right)\left(\frac{3}{2}S_{ij} - \Omega_{ij}\right)}}{K}\right)^{n} \frac{\left(\frac{3}{2}S_{ij} - \Omega_{ij}\right)}{\sqrt{\frac{2}{3}\left(\frac{3}{2}S_{ij} - \Omega_{ij}\right)\left(\frac{3}{2}S_{ij} - \Omega_{ij}\right)}} \tag{1}$$

$$\dot{\Omega}_{ij} = (n_1 + n_2)\dot{\varepsilon}_{ij}^{p} + \varepsilon_{ij}^{p}\left(\frac{\partial n_1}{\partial \Theta}\right)\dot{\Theta} - \left(\Omega_{ij} - \overset{o}{\Omega}_{ij} - n_1 c_{ij}\right)\left(\dot{G} - \frac{1}{n_2}\frac{\partial n2}{\partial \Theta}\dot{\Theta}\right) + \overset{\dot{o}}{\Omega}_{ij} \tag{2}$$

$$K = K_1 - K_2 e^{-n_7 R} - K_3 e^{-n_8 L} \tag{3}$$

$$\dot{\varepsilon}_{ij}^{p} = \frac{d}{dt}\left[(\delta_{ij}\lambda\varepsilon_{kk} + 2\mu\varepsilon_{ij} - \sigma_{ij} - \delta_{ij}(3\lambda + 2\mu)\int_{0}^{t}(\alpha\Theta \, d\xi)/2\mu\right] \tag{4}$$

$$\dot{G} = (n_3 + n_4 e^{-n_5 R})\dot{R} + n_6 \left(\frac{2}{3}\Omega_{ij}\Omega_{ij}\right)^{\frac{m-1}{2}} \tag{5}$$

$$\dot{R} = \sqrt{\frac{2}{3}\,\dot{\varepsilon}_{ij}^{p}\dot{\varepsilon}_{ij}^{p}} \tag{7}$$

$$\dot{L} = \left| \sqrt{\frac{2}{3}\,\dot{\varepsilon}_{ij}^{p}\dot{\varepsilon}_{ij}^{p}} - \left| \sqrt{\frac{2}{3}\,\dot{\varepsilon}_{ij}^{p}\varepsilon_{ij}^{p}} \right| \right| \tag{7}$$

$$\overset{\dot{o}}{\Omega}_{ij} = 3\overset{o}{\Omega}\left[\frac{\dot{\varepsilon}_{ik}\varepsilon_{kj}^{p}}{\varepsilon_{pq}^{p}\varepsilon_{pq}^{p}} + \frac{\varepsilon_{ik}\dot{\varepsilon}_{kj}^{p}}{\varepsilon_{pq}^{p}\varepsilon_{pq}^{p}} - \left(\frac{2\varepsilon_{ik}\varepsilon_{kj}^{p}}{\varepsilon_{pq}^{p}\varepsilon_{pq}^{p}}\right)\left(\frac{\varepsilon_{rs}\dot{\varepsilon}_{rs}^{p}}{\varepsilon_{uv}^{p}\varepsilon_{uv}^{p}}\right)\right] + \left[3\frac{\varepsilon_{ik}\varepsilon_{kj}^{p}}{\varepsilon_{pq}^{p}\varepsilon_{pq}^{p}} - \delta_{ij}\right]\frac{\partial \overset{o}{\Omega}}{\partial \Theta}\dot{\Theta} \tag{8}$$

$$S_{ij} = \sigma_{ij} - \frac{1}{3}\delta_{ij}\sigma_{kk} \tag{9}$$

Material Constants: λ, μ, $\overset{o}{\Omega}$, n, m, n_1, n_2, n_3, n_4, n_5, n_6, n_7, n_8, K_1, K_2, K_3 depend on temperature.

FIGURE 4.12. A SUMMARY OF WALKER'S MODEL.

testing of the precipitation aged materials is also a prime factor. No single series of tests can be performed (stress dip tests to probe for back stress, etc.) that will identify in a straightforward manner the evolution of the internal variables for materials of this type. If "trial and error" is required, optimization techniques can considerably facilitate the search.

As a result of the studies performed to date, several aspects of the use of optimization were found to be especially important. In addition, several variations of the basic approach were evaluated and still other variations identified for continued investigation. A description of these findings and the procedures used follows.

The interactive computer code which was developed as part of this effort is outlined in Figure 4.11(a) with additional details presented in Figure 4.11(b). The procedure normally followed in the use of the code begins with the selection of the data set from the HOST data base to be used in the optimization process. This data set is returned to the interactive control program as shown in Figure 4.11(a). The user then exercises a series of options as outlined in Figure 4.11(b). These include: 1) the option to reduce the number of data points in the file selected in order to control computation time, 2) the option to provide a weighting matrix to bias the least squares fit toward those aspects of the data (data fit at strain reversal point, for example) deemed most significant, 3) the ability to set limits or constraints on the magnitude of the constants based on prior information or physical limits, and finally, 4) to supply general control information such as convergence criterion and the type of optimization information desired.

The derivation of constitutive theories stems generally from two sources. The first source is the isolated mechanical behaviors observed in laboratory tests. Second, constitutive theories are derived from concepts and theories of physical metallurgy. Neither of these sources is entirely exclusive of the other or clearly sufficient in itself.

It is for this reason that a viable approach to the determination of model constants might proceed on the notion that the most appropriate tests from which to determine constants are those which most closely represent the application where the model is to be utilized. Preferably, this set of base or reference tests for model constant determination would span the range of conditions that are reasonably expected in hot section blade and vane applications; limited only by the usual limits imposed by use of laboratory equipment.

Based on the considerations outlined above, a study was initiated to determine to what extent useful constitutive model constants could be determined using cyclic data alone. More specifically, it was hypothesized that the most reliable source of constants would be obtained from a fatigue test with the most involved loading wave form. This approach was tested using 1600°F and 1800°F data from the HOST Isotropic Fatigue program. The results and conclusions are presented below.

The response of the material during a fully reversed dwell fatigue test (Specimen 27B) was selected as the base or reference data for selection of the model constants at 1600°F.

The model constants were found by optimizing a sum of squares parameter based on the residual deviations between the model predicted stress and the measured stress at each recorded data point. No constraints on the Walker constitutive model constants were imposed. The optimum fit of the data is compared against the measured data in Figure 4.13. The fit shown appears reasonable with the maximum difference at any strain between model predicted stress and data no more than 5% of the total stress range. However, a more interesting test of the validity of determining constants from cyclic data is to use the model constants to predict cyclic data at conditions which were not used to determine constants. This was done for a variety of test conditions, shown in Table 4.IV. The resulting comparisons of model prediction versus data at 1600°F are shown in Figures 4.14, 4.15, and 4.16 for one way rapid cycle, one way slow cycle, and fully reversed rapid cycle large strain conditions. The maximum deviations between model predicted stress and data are similar in magnitude to that found for the reference Specimen (27B) used to determine model constants at 1600°F.

While the approach of determining constants from cyclic data was successful in predicting the behavior at other cyclic load conditions at the same temperature, it was not successful in predicting the material behavior during a monotonic tensile test. Comparisons of the ability to predict high strain tensile data at two strain ramp rates from cyclically determined constants are shown in Figures 4.17 and 4.18. As readily noted, the high strain data fit is poor. Figure 4.19 presents a repeat of the condition of Figure 4.17, but with model constants determined from the data itself to illustrate that the optimization can readily tailor constants to individual data sets.

An additional approach to evaluating the validity of a constitutive model formulation is to compare the optimized constants from each test condition and observe the scatter between individual loading conditions. This comparison is shown for a partial list of the constants from the cyclic conditions at 1600°F in Table 4.V. It was found that the optimum constants were not influenced by varying cyclic strain rate, R-ratio, and loading wave form (triangle wave vs. hold periods).

Not unexpectedly the strain hardening exponent and the principal component of the drag stress, K_1, were influenced by a change in strain range as shown by a comparison of the constants for Specimens 31B and 27B in Table 4.V. This trend is similar to that observed from the comparisons of model prediction versus data for the tensile tests.

Constants for Walker's model were also determined at 1800°F. A comparison of the model using optimized constants with the corresponding data is shown in Figure 4.20 for a slow cycle fully reversed test. Figure 4.21 shows a comparison of model prediction with the tensile test data at 1800°F,

TABLE 4.IV

SPECIMEN TEST CONDITIONS USED IN WALKER'S MODEL EVALUATION

1600°F Data

Test Type	Spec.	%	R	Ramp Frequency Hz	Hold Period (Sec)	Notes
Dwell-Fatigue, Rapid Cycle	27B	.5	-1	.1520	60 Compression	Reference Case
Fatigue, Rapid Cycle	21B	.5	0	.1667	-	-
Fatigue, Slow Cycle	21A	.5	0	.00833	-	-
Fatigue, Slow Cycle	31B	.8	-1	.0104	-	-
Tensile, Rapid	2D	-	0	.005 in/in/min	-	-
Tensile, Slow	39A	-	0	.0005 in/in/min	-	-

1800°F Data

Test Type	Spec.	%	R	Ramp Frequency Hz	Hold Period (Sec)	Notes
Fatigue, Slow Cycle	29B	.8	-1	.0104	-	Reference Case
Tensile, Rapid	41B	-	-	.005 in/in/min	-	-

4-19

TABLE 4.V

PARTIAL LIST OF CONSTANTS FOR WALKER'S MODEL
DETERMINED BY OPTIMIZING ON CYCLIC DATA FROM INDIVIDUAL TESTS

		SPECIMEN TEST DESIGNATION*				
		27B (1600°F)	21B (1600°F)	21A (1600°F)	31B (1600°F)	29B (1800°F)
n	(Strain Hardening Exponent)	6.203	6.250	6.090	7.107	4.476
	Initial Equilibrium Stress Value (psi)	-2828.7	-2829.1	-2828.7	-2827.0	-3435.
K_1	Principal Component of Drag Stress	$.2288 \times 10^6$	$.2286 \times 10^6$	$.2288 \times 10^6$	$.1704 \times 10^6$	$.1839 \times 10^6$
n_1		.01340	.01337	.01338	.01336	.01338
n_2		$.1018 \times 10^9$	$.1019 \times 10^9$	$.1018 \times 10^9$	$.1015 \times 10^9$	$.9890 \times 10^8$
n_3		$.1990 \times 10^4$	$.1990 \times 10^4$	$.1990 \times 10^4$	$.1997 \times 10^4$	$.2022 \times 10^4$
n_6	**	.472	.472	.472	.472	.472
n_7		10.215	10.219	10.215	10.202	10.154
n_9		340.65	340.26	340.65	240.0	333.4
n_{11}		$.9989 \times 10^7$	$.1000 \times 10^8$	$.9989 \times 10^7$	$.9975 \times 10^7$	$.9973 \times 10^7$
m		1.0224	1.0197	1.0220	1.0337	1.2000
E	Young's Modulus	20.13×10^6	20.04×10^6	20.12×10^6	20.13×10^6	16.84×10^6

Remaining constants were not included either because they have been found not to contribute for precipitation hardened alloys or pertain only for non-proportional loading.

*Test conditions for each specimen shown in Table 4.III.

**Constants n_1, n_2, n_3, n_4, n_9, n_{11} and m influence the evolution of the equilibrium stress in Walker's model n_7 controls the rate of cyclic hardening.

FIGURE 4.13. OPTIMUM FIT OF 1600°F FULLY REVERSED COMPRESSION
DWELL DATA USING WALKER'S MODEL (SPECIMEN 27B).
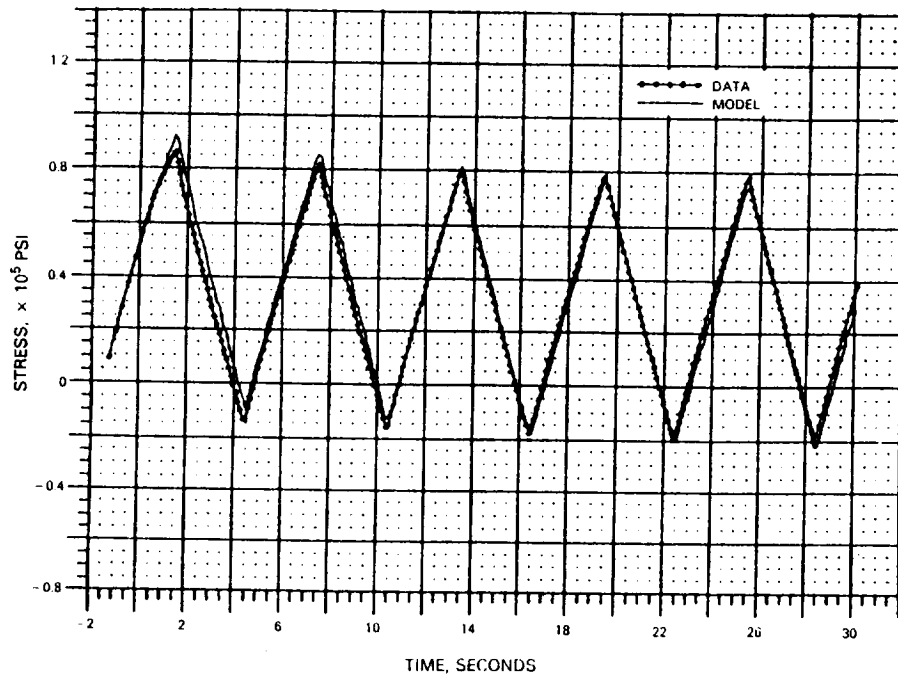
FIGURE 4.14. FIT OF 1600°F ONE WAY TENSILE, RAPID CYCLE
DATA (SPECIMEN 21B) USING WALKER'S MODEL
WITH CONSTANTS DERIVED FROM SPECIMEN 27B.

4-21
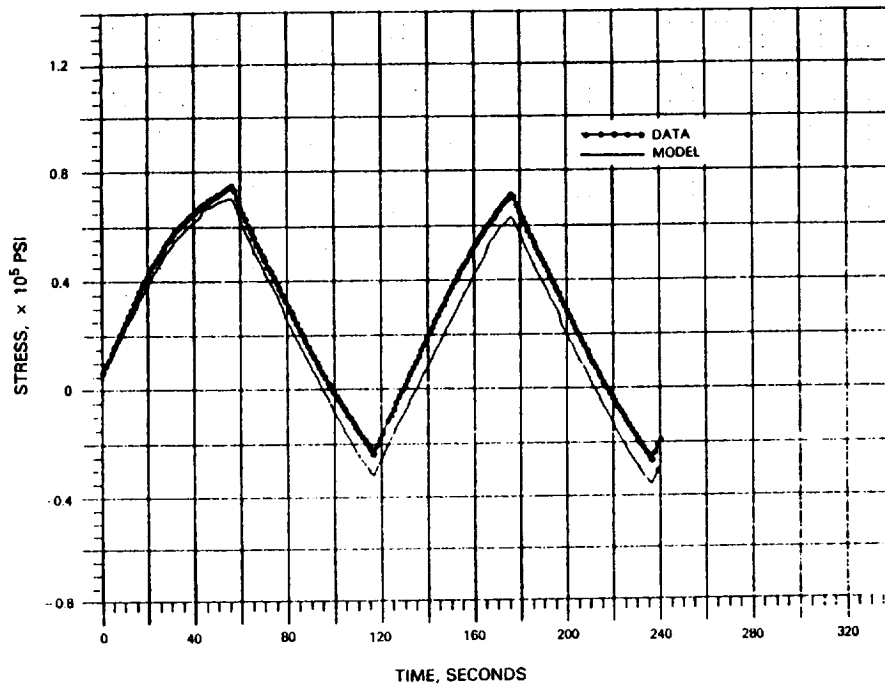
FIGURE 4.15. FIT OF 1600°F, ONE WAY TENSILE, SLOW CYCLE DATA (SPECIMEN 21A) USING WALKER'S MODEL WITH CONSTANTS DERIVED FROM SPECIMEN 27B.
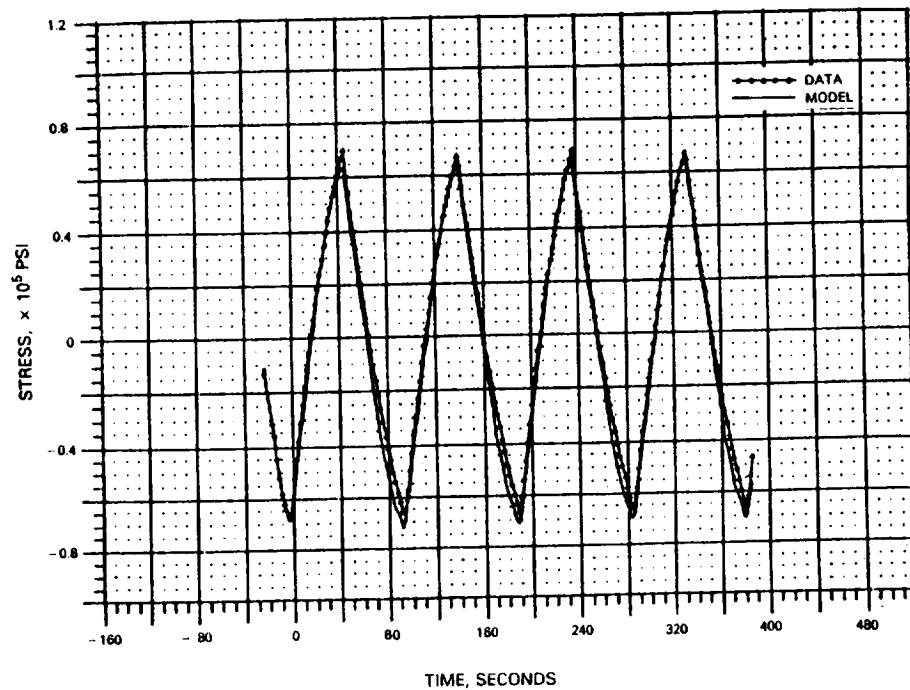
FIGURE 4.16. FIT OF 1600°F, FULLY REVERSED, RAPID CYCLE DATA AT +.4% (SPECIMEN 31B) USING WALKER'S MODEL WITH CONSTANTS DERIVED FROM SPECIMEN 27B.
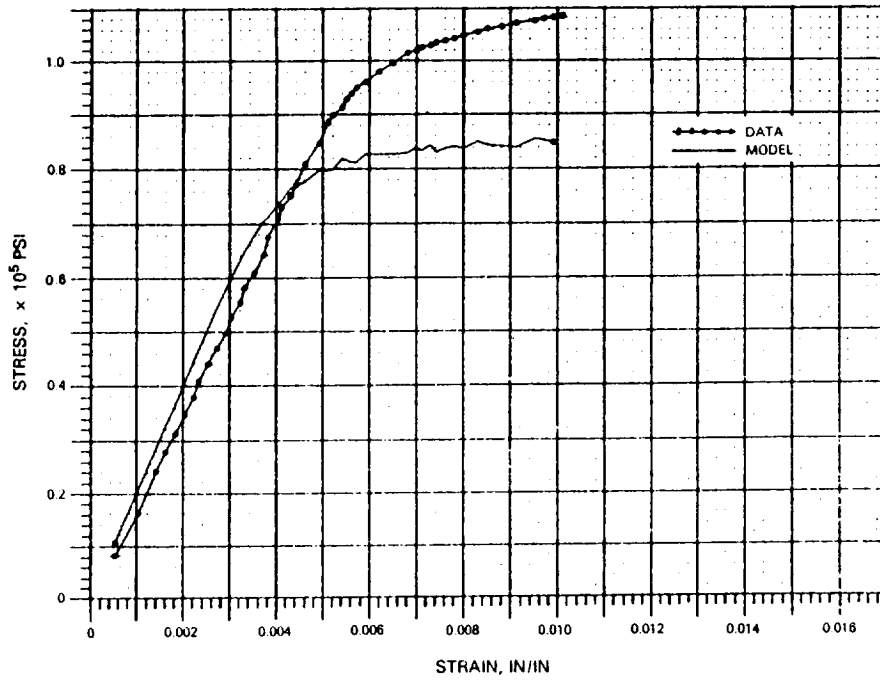
FIGURE 4.17.   FIT OF 1600°F MONOTONIC TENSILE DATA AT
A STRAIN RATE OF .5% PER MINUTE USING
WALKER'S MODEL WITH CONSTANTS DERIVED
FROM SPECIMEN 27B.
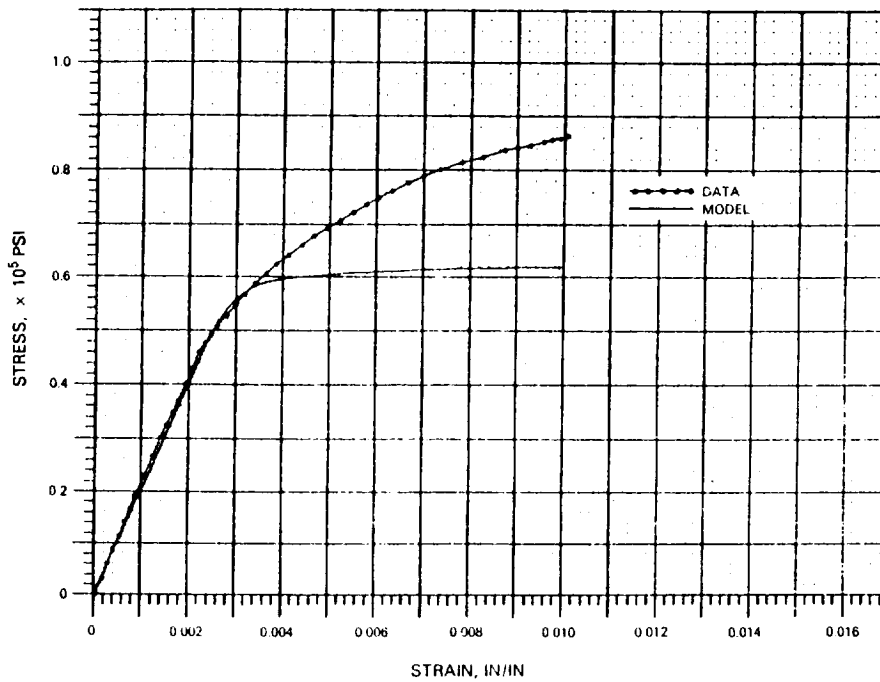
FIGURE 4.18.   FIT OF 1600°F MONOTONIC TENSILE DATA AT
A STRAIN RATE OF .05% PER MINUTE USING
WALKER'S MODEL WITH CONSTANTS DERIVED
FROM SPECIMEN 27B.
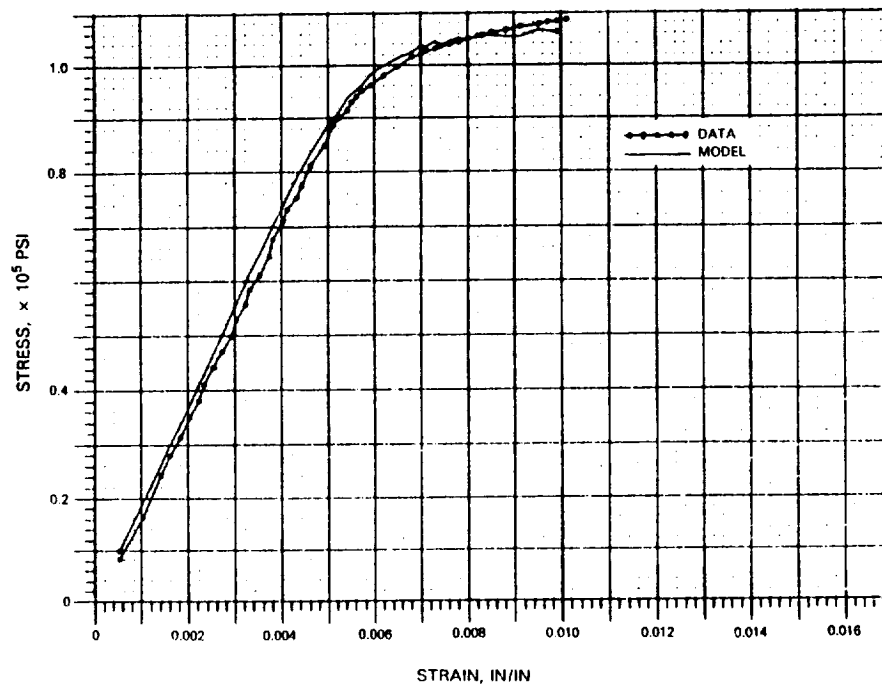
FIGURE 4.19.   OPTIMUM FIT OF 1600°F MONOTONIC TENSILE DATA
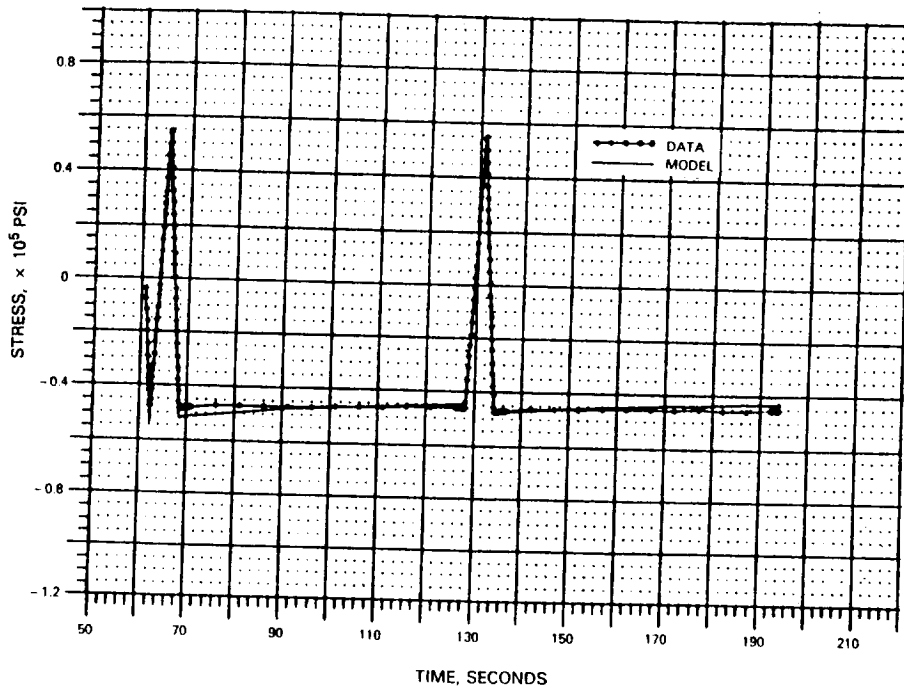AT A STRAIN RATE OF .5% PER MINUTE USING
WALKER'S MODEL.
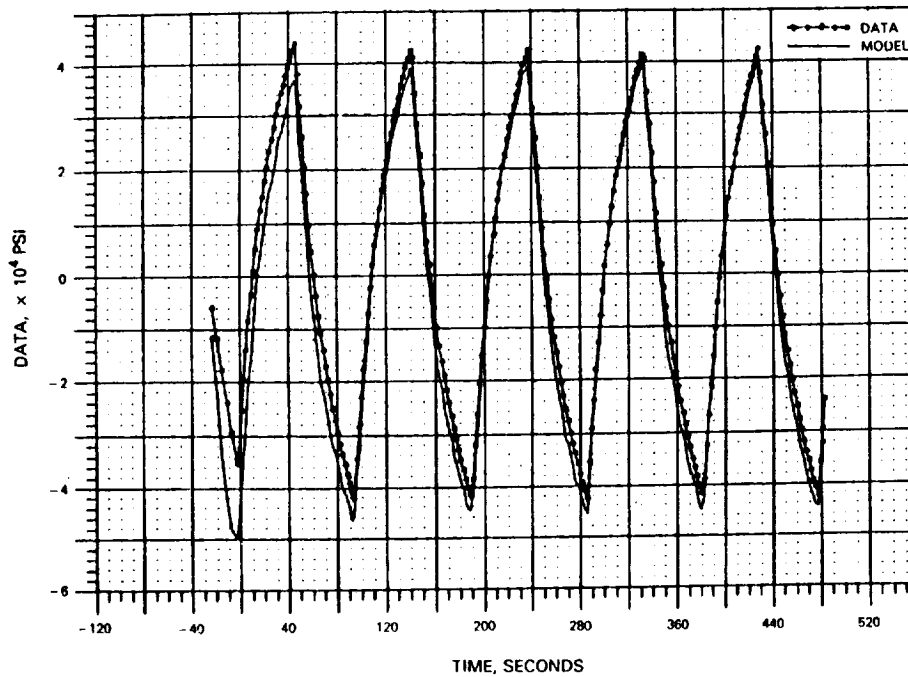
FIGURE 4.20.   OPTIMUM FIT OF 1800°F FULLY REVERSED, SLOW CYCLE
DATA USING WALKER'S MODEL (SPECIMEN 29B).
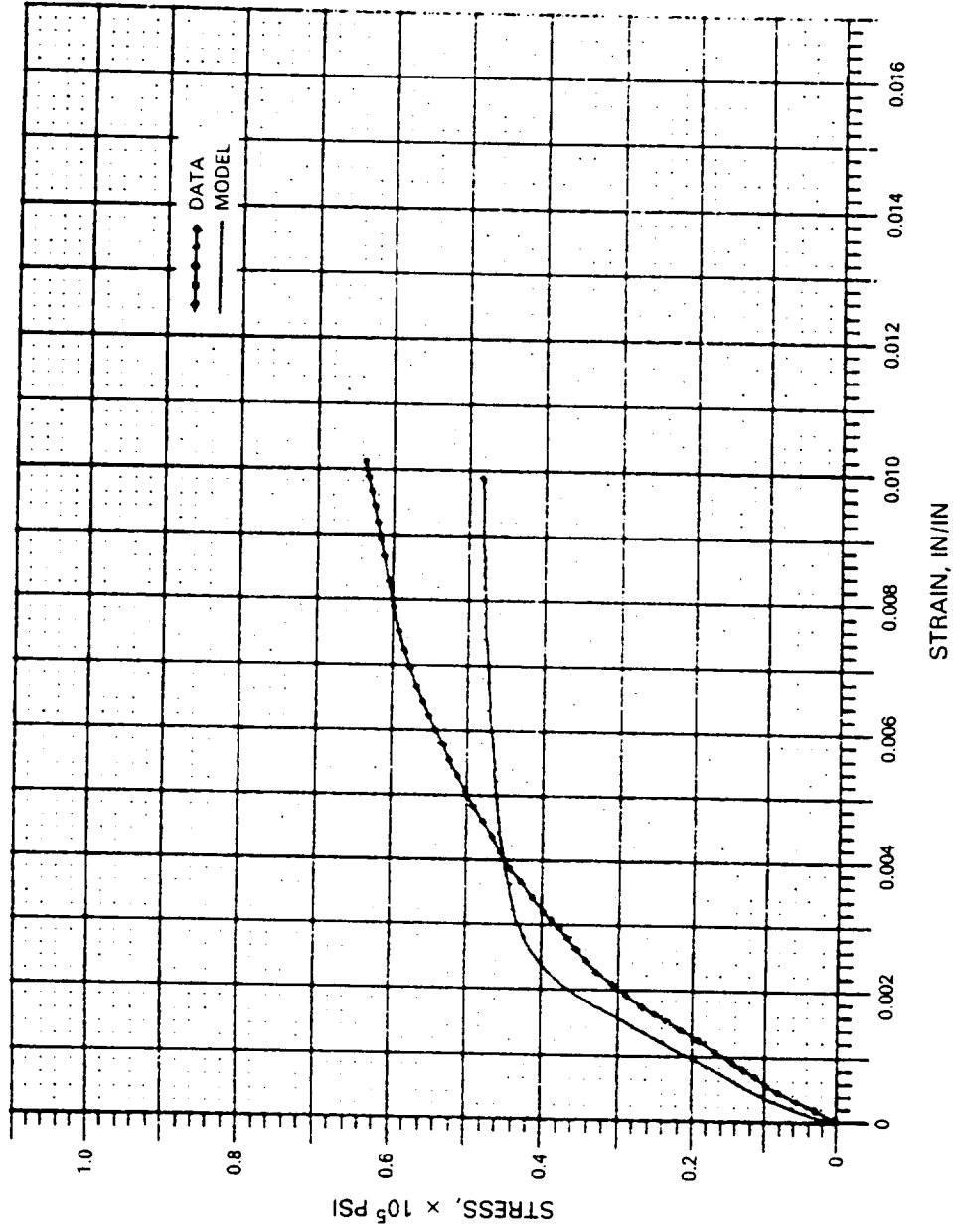
FIGURE 4.21. FIT OF 1800°F MONOTONIC TENSILE DATA AT A STRAIN RATE OF .5% PER MINUTE USING WALKER'S MODEL WITH CONSTANTS DERIVED FROM SPECIMEN 29B.

the constants derived from the cyclic test were used for this comparison. The same trends observed at 1600°F were found at 1800°F.

The method just described utilizes optimization of an objective function based upon the least squares parameter calculated from the residual deviation at each measured data point. Four rather specific strategies for the use of numerical optimization were tried. 1) Unrestrained optimizations on all constants simultaneously. 2) Progressive optimization on several types of cyclic tests using increasingly tight constraints on those constants determinable from prior data fitting, e.g., elastic constants. 3) A procedure which allowed constants to be fixed (equality type constraints), once determined, so that optimization can proceed on the remainder of the constant set. Of these three approaches, the first has surprisingly proven to be the most advantageous to date. The second approach was initially expected to be the ideal one, but the optimization algorithms used in this study tended to terminate the search procedures prematurely when the search limits (upper and lower bounds) were set close to one another. This limitation of the optimization procedures has been noted by the author of the CONMIN code, Dr. G. H. Vanderplaats.

The third strategy involved the temporary removal of the constrained variable from the list of those to be optimized. Removing a model constant from the variable list this way amounts to a practical way of providing an equality constraint on the constant. This approach yielded good results initially and will be explored further. The principal disadvantage of this approach is that it assumes that a particular constant is known exactly rather than within a narrow uncertainty band. This should not be a serious drawback in practice, however.

A fourth approach was the use of weighting factors applied to those points in the data cycle deemed most significant. The trials (e.g., increased significance given to data fit near strain reversal or null load points) using this approach showed no advantage on the limited data set evaluated.

Other strategies which remain to be explored are the use of constraints on dependent variables associated with the model and model constants and secondly, the use of alternative forms of the objective function. Two examples of dependent variable constraints which may prove useful are: 1) a narrow band around the actual measured response (e.g., measured stress) which might be made progressively more narrow in order to guide the optimization in the desired direction, and 2) a similar bound on the maximum residual deviation (e.g., the maximum absolute value of the differences between the measured and calculated stresses for all data points). This same maximum deviation should also be explored as an alternative to the sum of the squared deviations as an objective function to be minimized. It is considered likely that this would be a more sensitive parameter than the more usual sum of squared residuals. It may have the drawback, however, that it is overly sensitive to random fluctuations, or noise, in the measured stress data set and may not converge

due to minor discontinuities. A second alternative to the objective function which could possibly avoid sensitivity to data set noise would be weighted combination of the sum of squared residuals and the maximum deviation.

To summarize the experience with the use of optimization for determination of constitutive model constants, it is to a large degree a very successful approach. It is too early to say that the specific strategies used are the best ones to use. No one method has been found completely satisfactory at this time. However, it is clear that reasonable constant values can be determined with the relatively small expenditure of analysis time, which was the primary goal of the study to date.

5.0 TASK D. IMPLEMENTATION IN FINITE ELEMENT COMPUTER CODE

Any constitutive model being developed must be included in a structural analysis program. In this and two previous contract efforts [1 and 2], the MARC nonlinear finite element computer program was the vehicle for incorporating the viscoplastic models. The following section will be divided into three parts: 1) a brief discussion of the MARC code and the procedure for implementing a viscoplastic model, 2) a review of various integrating methods for viscoplastic theories considered to date in conjunction with the MARC code, 3) a summary of the approach being taken in Task D.

5.1 Description of the MARC Program

In References 1 and 2, the viscoplastic constitutive theories were incorporated into MARC program by means of an initial stress technique. All of the material nonlinearity in the constitutive equations is incorporated into an initial load vector and treated as a pseudo body force in the finite element equilibrium equations. Because the viscoplastic constitutive theories for a "stiff" system of differential equations, it is necessary to form the incremental constitutive equation appropriate to the finite element load increment by means of a subincrement technique.

In the subincrement technique the finite element load increment is split into a number of equal subincrements and the viscoplastic constitutive theories are integrated over the small subincrements to form an accurate representation of the incremental constitutive equation over the finite element load increment. Integration over each subincrement is accomplished by a number of techniques. Provided the subincrements are sufficiently small (so that the stability level of the integration method is not exceeded), the technique has been found to work efficiently and accurately, even for large finite element load increments. However, it is difficult for the user to pick efficient subincremental steps, and there is a considerable incentive to use as few subincrements as possible, consistent with the stability of the differential equations comprising the constitutive theory.

The MARC code allows the user to implement very general constitutive relationships into the program by means of the user subroutine HYPELA. Within this subroutine the user must specify the values of the elasticity matrix D_{ij} and the inelastic stress increment vector $\Delta \zeta_i$ in the incremental vector constitutive relationship

$$\Delta \sigma_i = D_{ij}(\Delta_j - \delta_j \alpha \Delta \Theta) - \Delta \zeta_i \qquad (5.1)$$

The inelastic stress increment vector $\Delta \zeta_i$ is computed in HYPELA from the viscoplastic constitutive relationships.

In Equation (5.) α denotes the coefficient of thermal expansion and δ_j is the vector Kronecker delta symbol,

$$\delta_j = \begin{cases} 1 \text{ if } 0 \leq j \leq 3 \\ 0 \text{ if } 3 < j \leq 6 \end{cases} \qquad (5.2)$$

For the class of nonlinear viscoplastic constitutive relationships under consideration in this contract, the incremental inelastic stress vector $\Delta\zeta_i$ depends in a highly nonlinear manner on the incremental strain vector $\Delta\epsilon_i$.

The solution of the incremental equilibrium is accomplished within the MARC code by the following algorithm. At the start of the increment the user subroutine HYPELA is entered to determine the elasticity matrix D_{ij} and the incremental inelastic stress vector $\Delta\zeta_i$. On entry to the subroutine the input consists of the strain increment vector $\Delta\epsilon_i$, the temperature increment $\Delta\Theta$, the time increment Δt over which the incremental external load vector ΔP_i is applied to the structure, and the values of the stress, strain, temperature and viscoplastic state variables at the beginning of the increment. Since the incremental strain vector, $\Delta\epsilon_i = B_{ij} \Delta u_j$, can only be accurately determined after the solution to the incremental equilibrium relationship has yielded the correct incremental solution Δu_j, the strain increment vector $\Delta\epsilon_i$ initially used to generate the $\Delta\zeta_i$ is assumed to be the value obtained for $\Delta\epsilon_i$ in the preceding increment. On exit from subroutine HYPELA the elasticity matrix D_{ij} and the estimated inelastic stress increment vector $\Delta\zeta_i$ are passed into the main program. After the values of D_{ij} and $\Delta\zeta_j$ are obtained for each integration point in the structure, the incremental equilibrium relationship is assembled and solved for the incremental node displacement vector Δu_i. The incremental strain vector, $\Delta\epsilon_i = B_{ij} \Delta u_j$, is then computed and compared with the initial guess for $\Delta\epsilon_i$ used to generate the inelastic incremental stress vector $\Delta\zeta_j$. If this incremental strain vector is equal, within a user specified tolerance, to the incremental strain vector used to compute $\Delta\zeta_j$ in the assembly phase, the solution is assumed to have converged. Otherwise, the updated strain increment vector, obtained from the solution of the equilibrium relations is passed into subroutine HYPELA, a new vector, $\Delta\zeta_j$, is computed, and the equilibrium equations resolved to yield an improved value of Δu_j and $\Delta\epsilon_i$. The process is repeated until the value of the vector $\Delta\epsilon_i$ on the assembly phase is equal, within a user specified tolerance, to the value of the vector $\Delta\epsilon_i$ on the solution phase. After convergence is achieved, the temperature, stress vector, strain vector and viscoplastic state variables are updated by adding the incremental values generated during the current increment to the values of these variables at the beginning of the increment. The program then passes on to the next load increment where the process is repeated.

5.2 Integration Methods for Viscoplastic Theories in the MARC Code

The values of D_{ij} and $\Delta\zeta_i$ in the incremental constitutive relation,

$$\Delta\sigma_i = D_{ij}(\Delta\epsilon_j - \delta_j \sigma\Delta\Theta) - \Delta\zeta_i \qquad (5.3)$$

are obtained by a subincrement method. Incremental values of the variables $\Delta \Theta$, Δt and ($\Delta \epsilon_i$ and δ_i $\alpha \Delta \Theta$) for the current finite element load increment are split into NSPLIT equal values, and the constitutive equations are integrated over the NSPLIT subincrements to provide accurate values of D_{ij} and $\Delta \zeta_i$. Each load increment in a MARC analysis is divided into NSPLIT subincrements. The integration of the constitutive equations is currently performed by using explicit Euler forward differences with a step size determined by dividing the MARC Load increment by NSPLIT.

Three methods for integrating the constitutive equations were examined in [2]: (1) an explicit Euler difference scheme with error estimates for revising the time step, (2) a backward difference scheme, and (3) integration of an integral form of the equations.

The forward difference integration, similar to [3], is based on an error estimate, ϵ, given by

$$\epsilon = \Delta R + \frac{\sqrt{3 \Delta J_2}}{2\mu} \tag{5.4}$$

where

$$\Delta R = \sqrt{\frac{2}{3} \Delta \epsilon_{ij}^p \Delta \epsilon_{ij}^p}$$

ϵ_{ij}^p is the inelastic strain

S_{ij} is the deviatoric stress

Δ of a quantity is the change in the quantity over time step Δt. If the error estimate is too large

$$\epsilon > \epsilon_1 \tag{5.5}$$

then the time step is halved and the step is repeated. If the error estimate is too small

$$\epsilon < \epsilon_2 \tag{5.6}$$

then the time step is doubled for the next integration step.

A backward difference algorithm was also developed in [2]. Although the forward difference worked adequately for all test cases considered, the backward difference convergence was slow in cases where the term n_6, in Walker's equation, was not equal to zero and the strain rate was smaller (i.e., on the order of 10^{-6}/sec). A quadratic Newton's method was also used to solve for ΔG and Ω_{ij}^{k+1} but there was no benefit over a linear Newton's method. Therefore, in these cases, a sufficiently small step size was required.

The equations for the modified Walker's theory have also been recast in integral form, [1].

The implicit integration for the evaluation of the integral form of the equations can be illustrated by considering the first order differential equation

$$\dot{y}(t) = f_0(t) - y(t)f_1(t) \tag{5.7}$$

where f_0 and f_1 are known functions of time, subject to the initial condition

$$y(0) = y_0 \tag{5.8}$$

Equations (5.7) and (5.8) have the solution

$$y(t) = y_0 e^{-Q(t)} + \int_0^t e^{-[Q(t)-Q(\xi)]} f_0(\xi)d\xi \tag{5.9}$$

where

$$Q(\xi) = \int_0^\xi f_1(\tau)d \tag{5.10}$$

From [1], for large times, Equation (5.9) is

$$y(t) \approx \frac{f_0}{f_1} - \frac{\dot{f}_0}{f_1^2} + \frac{\dot{f}_1 \dot{f}_0 + \dddot{f}_1}{f_1^3} \tag{5.11}$$

Equation (5.9) can be readily cast in an incremental form as

$$y(t_{N+1}) = y(t_N)e^{-[Q(t_{N+1})-Q(t_N)]} + \int_{t_N}^{t_{N+1}} e^{-[Q(t_{N+1})-Q(\xi)]} f_0(\xi)d\xi \qquad (5.12)$$

An approximate numerical integration of Equation (5.12) using Equation (5.11) is

$$y(t_{N+1}) = y(t_N)e^{-[Q(t_{N+1})-Q(t_N)]} + \frac{f_0(t_{N+1})}{f_1(t_{N+1})} \qquad (5.13)$$

where

$$-e^{-[Q(t_{N+1})-Q(t_N)]} \frac{f_0(t_N)}{f_1(t_N)} \qquad 1 + \frac{\Delta f_0}{f_0(t_N)} - \frac{\Delta f_1}{f_1(t_N)}$$

$$\Delta f_0 = f_0(t_{N+1}) - f_0(t_N), \quad \text{and} \quad \Delta f_1 = f_1(t_{N+1}) - f_1(t_N)$$

The evaluation of Q(t) is given by Equation (5.10)

$$Q(t_{N+1}) = Q(t_N) + \int_{t_N}^{t_{N+1}} f_1(\tau)d\tau \qquad (5.14)$$

and Equation (5.12) can be approximated by using a convenient numerical integration rule. For example, a rectangular rule gives

$$Q(t_{N+1}) = Q(t_N) + f_1(t_n) \Delta t \qquad (5.15)$$

where

$$\Delta t = t_{N+1} - t_N$$

or if desired, a trapezoidal rule can be used, then

$$Q(t_{N+1}) = Q(t_N) + \frac{1}{2} [f_1(t_N) + f_1(t_{N+1})] \Delta t \tag{5.16}$$

For large time steps, from Equation (5.13)

$$y(t_{N+1}) \approx \frac{f_0(t_{N+1})}{f_1(t_{N+1})} \tag{5.17}$$

which is the first term in Equation (5.11), and for small time step

$$y(t_{N+1}) \approx y(t_N)f_0(t_N) \Delta t - y(t_N)f_1(t_N) \Delta t \tag{5.18}$$

which is a first order Euler integration.

5.3   Summary of Approach to be Taken

Several numerical methods for implementing Bodner's and Walker's theory in the MARC finite element computer program are being considered in this Task. These include, but may not be limited to:

1) Explicit Euler integration with both a fixed and self-adaptive time step. This approach has been used successfully in the past with Walker's theory.

2) The NONSS method of Miller and Tanaka. This approach has been used successfully with Bodner-Partom's model. Recent work by Brockman have suggested a method for improving the efficiency of this approach [4].

3) Implicit integration of the integral form of the equations, as described above.

4) For completeness, a second order Runge-Kutta method with a self-adaptive time step will be considered. The existing HYPELA model for Walker's theory will be modified first. Each theory will be finally coded with at least two numerical integration algorithms.

5.4 References

1. K. P. Walker, "Research and Development Program for Nonlinear Structural Modeling with Advanced Time-Temperature Dependent Constitutive Relationships," Final Report NASA CR-165533, November 1981.

2. B. N. Cassenti, "Research and Development for the Development of Advanced Time-Temperature Dependent Constitutive Relationships," Vol. 1, 2 NASA CR-168191, July 1983.

3. V. Kumar, M. Morjaria and S. Mukherjee, "Numerical Integration of Some Stiff Constitutive Models of Inelastic Deformation," Transaction of the ASME, Journal of Engineering Materials and Technology, Vol. 102, pp. 92-96, January 1980.

4. R. A. Brockman, "Explicit Forms for the Tangent Modulus Tensor in Viscoplastic Stress Analysis," International Journal of Numerical Methods in Engineering, 20, pp. 315-319, 1984.

6.0   TASK E.   MULTIAXIAL EVALUATION OF CONSTITUTIVE MODELS

The literature review conducted in Task A reveals that several structural alloys including Hastelloy-X exhibit considerably more cyclic hardening when deformed under nonproportional loading paths than under proportional loads. To take into account this type of loading-path-proportionality-dependent hardening behavior, both the Bodner-Partom and the Walker models were modified by introducing new parameters in the evolution equation of the internal variables such that additional cyclic hardening would result under nonproportional paths. Summaries of the updated Bodner-Partom and Walker models are shown in Figure 4.2 and Figure 4.12, respectively. Preliminary calculations of cyclic stress-strain response of Hastelloy-X subjected to 90° out-of-phase combined tension/torsion loading indicate good correlation between experiment and theories, as shown in Figure 6.1. However, it should be noted that the cyclic stress-strain curve shown in Figure 6.1(b) for the Bodner-Partom model was obtained using uniaxial tensile data as input only, while the result shown in Figure 6.1(c) was obtained by fitting the Walker model to the experimental data in Figure 6.1(a).

The phase angle between the deviatoric stress and the plastic strain rate vectors of Hastelloy-X under 90° out-of-phase tension/torsion loading was also determined and the results are shown in Figure 6.2. Comparison of experimental data with preliminary calculations of Walker and Bodner-Partom models, also shown in Figure 6.2, indicate that the Walker model predicts non-coaxiality between the deviatoric stress and the plastic strain rate vectors, and the predicted phase angles which are approximately 5-15° are smaller than those observed experimentally. On the other hand, in the Bodner-Partom model, the plastic strain rate vector is always taken to be coaxial with the deviatoric stress vector. As a result, the predicted phase angles are always zero, as shown in Figure 6.2.
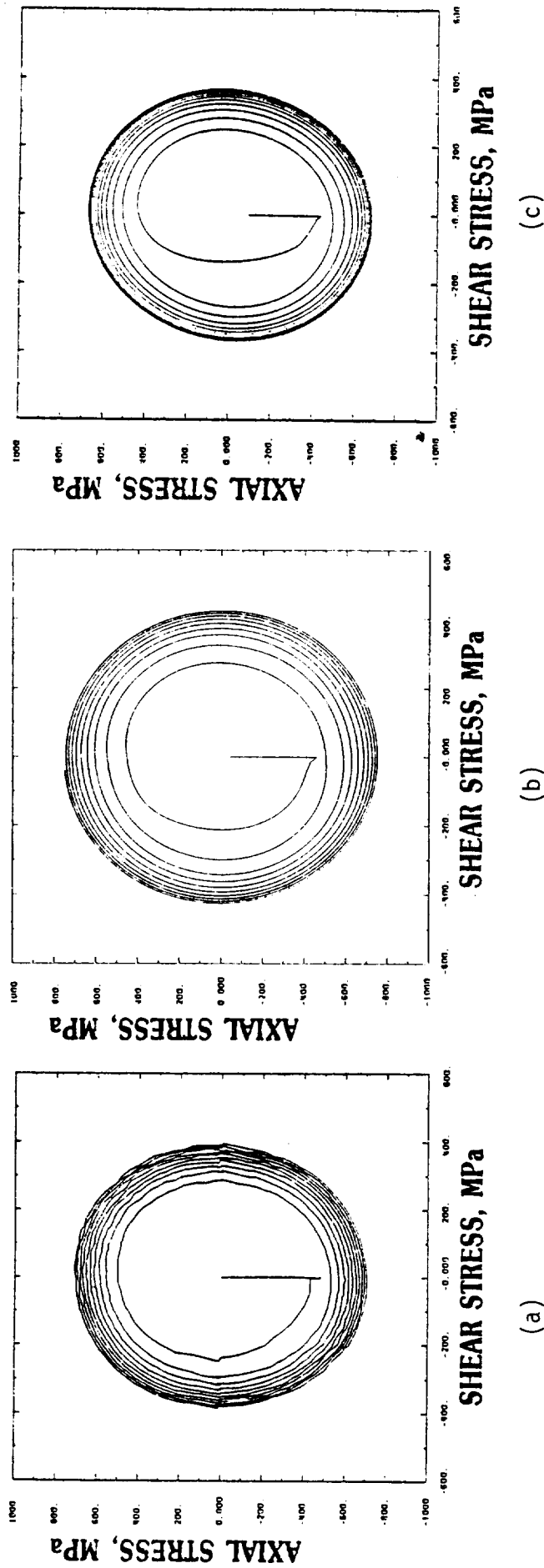
FIGURE 6.1   A COMPARISON OF BODNER-PARTOM AND WALKER THEORIES WITH EXPERIMENTAL RESULT ON THE STRESS-STRAIN RESPONSE OF HASTELLOY-X TESTED UNDER 90° OUT-OF-PHASE TENSION/TORSION LOADING AT ROOM TEMPERATURE: a) experimental data;   (b) Bodner-Partom theory;   (c) Walker theory.
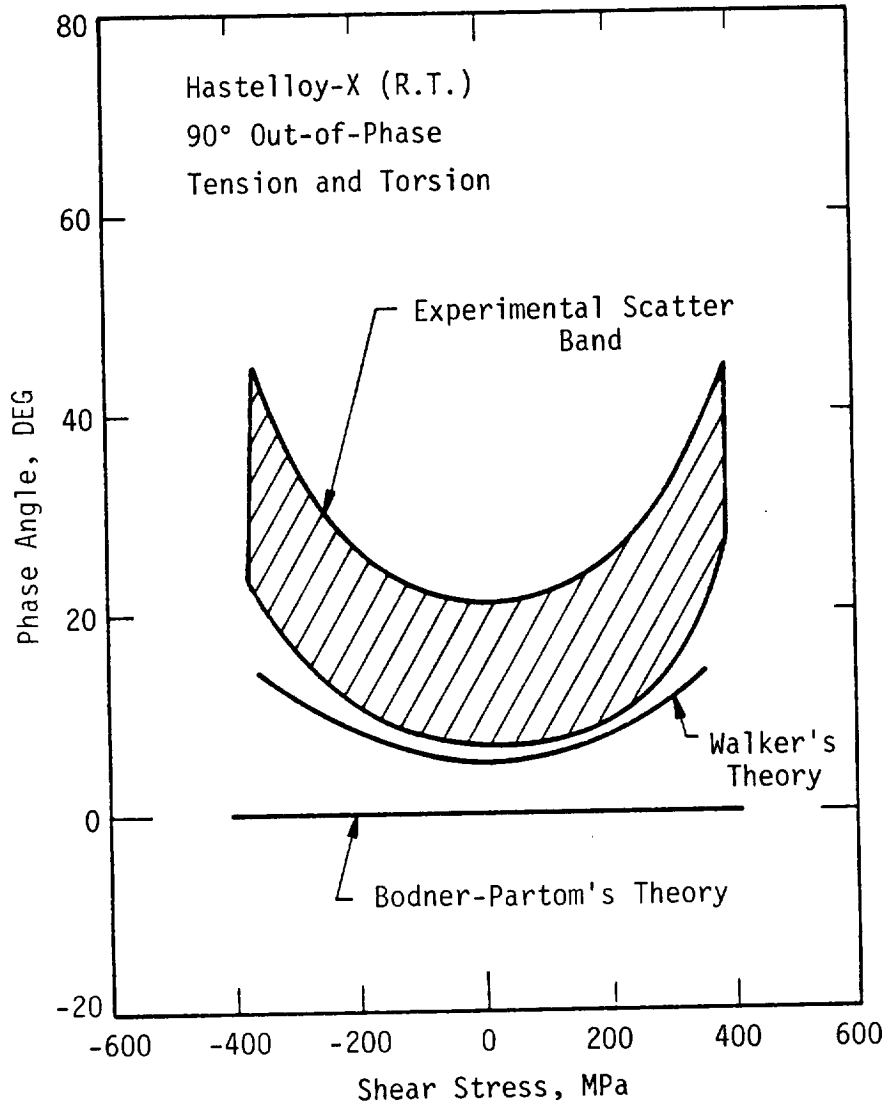
FIGURE 6.2. A COMPARISON OF BODNER-PARTOM AND WALKER
THEORIES WITH EXPERIMENTAL RESULT OF THE
PHASE ANGLE BETWEEN THE DEVIATORIC STRESS
AND THE PLASTIC STRAIN RATE VECTORS OB-
SERVED IN HASTELLOY-X TESTED UNDER 90°
OUT-OF-PHASE TENSION/TORSION LOADING AT
ROOM TEMPERATURE.

7.0 SUMMARY OF CURRENT RESULTS

During the first year of effort, the following tasks were accomplished and preliminary results obtained:

- A literature review of existing unified constitutive models for time and temperature dependent inelastic behavior of high temperature alloys was completed. All models contain three essential components - a flow law, a kinetic relationship between stress, inelastic strain rate and temperature, and evolutionary equations for the internal variable(s) describing work hardening. Ten different models were compared relative to these components.

- A review of numerical integration procedures applicable to these "stiff" equations was completed also.

- The particular models of Bodner and Partom and of Walker were selected for further detailed study and implementation in a FE code.

- The alloy selected for testing under the basic program was cast B1900+Hf. Specimens are being fabricated at PWA from a single heat of this material.

- Uniaxial tensile and creep tests have been completed at SwRI for a matrix including temperatures from room temperature to 2000°F and strain rates from 10^{-7} to 10^{-3} sec^{-1}.

- Initial correlations of the uniaxial data, both monotonic and cyclic, with the Bodner-Partom and Walker models indicate reasonable to good correlation. Procedures for determining best-fit constants for these models are being developed but need further refinement.

- Both models are being implemented in the MARC finite element computer code. At least two numerical integration algorithms will be used with each model.

- Preliminary data from the literature indicates cyclic biaxial hardening to be greater than under uniaxial or proportional cycling. Existing models do not include this effect. Several modifications were attempted to correct this situation with reasonable success.

8.0 FUTURE WORK

During the second year of the base program, the following work will be completed:

- Experimental test data will be obtained for B1900+Hf under isothermal and non-isothermal uniaxial strain controlled cyclic conditions, and proportional and non-proportional biaxial tension-torsion loading.

- The Bodner-Partom and Walker models will be implemented in the MARC finite element code. This code will then be utilized to correlate all the uniaxial and biaxial data.

- A notched specimen geometry will be selected and tested to provide benchmark data under a non-homogenous strain condition. This benchmark data will be compared with a FEM analysis of specimen utilizing the optimum constitutive model.

- A hot section component, probably a turbine blade, will be analyzed using the FEM code and optimum constitutive model to demonstrate advanced modeling capability.

- Finally, the FEM code with advanced unified constitutive model will be installed on the NASA Lewis computer facility.

APPENDIX A

LITERATURE REVIEW

1.0 INTRODUCTION

Constitutive theories based on the classical concepts of plasticity and creep generally decompose the inelastic strain rate into a time-independent plastic strain rate and a time-dependent creep rate with independent constitutive relations describing plastic and creep behavior. While this approach can be rationalized on historical grounds and perhaps on computational convenience, experimental evidence collected on structural alloys at elevated temperature indicates inherent time-dependency and creep/plasticity interactions [1,2]. This suggests that inelastic deformation might be primarily controlled by a single overall mechanism and should be treated in a unified manner.

Although much of the essential physics of time-dependent inelastic deformation of metals has been known for some time, attempts at a unified analytical formulation have been relatively recent. This seems to have been due to the success of elastic-plastic analyses in many areas of engineering and the tendency to treat time-dependent effects as special phenomena. Probably the first attempt at a unified treatment was that of J. J. Gilman and W. G. Johnston in the late 50's and early 60's who did some of the basic work in the field of "dislocation dynamics" [3-5]. They showed that a reasonably realistic stress-strain curve could be obtained by integrating expressions for the elastic and plastic strain rates which were both considered to be nonzero throughout the loading history.

In recent years, a number of formulations of elastic-viscoplastic constitutive equations have been presented in the engineering literature. Such equations are sometimes referred to as "unified" since inelastic deformations are represented and treated by a single kinetic equation and a discrete set of internal variables. In this context, creep, stress relaxation, and plastic flow are different manifestations of time-dependent inelastic deformations under particular loading conditions with consequently different response characteristics.

There are more than ten unified constitutive theories in the literature. A few of them were proposed in the last five years. These sets of constitutive equations have some common properties and some essential differences which have been reviewed recently by Walker [6]. Since then, there have been

more advances in the development of the unified theories. The purpose of this survey is to update Walker's previous work by reviewing the state-of-the-art and the numerical integration techniques for these unified theories. This survey also serves to identify areas for further model developments.

The unified theories which are reviewed in this survey include those of Walker [6], Bodner and Partom [7-9], Miller [10-12], Krieg, Swearengen and Rhode [13], Chaboche [14], Robinson [15], Hart and co-workers [16,17], Stouffer and Bodner [18,19], Lee and Zaverl [20], Ghosh [21], and Kagawa and Asada's modification of Miller's model [22].

2.0 GENERAL CHARACTERISTICS OF UNIFIED CONSTITUTIVE EQUATIONS FOR ELASTIC-VISCOPLASTIC MATERIALS

Constitutive equations for elastic-viscoplastic material could be formulated either with or without the use of a yield criterion. A basic assumption for this class of constitutive theories is that in the range where inelastic strains are present, the total strain rate $\dot{\varepsilon}_{ij}$ can be divided into elastic and inelastic components which are both nonzero, i.e.

$$\dot{\varepsilon}_{ij} = \dot{\varepsilon}_{ij}^{e} + \dot{\varepsilon}_{ij}^{p} \tag{1}$$

This equation is applicable for the small strain case and a similar decomposition is assumed to hold for the deformation rates in the case of large strains. These are equivalent to strain rates if the strains are small.

For elastic response the stresses are directly related to the deformation gradients with no memory effects. The elastic response is fully recoverable both thermodynamically and geometrically. In the case of small strains, as considered here, the elastic strain rate is given by the time derivative of Hooke's Law.

In the literature, see e.g. [23,24], there are alternative definitions for ε_{ij}^{p}, the inelastic strain. For our purposes here, and in the context of a "unified" theory, the inelastic strain rate $\dot{\varepsilon}_{ij}^{p}$ will be considered to include all strains that are not elastic, i.e. the difference between the total strain rate, $\dot{\varepsilon}_{ij}$, and the elastic strain-rate $\dot{\varepsilon}_{ij}^{e}$, (Eq. 1). Thus, the expression "unified" applied to the theories reviewed is taken to mean that all aspects of inelastic behavior such as plastic flow, creep, and stress relaxation characteristics for different loading histories. This broad definition of "unified" would admit theories with or without a yield criterion and with alternative specifications for $\dot{\varepsilon}_{ij}^{p}$. Alternative definitions of the inelastic strain increment that depend on a residual strain after loading and unloading from a stress increment are discussed by Lee [23] and Drucker [24]. Particular definitions of this type lead to the "normality" condition associated with strong material stability. With both loading and unloading increments time and temperature dependent, determination of an equilibrium residual plastic

strain component is difficult. Alternate uniqueness and stability criteria
for unified theories with internal variables are discussed in Section 2.5.
It is noted that the precise definition of inelastic strain rate in a con-
stitutive theory is given by the equations themselves.

Constitutive theories which are formulated without the use of a yield
criterion include that of Bodner and his associates [7-9], Walker [6], Miller
[10-]2], Krieg, Swearengen and Rhode [13]. Since these models do not con-
tain a completely elastic regime, the function that describes the inelastic
strain rate should have the property that the inelastic strain rate be very
small for low stress levels.

For theories with a yield criterion, $\dot{\varepsilon}_{ij}^{p}$ is identically zero until an
invariant function of the stress reaches a prescribed value; the function, by
definition, is independent of strain rate. For stresses at or exceeding the
yield value, Equation (1) applies and $\dot{\varepsilon}_{ij}^{p}$ and the stresses σ_{ij} are function-
ally related. The fully elastic state, i.e. $\dot{\varepsilon}_{ij}^{p} = 0$, would apply only for
stress states less than the rate independent yield value, and loading and un-
loading paths above that are controlled by the loading conditions through the
constitutive equations. Theories of this type have been developed by Perzyna
[25] for the case of isotropic hardening and by Chaboche [14], Robinson [15]
and Lee and Zaverl [20] for the case of both isotropic and directional harden-
ing. In these theories, loading above the elastic limit value and unloading
to it would generally not be fully elastic.

All the unified models are formulated on the basis of internal or struc-
tural variables which depend on the loading history. The essential features
of these unified theories are: (1) a flow law which functional form depends
on the method of treatment of directional (kinematic) hardening, (2) a kinetic
equation which is the temperature dependent functional relationship between
the strain rate and stress invariants and includes internal variables, and
(3) a set of evolution equations for describing the growth of the internal
variables. Here, the internal variables are used to represent the current

resistance to inelastic flow of the deformed solid. Two deforming solids with identical values of their internal variables would have identical inelastic responses under the same imposed stress state. Both the choice and the number of internal variables vary with the unified models. The number of independent internal variables that have been suggested ranges from one to as many as six reflecting the relative complexity of the model. Most of the unified models, however, use two internal variables or one variable with two components: one to represent isotropic hardening and another to represent directional (kinematic) hardening. In most models, the isotropic hardening variable is represented by a scalar quantity, either the drag stress (K) or the yield stress (Y), while directional hardening is represented by a second order tensor Ω_{ij} or a scalar function of such a tensor.

2.1 Basic Flow Laws

Four basic forms of the inelastic flow law have been identified. Plastic incompressibility is always assumed and these flow laws are:

$$(1) \quad \dot{\varepsilon}_{ij}^{p} = \lambda_1 S_{ij} \quad , \quad \dot{\varepsilon}_{kk}^{p} = 0 \tag{2a}$$

$$(2) \quad \dot{\varepsilon}_{ij}^{p} = \lambda_2 \Sigma_{ij} = \lambda_2 (S_{ij} - \Omega_{ij}) \quad , \quad \dot{\varepsilon}_{kk}^{p} = 0 \tag{2b}$$

$$(3) \quad \dot{\varepsilon}_{ij}^{p} = \lambda_{ijkl} S_{kl} \quad , \quad \dot{\varepsilon}_{iikl}^{p} = \dot{\varepsilon}_{ijkk}^{p} = 0 \tag{2c}$$

$$(4) \quad \dot{\varepsilon}_{ij}^{p} = \frac{\partial f}{\partial \sigma_{ij}} \quad , \quad \dot{\varepsilon}_{kk}^{p} = 0 \tag{2d}$$

where S_{ij}, σ_{ij}, and Σ_{ij} are the deviatoric, direct and effective stresses, respectively. The tensor Ω_{ij} represents the "equilibrium stress" which has also been referred to as the "back stress" and the "rest stress". The parameter f is a yield function or a flow potential. It should be noted that the first three laws can be considered or can be derived from Equation (2d) if they are associated with a flow potential.

Equation (2a) is the Prandtl-Reuss flow law associated with the von Mises yield criterion. However, it can be considered as a basic material equation in its own right independently of a yield condition. As such, this

A-6

equation is usually taken to be applicable for proportional loading conditions for which isotropic hardening would be appropriate. The equation states that the material response (i.e., the plastic strain rate) to stress is isotropic even though λ_1 could be stress history dependent. Since stress is directional, λ_1 could have a directional character within the context of incremental isotropic response and thereby account for induced directional hardening effects. This situation would be analogous to finite strain elasticity in which the coefficients are stress history dependent.

Equation (2b) is the flow law obtained by introducing the kinematic hardening variable of Prager into the classical plasticity formulation to account for directional hardening (the Bauschinger effect) [26]. In this context, the term Ω_{ij} would represent the new origin of a translating von Mises yield surface in deviatoric stress space, and Equation (2b) would be the associated flow rule. As before, Equation (2b) can be taken to be a basic material equation in a formulation without a yield criterion and the "equilibrium stress" tensor Ω_{ij} is generally intended to serve the following functions:

(a) to account for directional hardening (the multi-dimensional Bauschinger effect), and for the non-coaxiality of $\dot{\varepsilon}_{ij}^{p}$ and S_{ij} under non-proportional loading histories (Figure 1);

(b) to account for reversed plastic straining effects, e.g. reversed creep, relaxation through zero stress, when the effective stress Σ_{ij} is negative;

(c) for theories without a fully elastic range (i.e., a yield criterion), to account for low plastic straining within a given range.

Equation (2b) has been used by many investigators as the basic flow rule and appears to be particularly useful in representing directional hardening effects. In Equation (2b), λ_2 is a scalar function of the isotropic hardening variable K and the tensor Ω_{ij}. The evolution equation for Ω_{ij} is generally dependent on a hardening term in the direction of $\dot{\varepsilon}_{ij}^{p}$ and on so called "dynamic" and "static" (or thermal) recovery terms in the direction of Ω_{ij}. As such, Ω_{ij} is a deviatoric quantity, i.e. traceless.

Although attempts have been made to interpret Ω_{ij} physically in terms of residual stresses, this turns out to be difficult but is not essential from

DEVIATORIC STRESS SPACE
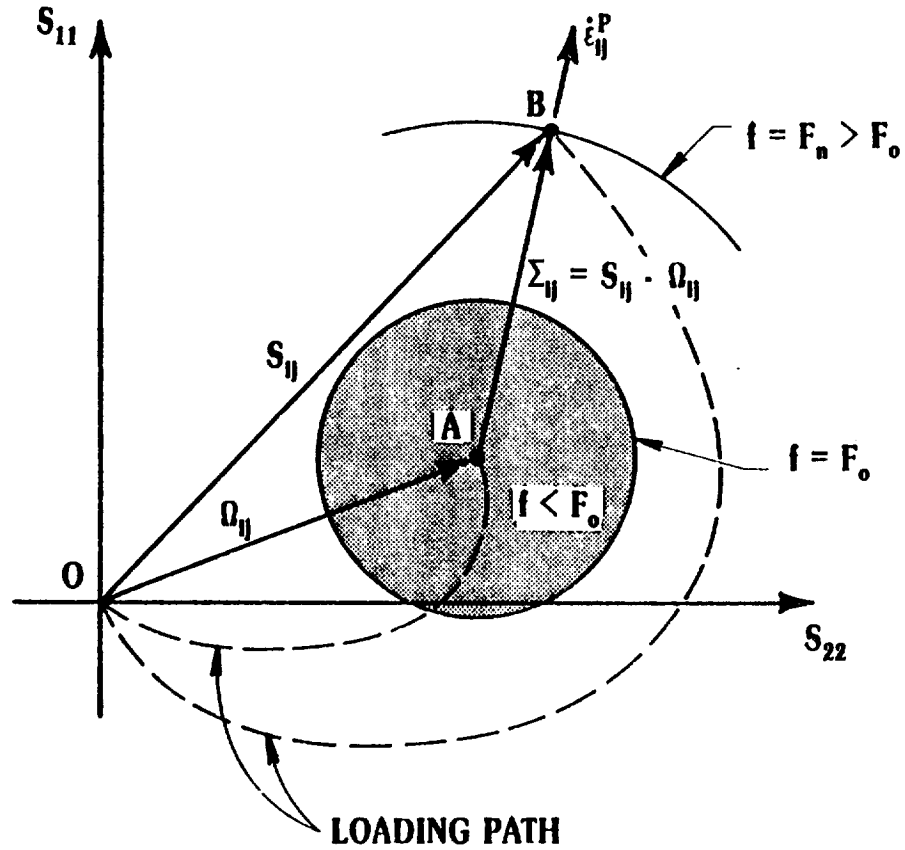
FIGURE 1. GRAPHICAL REPRESENTATION OF THE BASIC FLOW LAWS USED IN THE UNIFIED CONSTITUTIVE THEORIES. For theories based on an equilibrium stress, the inelastic strain rate vector $\dot{\varepsilon}^P_{ij}$ is coaxial with the effective stress Σ_{ij} and normal to the flow potential f if such a concept is used. For theories which do not include an equilibrium stress, $\dot{\varepsilon}^P_{ij}$ is coaxial with the deviatoric stress S_{ij} for both isotropic and incrementally isotropic cases but is noncoaxial with S_{ij} for generalized anisotropic cases.

the viewpoint of its possible utility in constitutive equations. The term "equilibrium stress" is usually applied to Ω_{ij} since it would correspond to the asymptotic stress state under relaxation conditions, but such a stress state is difficult to determine by direct experimentation. A possible criticism of Equation (2b) is that the "equilibrium stress" is a load history dependent material property which is subtracted from the applied stress which is a kinetic quantity. It is noted that difficulties are experienced in generalizing the flow law (2b) to the case of large strains because different transformation rules are required for S_{ij} and for Ω_{ij}, e.g. recent papers by E. H. Lee [27].

For cycling under proportional stress states, Equation (2a) with a stress history dependent coefficient can be shown to be equivalent to Equation (2b). The real differences in these equations would show up for non-proportional loading histories.

Equation (2c) is the general anisotropic form of the Prandtl-Reuss flow law which can be rewritten in a 6D stress and strain rate space to take the form,

$$\dot{E}^P_\alpha = \Lambda_{\alpha\beta} T_\beta \qquad \begin{array}{l} \alpha = 1, ---6 \\ \beta = 1, ---6 \end{array} \qquad (3)$$

where $\dot{E}_\alpha$ and T_β are related to the usual plastic strain rates and stresses in a simple manner, see [18,19], and $\Lambda_{\alpha\beta}$ is the 6x6 matrix of coefficients. If the material is initially isotropic and the law for plastically induced directional hardening does not lead to off diagonal terms, then $\Lambda_{\alpha\beta}$ is initially and remains diagonal. Under these conditions, Equation (2c) is equivalent to Equation (2b) since 6 material constants determine the anisotropic flow behavior (Ω_{ij} in Equation (2b) has 6 components). All the flow equations, Equations (2a,b,c), would be equivalent for the case of proportional loading, including cyclic conditions.

Although Equation (2c) can be used for materials that are initially non-isotropic with regard to inelastic response, it is obviously a complicated equation to manage. There has been relatively little experience in using Equation (2c) for such cases.

For constitutive theories with a flow potential, both the flow law and the growth law of the kinematic hardening variable Ω_{ij} are derivable from a single flow potential, Equation (2d). A basic form of such a flow potential is [13,28].

$$f = f(\sigma_{ij}, \Omega_{ij}) = F(J_2') + G(T_2) \tag{4}$$

where $J_2' = 1/2 (\sigma_{ij} - \Omega_{ij})(\sigma_{ij} - \Omega_{ij})$

$$T_2 = 1/2 \Omega_{ij} \Omega_{ij}$$

If the function $F(J_2')$ is taken as [15]

$$F(J_2) = \frac{K^2}{\mu(n+1)} F^{\frac{n+1}{2}} \tag{5}$$

where $F = \frac{J_2'}{K^2} - 1$ is the von Mises yield function, n and μ are material parameters, and recalling that K is the isotropic hardening variable. The associated flow law, from Equation (2d) then becomes

$$\dot{\varepsilon}_{ij}^p = \frac{1}{2\mu} F^{\frac{n-1}{2}} (\sigma_{ij} - \Omega_{ij}) \qquad \text{for inelastic loading} \tag{6a}$$

and $\dot{\varepsilon}_{ij}^p = 0$ for elastic unloading (6b)

The conditions for inelastic loading and elastic unloading have been identified in [15]. It can be easily seen that (6a) and (2b) are equivalent. In both cases, the direction of the inelastic strain rate vector is coaxial with the current effective stress vector (see Figure 1). Robinson [15] has recognized the equivalence and pointed out that the existence of a flow potential is not strictly necessary for the development of the flow law represented by (6a); the flow law can simply be stated without reference to their derivability from a potential function, as done in models which do not include a yield surface or flow potential.

2.2 Kinetic Equations

The flow laws, Equations (2a) and (2b) can be squared to give respectively,

$$\lambda_1 = [D_2^p/J_2]^{1/2} \tag{7a}$$

$$\lambda_2 = [D_2^P/J_2']^{1/2} \tag{7b}$$

where D_2^P is the second invariant of the plastic strain rate, $D_2^P = (1/2) \dot{\varepsilon}_{ij}^P \dot{\varepsilon}_{ij}^P$, and J_2 and J_2' are the second invariants of the deviatoric stress and effective deviatoric stress, respectively,

$$J_2 = (1/2) S_{ij} S_{ij} \tag{8a}$$

$$J_2' = (1/2) (S_{ij} - \Omega_{ij})(S_{ij} - \Omega_{ij}) \tag{8b}$$

Fundamental to all "unified" viscoplastic formulations based on flow laws of the forms listed in Equations (2) is that inelastic deformations are governed by a functional relation between D_2^P and J_2 (or J_2') that could involve load history dependent variables. These variables are intended to represent properties of the inelastic state with respect to resistance to plastic flow, e.g. hardening and damage. Some functions that have been suggested are the following.

(a) $$D_2^P = D_o X^n \tag{9a}$$

(b) $$D_2^P = D_o \exp\left[-\left(\frac{1}{X}\right)^n\right] \tag{9b}$$

(c) $$D_2^P = D_o \left[\sinh(X)^m\right]^n \tag{9c}$$

where $X = 3J_2/K^2$, or $3J_2'/K^2$

and n, m, and D_o are constants. The inelastic strain rate components can then be obtained as a function of the stress by the use of Equation (2a) or (2b) and one of Equations (9). Expression (9b) has some advantage over (9a or c) in theories without a yield criterion in that the value of D_2^P is almost zero for some extended range of J_2 regardless of the value of n. In (9b), D_o is the limiting value of the inelastic strain rate in shear; (9a) and (9b) do not contain such a limit. These differences between the kinetic equations are illustrated in a normalized plot of log (D_2^P/D_o) vs X in Figure 2 for the case of n = 3 and m = 1.0. Experimental support for Equation (9b) is shown in Figure 3 which indicates that a limiting inelastic strain rate of 2×10^5 sec^{-1} occurs in 1100-aluminum [29]. On the other hand, the power law expression has

KINETIC RELATIONS
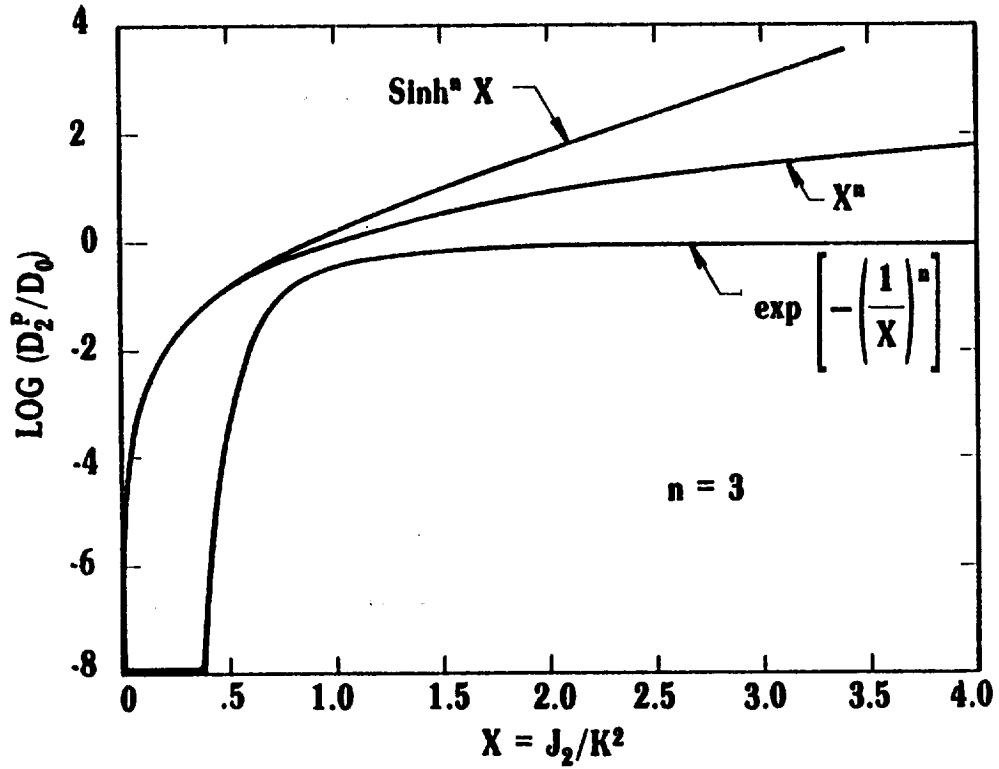
FIGURE 2. FUNCTIONAL BEHAVIOR OF THE KINETIC EQUATIONS USED IN THE UNIFIED CONSTITUTIVE THEORIES. The exponential formulation in Bodner-Partom's theory is seen to give a limiting inelastic strain rate of D_0.
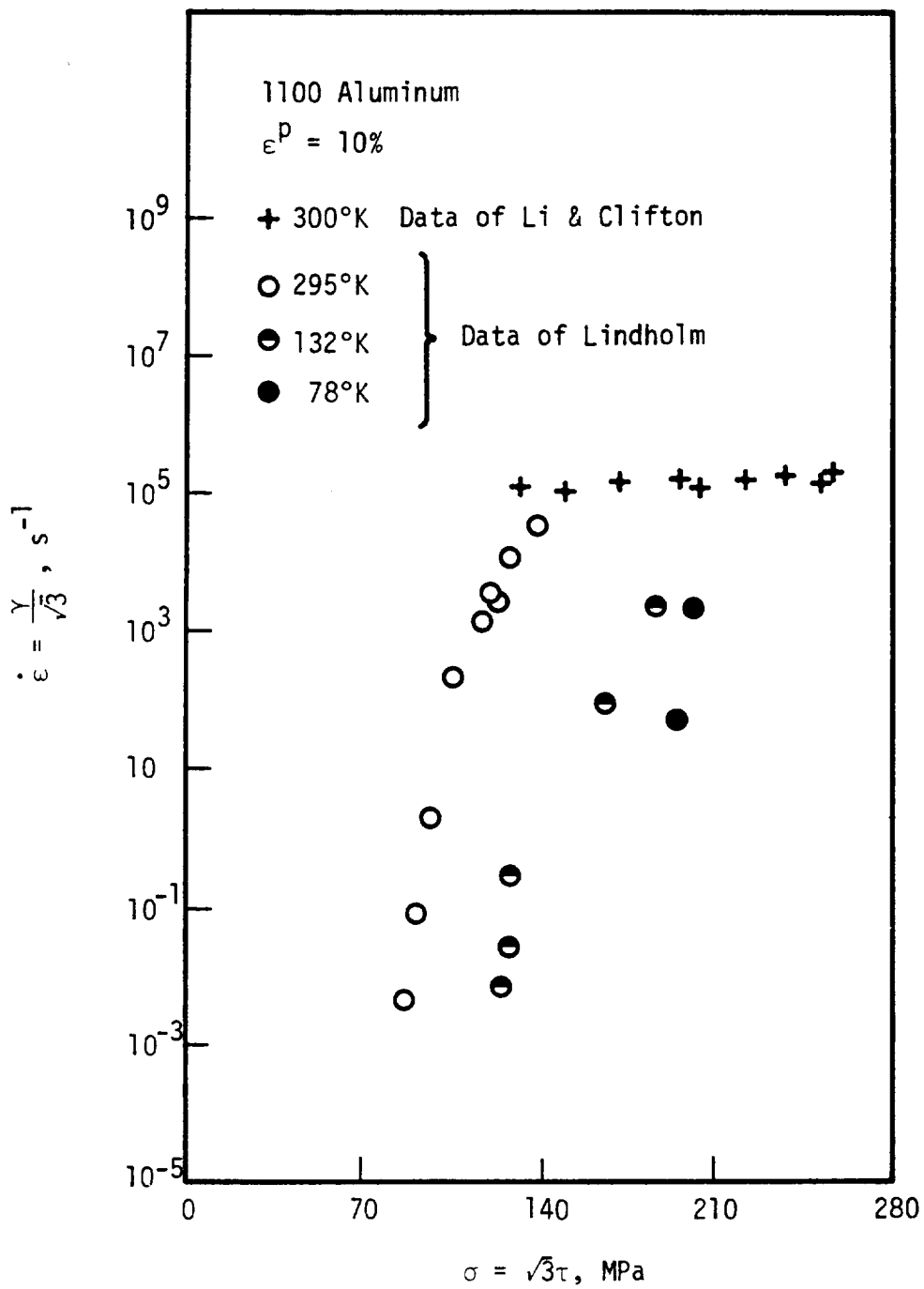
FIGURE 3.   STRAIN RATE AS A FUNCTION OF STRESS FOR 1100 ALUMINUM
            INDICATING A LIMITING STRAIN RATE OF 2×10^5 SEC^{-1},
            FROM [27]

been found to overpredict values of stress in a constant strain rate tensile test when the strain rates are greater than 10^{-2} sec^{-1} [13,30].

In all the preceding equations (9a,b,c) the exponent n influences the slope of the D_2, J_2 relation and therefore has the major influence on strain rate sensitivity. That parameter also affects the overall level of stress-strain curves although the level also depends on the hardening parameter K.

Temperature (T) dependence of plastic flow is a first order phenomenon comparable to strain rate sensitivity and should appear directly in the kinetic equation. In the case of Equations (9a,b), this can be achieved by taking the exponent n to be a function of T, e.g. n = c/kT (k is Boltzmann's constant and c a material constant) which leads to strong temperature dependence of the stress parameter $X=3J_2/K^2$ (or $3J_2'/K^2$). Numerical results for this dependence are shown in Figure 4 for both the power law and exponential kinetic equations at different non-dimensionalized strain rates. These trends appear to be consistent with experimental results shown in Figures 5 and 6 which are plotted in a similar manner.

The method of including temperature dependence in Equations (9) can be derived from an activation energy formulation. Table I lists temperature-dependent kinetic equations based on four different functional expressions for the activation energy. Some of the consequences of the various relations are discussed in [29].

Another procedure for including temperature dependence in the kinetic equations is to multiply the stress function, the right hand side of equations (9) by a temperature function. The temperature factor can again be motivated by thermal activation considerations and the Arrhenius expression seems to be the reasonable function to use at the higher temperatures. This is the approach taken in [10]. Additional discussion of temperature effects in the constitutive equations is given in a subsequent section.

2.3 Evolutionary Equations for Internal Variables

An important feature of the unified approach is the use of a set of discrete evolutionary equations to describe the change in hardening behavior of
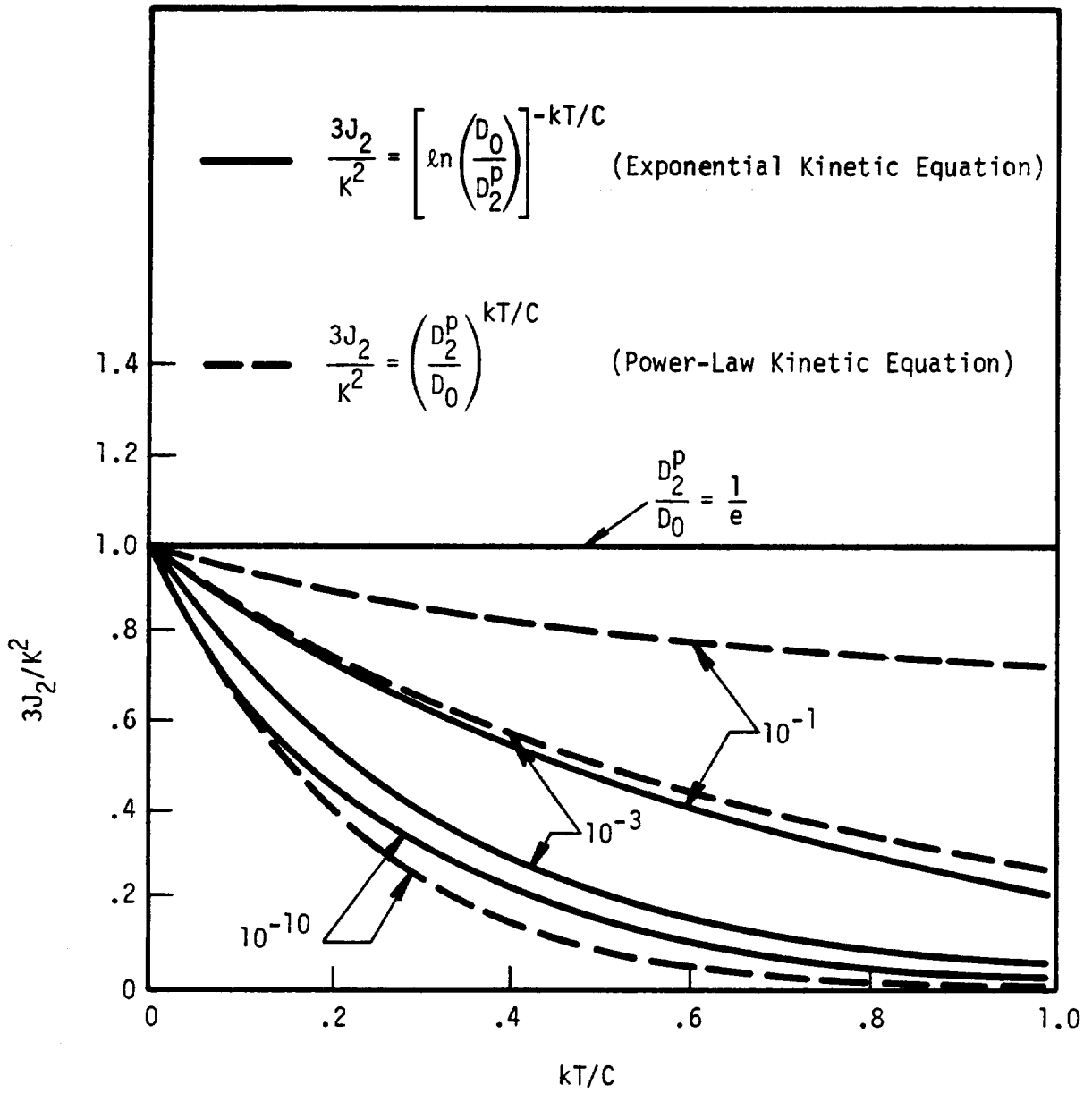
FIGURE 4. FUNCTIONAL BEHAVIOR OF TEMPERATURE-DEPENDENT KINETIC
EQUATIONS UTILIZED IN BODNER-PARTOM AND WALKER
THEORIES

A-15

FIGURE 6.   FLOW STRESS OF IRON AS A FUNCTION OF TEMPERATURE AT TWO STRAIN RATES, FROM [37]

FIGURE 5.   FLOW STRESS OF 1100 ALUMINUM AS A FUNCTION OF TEMPERATURE AT VARIOUS STRAIN RATES, FROM [27]

TABLE I

FIVE FORMS OF TEMPERATURE-DEPENDENT KINETIC EQUATIONS WITH
THE CORRESPONDING ACTIVATION ENERGY FUNCTION

Activation Energy	Temperature-Dependent Kinetic Equations
$\Delta H = C \ln\left(\dfrac{K^2}{3J_2}\right)$	$D_2^p = D_0\left[\dfrac{3J_2}{K^2}\right]^{C/kT}$
$\Delta H = H_0 - Vg(J_2)$	$D_2^p = D_0 \exp\left[-\dfrac{H_0 - Vg(J_2)}{kT}\right]$
$\Delta H = \dfrac{H*K^2}{3J_2}$	$D_2^p = D_0 \exp\left[-\dfrac{H*}{kT}\left(\dfrac{K^2}{3J_2}\right)\right]$
$\Delta H = kT\left[\dfrac{K^2}{3J_2}\right]^{C/kT}$	$D_2^p = D_0 \exp\left[-\left(\dfrac{K^2}{3J_2}\right)^{C/kT}\right]$
$\Delta H = Q$	$D_2^p = D_0 \exp\left[-\dfrac{Q}{kT}\right]\left[\sinh\left(\dfrac{3J_2}{K^2}\right)^m\right]^n$

where C, D_0, H*, H_0, Q, m, and n are constants; V is the activation
volume; and k is the Boltzmann's constant.

materials undergoing inelastic deformation. The same set of internal variables and evolutionary equations is used to govern all aspects of inelastic deformation including plastic flow, creep, and stress relaxation. The general framework of the evolutionary equations of internal variables is based on the now well-accepted Bailey-Orowan theory [31-32] which theorizes inelastic deformation to occur under the actions of two simultaneously competing mechanisms, a hardening process proceeding with accumulated deformation and a recovery or softening process proceeding with time. The evolution rate of an internal variable is then the difference between the hardening rate and the recovery rate as given by

$$\dot{X}_i = h_1(X_i)\,\dot{M}_1 - r_1(X_i, T) \tag{10}$$

where $\dot{X}_i$ is the evolution rate of the internal variable X_i, and h_1 and r_1 are the hardening and the thermal recovery functions, respectively. h_1 and r_1 are functions of X_i, temperature (T), and the hardening measure ($\dot{M}_1$) is either $\dot{\varepsilon}_{ij}^P$ or $\dot{W}_P$ depending on the model. A summary of the hardening measures utilized in the various unified theories is shown in Table II.

(1.) <u>Isotropic Hardening</u>

The quantity K in Equation (9) is usually interpreted as the isotropic hardening internal variable and is often referred to as the drag stress. Evolutionary equations for the isotropic hardening parameter generally follow the hardening/recovery format shown in Equation (10). A comparison of these hardening and recovery functions in various unified theories is shown in Table III. The rate of isotropic hardening is usually given by a function of the hardening variable K, which may saturate to a limiting value, shown as K_1 in Table III, multiplied by a measure of the hardening rate. Both the inelastic work rate and the effective inelastic strain rate have been proposed as the scaler hardening measure. At present, it is not obvious which hardening measure leads to better overall agreement with experiments. A recent proposal is to take the measure to be a functional of the strain rate history [33]. On the other hand, the rate of softening or recovery is often taken to be a power function of K and a temperature-dependent constant K_o which value represents the reference state for that particular temperature.

A-18

TABLE II

THE CHOICE OF INTERNAL VARIABLES AND MEASURES OF
HARDENING IN SELECTED UNIFIED CONSTITUTIVE THEORIES

MODEL	INTERNAL VARIABLES	MEASURE ($\dot{M}_1$)
BODNER & PARTOM	Z^I, Z^D	$\dot{W}_P$
WALKER	K, Ω	$\dot{\varepsilon}^P$
KRIEG ET AL	K, Ω	$\dot{\varepsilon}^P$
ROBINSON	Y, Ω	$\dot{\varepsilon}^P$
CHABOCHE	Y, Ω	$\dot{\varepsilon}^P$
LEE & ZAVERL	Y, Ω	$\dot{\varepsilon}^P$
HART	Ω_1, Ω_2	$\dot{\varepsilon}^P$
GHOSH	g	$\dot{\varepsilon}^P$
MILLER	$K_1, K_2, \Omega_1, \Omega_2, F_{sol_1}, F_{sol_2}$	$\dot{\varepsilon}^P$

TABLE III

THE SPECIFIC FORMS OF ISOTROPIC HARDENING AND STATIC THERMAL RECOVERY FUNCTIONS USED IN THE SELECTED UNIFIED CONSTITUTIVE THEORIES

$$\dot{K} = h_1(K)\dot{M}_1 - r_1(T,K)$$

$$\text{where} \quad \dot{M}_1 = \dot{\bar{\epsilon}}; \quad \dot{\bar{\epsilon}} = \sqrt{\frac{2}{3} \dot{\epsilon}_{ij}^p \dot{\epsilon}_{ij}^p}$$

$$\text{or} \quad \dot{M}_1 = \dot{W}_p \quad \text{(Bodner-Partom's Theory)}$$

Model	Hardening Function, $h_1(K)$	Static Thermal Recovery Function, $r_1(T,K)$
Bodner-Partom	$C_1(K_1 - K)$	$C_2(K - K_0)^p$
Walker	$C_1(K_1 - K)$	-
Krieg et al	C_1	$C_2(K - K_0)^p$
Robinson	C_1	-
Chaboche	$C_1(K_1 - K) + f_1(\bar{\epsilon}, \dot{\bar{\epsilon}}, \Omega_{ij})$	-
Lee and Zaverl	$C_1(K_1^* - K)/\sqrt{J_2}$	-
Hart	-	-
Ghosh	$C_1 K^{-q}$	$C_2(K - K_0)^p$
Miller	$C_1[K_1 - C_4(\sinh^{-1} C_3|\dot{\bar{\epsilon}}|)^q K^m]$	$C_2[\sinh C_3 K^m]^p$

where C_1, C_2, C_3, C_4, C_5, m, p, q, K_0, and K_1 are material constants; K_1^* is the saturated value of K; K_1^* is governed by an evolutionary equation which is function of $\dot{\bar{\epsilon}}$ and J_2.

This recovery model, sometimes credited to Friedel [34], theorizes that recovery occurs only when the current internal state exceeds the reference state.

(2.) Directional or Kinematic Hardening

Probably the main difference in the various unified theories is the treatment of directional or kinematic hardening. Differences exist not only in the choice of the flow law but also in the evolutionary equations. The general framework of these evolutionary equations follows the hardening/recovery formulation represented in Equation (10) with indexes to indicate the directions of hardening and recovery.

$$\dot{\Omega}_{ij} = h_2 \, (\Omega_{ij})\dot{M}_{ij} - d(\Omega_{ij}, \, T)\dot{N}_{ij} - r_2(\Omega_{ij}, \tau)V_{ij} + \Theta(\Omega_{ij}, T)\dot{T} \, W_{ij} \qquad (11)$$

where h_2, d, and r_2 are the hardening, "dynamic recovery", and static thermal recovery functions, respectively. Θ represents hardening and/or recovery associated with the rate of temperature change. $\dot{M}_{ij}$, $\dot{N}_{ij}$, V_{ij} and W_{ij} are the directional indexes of h_2, d, r_2, and Θ, respectively. The main differences among the various theories, as summarized in Table IV, are in the choices of the directional index and the hardening and recovery functions.

As indicated in Table IV, unified models based on the equilibrium stress utilize the inelastic strain rate as the directional index for hardening and contain a "dynamic recovery" term in the hardening function. The proposed hardening rule is thus similar to the Prager rule [26] in conventional plasticity which requires the translation of a yield surface to occur in the direction of the plastic strain increment. On the other hand, the evolutionary equation proposed in conjunction with Equation (2a) is based on the direct stress as the index for directional hardening [8,9]. This formulation avoids the cross-softening effect associated with inelastic strain rate as the index and the theory is more compatible with Ziegler's modification [35] of the Prager hardening rule.

The directional index for "dynamic recovery" is generally in the opposite direction of the directional hardening variable Ω_{ij}. The "dynamic recovery" term is treated in [7-9] as a saturation term in the direction of the direct stress but the index has recently been modified to be in the direction of $- \Omega_{ij}$ also [36].

TABLE IV

THE SPECIFIC FUNCTIONS OF ANISOTROPIC HARDENING, DYNAMIC RECOVERY, STATIC THERMAL RECOVERY, AND THE TEMPERATURE RATE TERM IN SELECTED UNIFIED CONSTITUTIVE THEORIES

$$\dot{\Omega}_{ij} = h_2(u_{ij})\dot{H}_{ij} - d(\Omega_{ij}, T)\dot{H}_{ij} - r_2(u_{ij}, T)v_{ij} + \dot{\sigma}(u_{ij}, T)Tw_{ij}$$

where: $v_{ij} = u_{ij}/[I_2]^{1/2}$, $I_2 = B/2 \; \Omega_{k\ell}\Omega_{k\ell}$ (except Walker, $v_{ij} = g_{ij}$)

$$g_{ij} = \Omega_{ij} - \dot{\Omega}_{ij} - n_1 i_{ij}$$

Model	Hardening Function, h_2	$\dot{H}_{ij}$	Dynamic Recovery Function, d	$\dot{H}_{ij}$	Static Thermal Recovery Function, r_2	Temperature Rate Function, Θ	w_{ij}
Bodner-Partom	$n_1 n_2$	$\dot{w}_p u_{ij}$	$n_1[I_2]^{1/2}$	$\dot{w}_p v_{ij}$	$n_3 I_2^s$	-	-
Walker	$n_1 + n_2$	$\dot{i}_{ij}$	f_1	$\dot{\epsilon}g_{ij}$	$n_6 I_2^s$	$\frac{\partial n_1}{\partial T}, \frac{1}{n_2}\frac{\partial n_2}{\partial T}$	ϵ_{ij}, g_{ij}
Krieg et al	$n_1 + n_2\exp[-f_0/n_2]$	$\dot{\epsilon}_{ij}$	-	-	$n_3 I_2^s$	-	-
Robinson	$n_1 I_2^{-s}$	$\dot{\epsilon}_{ij}$	-	-	$n_2 I_2^b$	-	-
Chaboche	$n_1 n_2 f_2$	$\dot{\epsilon}_{ij}$	$n_2 f_2$	$\dot{\epsilon}\Omega_{ij}$	$n_3 n_2 I_2^s$	f_3	Ω_{ij}
Lee and Zaverl	$1.5n_1[J_2^{\cdot}]^{-1/2}$	$\dot{\epsilon}\Omega_{ij}^{\ast}$	$1.5n_1[J_2^{\cdot}]^{-1/2}$	$\dot{\epsilon}\Omega_{ij}$	$n_2 n_3\left(\frac{\sigma_1^{\ast}}{\mu}\right)^b\left[\log\left(\frac{\sigma_1^{\ast}}{\sqrt{J_2}}\right)\right]^{-s}$	-	-
Hart	n_1	$\dot{\epsilon}_{ij}$	-	-	-	-	-
Ghosh	-	-	-	-	-	-	-
Miller	n_1	$\dot{\epsilon}_{ij}$	n_2/f_4	$\dot{\epsilon}\Omega_{ij}$	$n_3[\sinh n_4\sqrt{I_2}]^s$	-	-

where: $f_0 = (\sigma_{ij} - \Omega_{ij})\Omega_{ij}$

$f_1 = n_3 + n_4\exp(-n_5\bar{\epsilon})$

$J_2^{\cdot} = 1/2(s_{ij} - \Omega_{ij})(s_{ij} - \Omega_{ij})$

$f_2 = n_4 + (1 - n_4)\exp(-n_5\bar{\epsilon})$

$B = 1, 2, \text{ or } 4/3, \text{ depending on the model}$

$f_3 = \frac{1}{n_2}\frac{\partial n_2}{\partial T} + \frac{1}{n_1}\frac{\partial n_1}{\partial T} + \frac{1}{f_2}\frac{\partial f_2}{\partial T}$

$n_1, n_2, n_3, n_4, n_5, n_6, b, \text{ and } s \text{ are material constants.}$

$\Omega_{ij}^{\ast}$ are the saturated values of $\Omega_{ij}; \dot{\Omega}_{ij}^{\ast}$ are governed by evolutionary equations which are functions of $\bar{\epsilon}$ and $J_2^{\cdot}$.

$f_4 = \sinh^{-1}(n_5\bar{\epsilon})^b$

The unit vector which represents the direction cosines of the directional hardening variable is usually taken to be the directional index for static thermal recovery. Recovery always occurs in the opposite direction of the unit vector and tends to reduce the magnitude of the directional (kinematic) hardening variable. Most unified theories utilize Friedel's recovery model and take zero magnitude of Ω_{ij} as the reference state. Table IV shows that a temperature rate term is also included in the theories of Walker and Chaboche. In principle, similar terms could be added to the other theories.

The various hardening terms in the evolution equation of the directional hardening variable have profound effects on the shape of the cyclic hysteresis loops. Unified models which contain at least two hardening terms to describe the evolution of the equilibrium stress with strain history include that of Walker [6], Hart and co-workers [17], and Miller [12]. The contribution to the equilibrium stress from each of the four hardening terms used in the Walker theory may be seen in Figure 7. The term Ω_{ij}^o describes the difference between the tensile and compressive behavior of the equilibrium stress variable, and this difference gives a stress-strain response which differs in tension and compression. The linear term $n_1 \dot{e}_{ij}^p$ allows the asymptotic stress-strain response to exhibit a linear behavior at large strain values. The integral term containing n_2 allows the equilibrium stress to grow and saturate rapidly when cycling under small strain amplitudes, while the integral term containing n_8 gives a more gradual growth of the internal variable. These two integral terms allow the cyclic hysteresis behavior to be reproduced for both small and large strain amplitude loading conditions.

2.4   Temperature Dependence of Inelastic Flow

Temperature effects are taken into account in most unified models by assuming the material constants in the kinetic equation and the evolutionary equations of the internal variables to be temperature dependent. Lindholm and Bodner [29] recently examined this issue and made an attempt to model temperature dependence of inelastic flow by incorporating a reaction rate theory into Orowan's kinetic relation. By assuming appropriate functions for the activation energy, Lindholm and Bodner were able to obtain four different formulations of temperature-dependent kinetic relations. These kinetics relations and the corresponding activation energy are rewritten in terms of deviatoric

$$n_1 \epsilon^P + n_2 \int_0^t e^{-[G_1(t) - G_1(\xi)]} \frac{\partial \epsilon^P}{\partial \xi} d\xi + n_8 \int_0^t e^{-[G_2(t) - G_2(\xi)]} \frac{\partial \epsilon^P}{\partial \xi} d\zeta$$

$\sigma = \Omega + K \dot{\epsilon}^{P \; 1/n}$

$$\Omega = \overset{\circ}{\Omega} + n_1 \epsilon^P + n_2 \int_0^t e^{-[G_1(t) - G_1(\xi)]} \frac{\partial \epsilon^P}{\partial \xi} d\xi + n_8 \int_0^t e^{-[G_2(t) - G_2(\xi)]} \frac{\partial \epsilon^P}{\partial \xi}$$

$$n_8 \int_0^t e^{-[G_2(t) - G_2(\xi)]} \frac{\partial \epsilon^P}{\partial \xi} d\xi$$

$$n_2 \int_0^t e^{-[G_1(t) - G_1(\xi)]} \frac{\partial \epsilon^P}{\partial \xi} d\xi$$

$n_1 \epsilon^P$

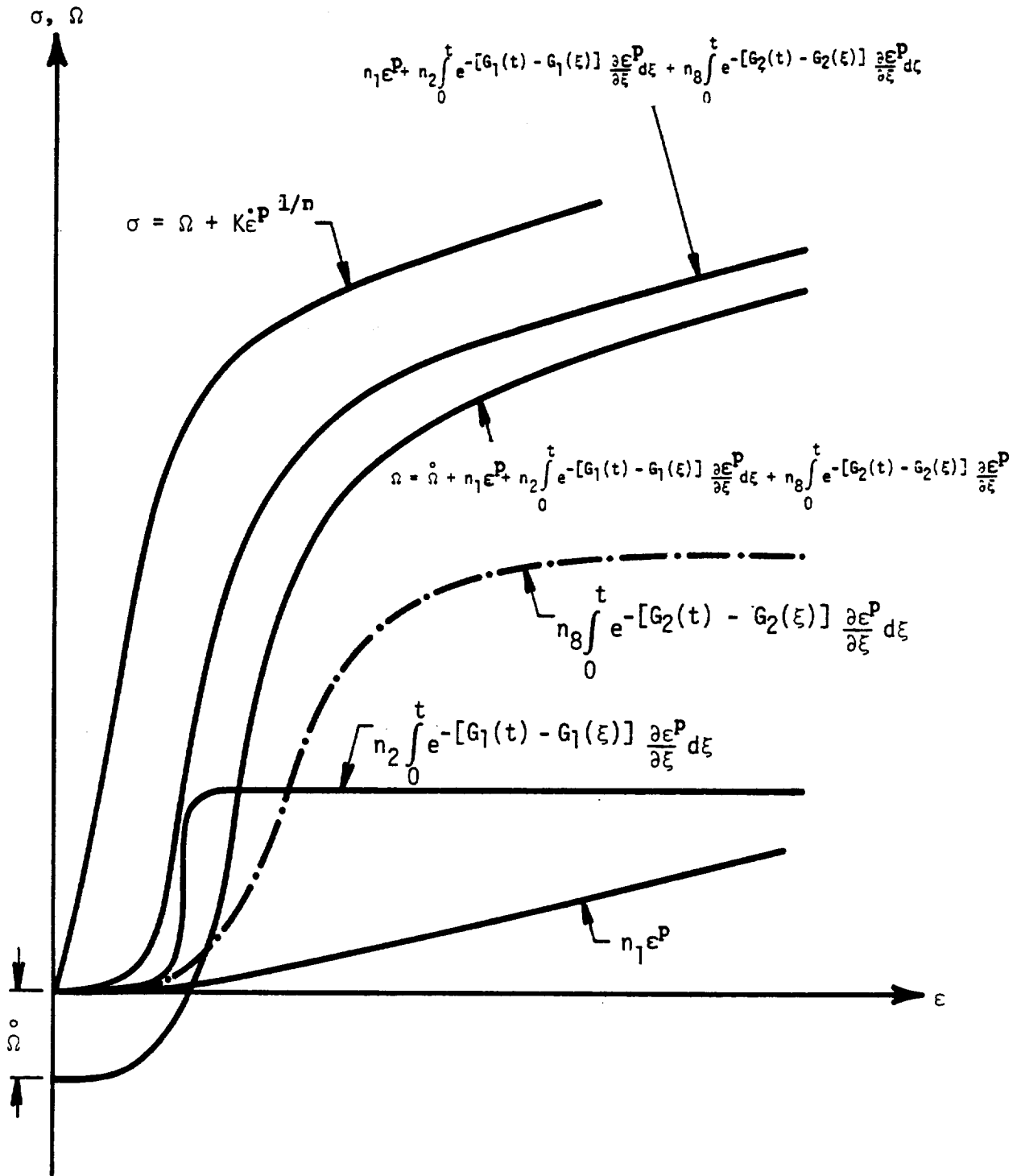σ, Ω

ϵ

$\overset{\circ}{\Omega}$

FIGURE 7.   CONTRIBUTIONS OF EQUILIBRIUM STRESS TERMS TO THE
STRESS-STRAIN BEHAVIOR IN WALKER'S MODEL

invariants, summarized in Table I. Figure 4 demonstrates the similarities between the functional behavior of the first and fourth formulations which correspond to the kinetic relation utilized in the Walker and Bodner models, respectively. Experimental evidence in Figures 5 and 6 for aluminum [29] and iron [37], respectively, tend to indicate both formulations are adequate and justified.

Another approach for incorporating temperature dependence into a unified theory is taken by Miller [10]. Temperature dependence of inelastic flow is modeled on the basis of creep phenomenology and an Arrhenius expression is modified to reflect the temperature dependence of the activation energy for diffusion (or creep). To cover a wide range of temperature, both lattice diffusion and pipe diffusion have been considered. The resulting Arrhenius expression which is also shown in Table I is included in both the kinetic relation and the recovery term of the evolutionary equations. With the exception of the elastic constants, material constants in Miller's model are independent of temperature. There are, however, indications that the model would yield better results for thermomechanical loading if some of the material constants are allowed to change with temperature [6].

Walker and his co-workers at Pratt & Whitney Aircraft have compared the predictive capabilities of three unified models for applications under thermomechanical cycling conditions. Their experience with the unified models to date indicates that all the material constants in the formulations would depend on temperature and must be evaluated at a number of base temperatures. Suitable interpolation methods must be developed for evaluating the values of these material constants at other temperatures. The predicted results would therefore depend on the interpolation method [6].

The temperature dependence of the internal variables is also important. Comparisons of experimental and theoretical results on thermomechancial constitutive behavior of Hastelloy-X in Reference 6 indicate that the shape of the predicted thermomechanical loop depends critically on the growth of the equilibrium stress with temperature. Most thermomechanical loops are necessarily of small strain amplitude. Hence, at the points of strain reversal, the equilibrium stress is in the initial growth phase and is changing rapidly with strain. Depending on the rapidity with which the equilibrium stress

grows with inelastic strain after a strain reversal, the equilibrium stress may be in the process of almost saturating at the next strain reversal. This can change the predicted shape of the thermomechanical stress-strain hysteresis loop quite dramatically.

2.5 Uniqueness and Stability Criteria

All the proposed kinetic and evolutionary equations of the internal variables are based on a combination of phenomenology and physical mechanisms. There are certain continuum properties which are required of these constitutive relationships in order to ensure that the resulting boundary value problems are well-posed. The required properties are the uniqueness and the stability of the solution. For stability, unified theories with internal variables must, according to Ponter [38], obey the following inequality:

$$d\sigma_{ij} \, d\dot{\varepsilon}_{ij}^{P} - dX_i \, d\dot{X}_i \geq 0 \qquad (12)$$

where $d\sigma_{ij}$, $d\dot{\varepsilon}_{ij}^{P}$, dX_i, and $d\dot{X}_i$ represent incremental changes in stress, inelastic strain rate, the current value and the evolution rate of the internal variables. The inequality admits classical plastic flow, creep, and stress relaxation behavior. It also admits recovery phenomena involving negative inelastic work provided that the corresponding changes in the internal variables are sufficiently large to make the inequality in Equation (12) remain valid. The basic requirement of Equation (12) is that the dissipation rate must be nonnegative.

For a constant internal state, a small change in σ_{ij} results in a corresponding change in $\dot{\varepsilon}_{ij}^{P}$ so that [38]

$$d\sigma_{ij} \, d\dot{\varepsilon}_{ij}^{P} \geq 0 \qquad , \qquad \dot{X}_i = 0 \qquad (13)$$

The inelastic work inequality which is identical to Drucker's postulate [39] in classical plasticity requires that for a stable material flow the plastic work done must be nonnegative. For proportional loading the kinetic equations represented in Equation (9a) to Equation (9c) all yield convex flow potentials to which the inelastic strain rate vectors are normal. The consequence

is that the inelastic work is always positive, and unified theories based on Equation (9a) to (9c) obey the inelastic work inequality.

For loading involving constant σ_{ij} as in creep, the inequality in Equation (12) requires that a small change in dX_i produces a change in the evolution rate such that

$$- dX_i \; d\dot{X}_i \; \geqslant \; 0 \qquad , \quad d\sigma_{ij} \; = \; 0 \qquad\qquad (14)$$

It is clear that both Equation (13) and (14) would be obeyed by any constitutive model if these two conditions are satisfied:

(1) An increase in strain rate ($d\dot{\varepsilon}_{ij}^{p} \geqslant 0$) results in an increase in flow stress ($d\sigma_{ij} \geqslant 0$) or vice versa; and

(2) An increase in the value of an internal variable ($dX_i \geqslant 0$) results in a decrease in the evolution rate ($d\dot{X}_i \leqslant 0$) or vice versa.

Some of the ramifications of Drucker's inequality in classical rate independent plasticity are that the stress-strain curve must have a positive slope for stable flow and strain must be a single-valued function of stress for uniqueness. Ponter's inequality exerts similar ramifications on visco-plastic unified theories. For uniqueness, it appears that the inelastic strain rate must be a single-valued function of stress and internal variables. To satisfy the requirement for stable flow, Equation (12) dictates that stress-strain curves at constant strain rate must have positive slope but must decrease with increasing strain. On the other hand, stress-strain curves at constant value of plastic strain or plastic work must have positive slope, but the slope may either increase or decrease with increasing strain rate [38].

Most (if not all) of the unified theories listed in Table II satisfy the Ponter inequalities and meet the uniqueness and stability requirements. The stability requirement is, however, not essential for constitutive theory developments. Unified theories admit unstable inelastic flow and are generally modeled by including softening mechanisms such as thermal softening and continuum damage in the evolution and/or kinetic equations. Negative strain rate sensitivity and strain (or work) softening phenomena have also been modeled [11,12].

2.6   Constitutive Behavior Under Nonproportional Loading

Cyclic constitutive behavior of materials subjected to nonproportional loading conditions is still poorly understood. Recent studies on Hastelloy-X [36], copper [40], 1% Cr-Mo-V steel [41], and 316 stainless steel [42] all indicate that these materials exhibit considerably more cyclic hardening when tested under nonproportional paths of combined tension and torsion than under proportional paths of tension or torsion only. A comparison of the hardening behavior of Hastelloy-X alloy subjected to tension, torsion, and combined, nonproportional tension-torsion loading is shown in Figure 8 [36]. In this plot of effective stress vs cumulative effective plastic strain, where the effective stress and strain are computed based on the von Mises criterion, and the cumulative effective plastic strain is number of cycles times the effective plastic strain range per cycle, an apparent increase of hardening is observed in the case for 90° out-of-phase loading. This apparent hardening can arise from three different sources: (1) nonproportional loading induces additional hardening; (2) the von Mises criterion is not appropriate for this material; and (3) testing was not done at the same "effective" strain levels. Efforts to delineate the relative contribution of these factors indicate the first factor to be important. As a result, all of the constitutive models need to be modified to take into account the hardening behavior due to out-of-phase loading.

Another question concerning the nonproportional, multiaxial deformation is whether or not the inelastic strain rate vector is coaxial with the deviatoric stress vector under nonproportional loading paths. The works of Ohashi and co-workers [43-45], and Meguid [46] indicate that the deviatoric stress and the inelastic strain rate vectors become noncoaxial just after an abrupt change of deformation path but become coaxial again as inelastic deformation develops along the subsequent path. Current work by the authors on 90° out-of-phase cyclic loading of Hastelloy-X under combined tension and torsion indicates that the inelastic strain rate vector leads the deviatoric stress vector by an angle which ranges from 10 to 40 degrees [36]. These findings tend to suggest that, as a result of the apparent noncoaxiality, the isotropic Prandtl-Reuss flow laws might not be adequate for nonproportional loading

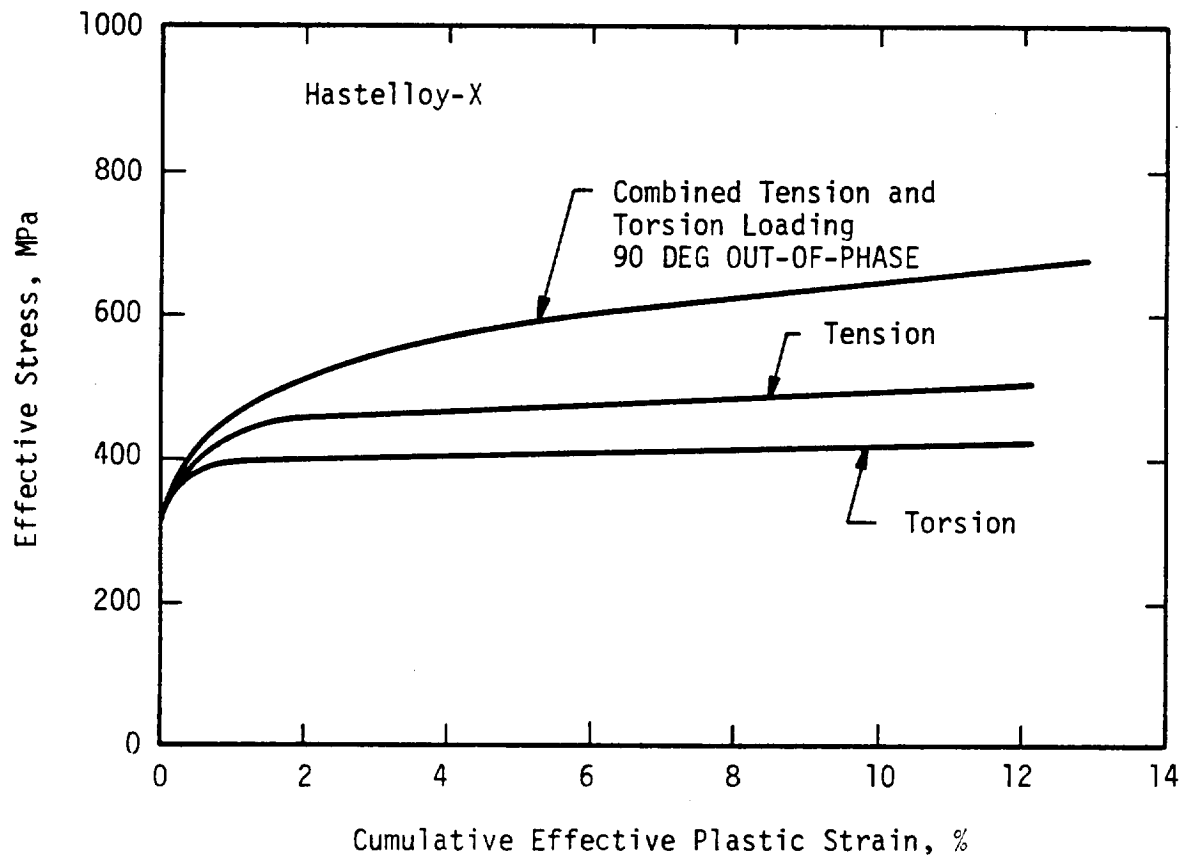FIGURE 8. A COMPARISON OF THE EFFECTIVE STRESS-CUMULATIVE EFFECTIVE STRAIN BEHAVIOR OF HASTELLOY-X UNDER TENSION, TORSION, AND COMBINED, NONPROPORTIONAL TENSION AND TORSION LOADINGS

paths. On the other hand, the noncoaxiality between inelastic strain rate and deviatoric stress can be accounted for by using either a generalized anisotropic Prandtl-Reuss flow law or a flow law based on an "equilibrium stress."

3.0 REVIEW OF NUMERICAL METHODS FOR INTEGRATING UNIFIED CONSTITUTIVE EQUATIONS

3.1 Numerical Integration Techniques

A literature review indicated that no systematic studies which compare the integrability of unified constitutive equations have been performed. The evaluations that have been done support the existing consensus that this family of differential equations can be characterized as mathematically "stiff." That is, in these equations, dependent variables are susceptible to large changes from small increments of the independent variables or from small time steps. This "stiff" behavior occurs usually with the onset of a significant amount of inelastic strain in the loading cycle and is due to the generally nonlinear nature of the functional forms that are employed in the kinetic equations of these theories.

Probably of greater importance than differences in stiffness of individual constitutive theories are the methods used to integrate them. A systematic comparison of a variety of approaches has been reported by Kumar, Morjaria, and Mukherjee [47]. Specifically, they compared simple Euler forward method, two-step Adam's method, predictor-corrector method, and the Gear method. This study concluded that for the constitutive theory of Hart, a relatively simple Euler integration method, together with a time step control strategy, was optimal when compared with the more sophisticated methods. Similar conclusions were obtained by Krieg [48] who rearranged various unified constitutive theories into a skeletal model to illustrate the numerical difficulties in the integration of constitutive equations and to discuss the viability of various integrators.

Tanaka and Miller recently developed a noniterative, self-correcting solution (NONSS) method for integrating stiff time-dependent constitutive equations [49]. The NONSS method is basically an extension of the α-method which is used in creep and heat transfer analysis [50]. In this approach, the stress, inelastic rate, and evolutionary rate of the internal variables at $t+\alpha\Delta t$ are expressed as:

$$\sigma(t+\alpha\Delta t) = (1-\alpha)\sigma(t) + \alpha\sigma(t+\Delta t)$$

$$\dot{\varepsilon}(t+\alpha\Delta t) = (1-\alpha)\dot{\varepsilon}(t) + \alpha\dot{\varepsilon}(t+\Delta t) \tag{15}$$

$$\dot{X}_i(t+\alpha\Delta t) = (1-\alpha)\dot{X}_i(t) + \alpha\dot{X}_i(t+\Delta t)$$

with $0 \leqslant \alpha \leqslant 1$. The method reduces to the Euler forward difference method when $\alpha = 0$ and is an implicit technique when $\alpha > 0$, because the unknown quantities $\sigma(t+\Delta t)$, $\dot{\varepsilon}(t+\Delta t)$, and $\dot{X}_i(t+\Delta t)$ enter into the solution. Implicit quantities are removed in the NONSS method by Taylor expansions of σ, $\dot{\varepsilon}$, and $\dot{X}_i$. The method is unconditionally stable for $\alpha \geqslant 1/2$ and noniterative, but requires setting up of a Jacobian matrix and solving a set of linear equations at each time-step. Accuracy is maintained through self-adaptive time control and by correcting previous errors at the current step. This method has been used in one-element applications only. The applicability of this approach to finite-element analysis remains to be seen.

At Pratt and Whitney Aircraft and at the United Technologies Research Center, work has been done using the Euler single step approach usually without automatic time step control, but rather by determining an optimum step size for each problem experimentally. Efficiency obtained by using this approach has been acceptable and has shown considerable improvement over more sophisticated approaches such as higher order Runge-Kutta methods.

One way of incorporating a self-adaptive time control technique into the integration procedure is by expressing the inelastic strain at time $t+\Delta t$ in a Taylor series and ensuring that the higher order terms are small in comparison to the first order term. For example, the inelastic strain at time $t+\Delta t$ may be written in the Taylor series

$$\dot{\varepsilon}(t+\Delta t) = \dot{\varepsilon}(t) + \ddot{\varepsilon}\,\Delta t + 1/2\,\dddot{\varepsilon}\,(\Delta t)^2 +\ldots \tag{16}$$

The time step Δt can then be chosen so that the third term in the series is some small fraction, γ say, of the second term in the series. In this way one obtains

$$\Delta t = \frac{2\gamma|\dot{\varepsilon}|}{|\ddot{\varepsilon}|} \tag{17}$$

where $|\dot{\varepsilon}|$ and $|\ddot{\varepsilon}|$ are the magnitude of the maximum components of $\dot{\varepsilon}$ and $\ddot{\varepsilon}$, respectively.

A-32

Alternatively, implicit methods can be used. An implicit method for use with an integral constitutive formulation was outlined in Reference 6 and the technique gave good results.

A summary of these various numerical techniques and their applications to several unified theories as well as to Norton's law for integrating a uniaxial stress-strain curve to a total strain of 1-2% is shown in Table V. As illustrated in Table V, the explicit Euler method is stable when the size of the strain increment is kept below 10^{-4}. The size of the strain increment can be increased by using an implicit method such as the NONSS or α-method with $\alpha = 1$ (implicit Euler). By restricting the comparison to the explicit methods only, it appears that there is no substantial difference between the integrability of Walker [6,51] and Miller [52] theories nor between these unified theories and the classical Norton law [52]. The size of the strain increment is, however, somewhat sensitive to the values of model constants which describe material strain rate sensitivity.

3.2 Integration of Unified Theories in Finite Element Analysis

The question of which integration method to use for integrating unified theories in finite element analysis appears to be code and problem dependent. For example, the MARC code solves the finite element equilibrium equations by a Picard, or successive substitution, method. The finite element equilibrium equations may be written in the form

$$\Sigma \int_V B^T \sigma(u) dV = P \tag{18}$$

P being the applied load sector and $\sigma(u)$ being the corresponding stresses due to the nodal displacement u.

The MARC program solves the incremental form of equation, viz.

$$\left(\Sigma \int_V B^T D B dV \right) \Delta u_{i+1} = \Delta P - \Sigma \int_V B^T \Delta \zeta (\Delta u_i) dV, \tag{19}$$

where $\Delta \zeta$ is the inelastic stress increment in the relation

$$\Delta \sigma = D \Delta \varepsilon + \Delta \zeta \ , \tag{20}$$

A-33

TABLE V

COMPARISONS OF THE INTEGRATABILITY OF VARIOUS CONSTITUTIVE MODELS

Comparison is based on the size of the average strain increment per step for integrating a uniaxial tensile stress-strain curve to a total strain of 1-2%

Constitutive Model	Integration Method	Strain Increment Per Step	Automatic Time or Strain Increment Control	Stability	Reference
Walker	Explicit Euler	10^{-5} to 10^{-4}	No	Stable	Walker [6]; Cassenti [51]
Bodner-Parton	NONSS (α-Method)				Present Investigation
	$\alpha = .1$	1×10^{-4}	No	Stable	
	$\alpha = .5$	1×10^{-4}		Stable	
	$\alpha = 1$	1×10^{-3}		Stable	
Miller	Explicit Euler	4×10^{-4}	No	Unstable	Lee et al [52]
	Tayler Series Modified Euler	4×10^{-4}	No	Stable	Lee et al
	NONSS (α-Method, $\alpha = 1$)	3×10^{-3}*	Yes	Stable	Tanaka [49]
Hart	Explicit Euler	2×10^{-5}*	Yes	Stable	Kumar et al [47]
	Predictor-Corrector	3×10^{-5}*	Yes	Stable	Kumar et al
	High Order Predictor-Corrector	3×10^{-5}*	Yes	Stable	Kumar et al
	Two-Step Adam	2×10^{-5}*	Yes	Stable	Kumar et al
Norton	Explicit Euler	1×10^{-3}	No	Unstable	Lee et al [52]
	Tayler Series Modified Euler	5×10^{-4}	No	Stable	Lee et al
		1×10^{-3}	No	Stable	Lee et al

* Average strain increment per step = total strain/number of time steps.

and Δu_{i+1} are the nodal displacement increments in the (i+1) the interation. The load ΔP in Equation (19) represents the current load increment plus the out-of-equilibrium load from the previous increment.

For crack problems the preceding interation method can converge very slowly and very small finite element load steps must then be taken. The ABAQUS code solves the finite element equilibrium equations directly by a Newton-Raphson method, so that Equation (18) is solved in the form

$$\left(\Sigma \int_v B^T \left(\frac{\partial \sigma}{\partial \varepsilon} \right) Bdv \right) C_{i+1} = P - \Sigma \int_v B^T \sigma(u_i)dV \qquad (21)$$

where

$$u_{i+1} = u_i + C_{i+1}$$

and C_{i+1} is the (i+1) th interative correction to the total nodal displacement at the end of the increment. For crack problems small steps must still be taken, but now the convergence of the finite element equilibrium equations is quadratic, as opposed to the slow linear convergence of the successive substitution method.

To obtain the quadratic convergence it is necessary to evaluate the Jacobian matrix $\partial \sigma / \partial \varepsilon$. Since subincremental procedures are usually used to integrate the unified models over the finite element increment, the Jacobian matrix cannot be obtained analytically. It may be determined by perturbing each component of the strain increment tensor and obtaining $\partial \sigma / \partial \varepsilon$ numerically. It is then necessary to use the same number of subincrements in each of the perturbations so that $\partial \sigma / \partial \varepsilon$ is consistent and does not include contributions from changes in the number of subincrements. In this case it is better not to use a self adaptive integration procedure. A maximum strain increment of, say 10^{-4}, can be prescribed. The finite element strain increment can then be divided by 10^{-4} to obtain the number of subincrements in the step at the particular Gauss integration point. If instability is detected during the finite element load step, the integration can be repeated using triple the number of

subincrements until the stability criterion is met. This number of subincre-
ments is then used in each integration of the perturbed strain increment
tensor to obtain the Jacobian matrix $\partial\sigma/\partial\varepsilon$.

This procedure has been implemented in the ABAQUS code to solve crack
growth problems with a unified model [53]. Typically at the integration point
closest to the crack tip, as many as fifty subincrements may be required.
However, since the strain increments at integration points far removed from
the crack tip are small in comparison with those at the crack tip, only two
subincrements may be needed at most of the other integration points in the
structural model. Since small finite element increments are required to solve
crack problems, and only two or three subincrements are required at most of
the Gaussian integration points away from the crack tip vicinity, it may ac-
tually be computationally inefficient to use an implicit integration method
for the unified models for this class of structural problems.

3.3   Comparison of the Integrabilities of Unified and Classical Theories

In order to better understand the problem of efficient computing algo-
rithms for utilizing unified constitutive models, a summary of computing times
for typical non-linear finite element analyses has been compiled along with a
comparison with classical approaches for the same analysis cases. A summary
of this study is shown in Table VI. This table lists two small structural
models and some single element models which were performed at Pratt and
Whitney using the MARC non-linear finite element code. Each of the three
structural models shown in Table VI was run using two or more approaches for
modeling the material behavior as indicated. It should be noted that each of
the variations was run on a single computing system, but that analyses 2 and
3 were run on a computing system that was approximately 30% slower than for
the structural model used for analysis number 1, the Burner Liner Crack Anal-
ysis. Thus, any attempt to make comparisons between structural models may be
misleading. Aside from this limitation, it can be seen that experience to
date using the unified model of Walker has involved more computing time than
the classical approach using a time independent plasticity model and alternate
load increments using a time dependent creep model. Also shown in Table VI

TABLE VI

RUN TIME COMPARISONS FOR UNIFIED CONSTITUTIVE MODEL APPLICATIONS

1. Burner Liner Crack Analysis

   Problem Size: 50 elements, 181 nodes, 350 degrees of freedom, 40 load increments

	Method	Computing Time (Seconds)
a.	Classical plasticity/creep	365
b.	Integral form of Walker's theory	322
c.	Walker integral form with 2 subincrements	382
d.	Walker integral form with 5 subincrements	493

2. Hot Spot Blister Analysis

   Problem Size: 23 elements, 103 nodes, 198 degrees of freedom, 51 or 64 load increments

	Method	Computing Time (Seconds)
a.	Classical plasticity/creep (64 load increments)	444
b.	Differential form of Walker's model (51 load increments)	614

3. Uniaxial Analysis

   Problem Size: 1 elements, 8 nodes, 12 degrees of freedom, 35 or 48 load increments

	Method	Computing Time (Seconds)
a.	Elastic Analysis (35 load increments)	14
b.	Classical plasticity/creep (35 load increments)	18
c.	Walker's theory, integral form (48 load increments)	32
d.	Walker's theory, integral form (48 load increments with 5 subincrements per load step)	48

are comparisons of computing time for variation of integration method for Walker's constitutive theory. These should not be regarded as a measure of efficiency in any absolute sense since no attempt was made to optimize the approaches used, but rather are intended to provide some indication of current experience for computing times and to provide an informal basis against which to judge the computing efficiency of the unified theories.

4.0 REVIEW OF SPECIFIC UNIFIED THEORIES

There are at least 12 viscoplastic constitutive theories which are based on the unified approach in the literature. These theories are reviewed individually as follows.

Other unified theories include that of Lee and Zaverl [20], Cernocky and Krempl [30], and Anand [59]. The model of Lee and Zaverl is a generalized anisotropic theory based on a yield surface concept. This model and that proposed by Cernocky and Krempl have recently been reviewed by Walker [6]. Anand's model is in uniaxial form with isotropic hardening only, and its formulation is very similar to Bodner and Partom's theory.

4.1 Robinson's Theory

Robinson's model [15] is based on a flow potential from which the flow law and the growth laws of the internal variables are derived. For stress states inside the flow potential, the material is elastic, while for stress states on the flow potential, the material response is viscoplastic. Different forms of flow and growth laws are derived for loading and unloading, together with inequalities defining boundaries across which the flow and evolutionary equations change form discontinuously. The model employs an equilibrium stress internal variable Ω_{ij} and a drag stress internal variable K to represent kinematic and isotropic hardening, respectively. The use of different growth laws allows the equilibrium stress to grow rapidly with inelastic strain just after a stress or strain reversal, but to grow more slowly with inelastic strain at a large distance (in strain space) from the strain or stress reversal. As a result, the model can reproduce rounded, cyclic hysteresis loops for both large and small strain amplitudes without employing two hardening terms in the equilibrium stress evolutionary equations.

The model contains eight temperature-independent and four temperature-dependent material constants. The model has been used for predicting material behavior under monotonic, cyclic, creep, stress relaxation, and nonisothermal cycling loading conditions. [53].

4.2 Walker's Functional Theory

This theory was developed by modifying the constitutive relation for a three-parameter viscoelastic solid. Two internal variables were introduced into the viscoelastic theory to account for the effects of viscoplasticity. The equilibrium stress Ω_{ij} represents nonlinear kinematic hardening and accounts for the Bauschinger effect, while the drag stress K represents isotropic hardening and accounts for cyclic hardening of the material. Both the integral and the differential forms of the theory are summarized in Reference 6.

The growth law for the equilibrium stress contains both dynamic recovery and static thermal recovery terms. At high strain rates, the thermal recovery term becomes insignificant in comparison with the dynamic recovery term, and the equilibrium stress becomes independent of strain rate. The equilibrium stress expression contains a temperature rate term, which allows the equilibrium stress to change during nonisothermal elastic excursions, and a Ω_{ij}^{o} term to account for asymmetric cyclic hysteresis behavior. Static thermal recovery terms have been omitted in the growth law for the drag stress. This form has been found adequate in the modeling of Hastelloy-X behavior [6], but future applications may require the inclusion of static thermal recovery in the drag stress evolution law.

The kinetic relation is formulated in terms of a power law in [6] and in terms of an exponential law in [53]. The power law expression has been found adequate for the representation of creep, stress relaxation, and strain rate effects encountered in a combustor liner material under service conditions where strain rates may vary from 10^{-6} sec^{-1} to 10^{-3} sec^{-1}. However, it appears that an exponential law is necessary if strain rates greater than about 10^{-2} sec^{-1} are encountered. In particular, at higher strain rates, the power law expression for the inelastic strain rate and predicts values of stress in a constant strain rate tensile test which are too large [13, 30].

The model contains 14 temperature-dependent material constants. The model has been applied successfully for predicting creep, stress relation, cyclic, and thermomechanical hysteresis behavior of Hastelloy-X alloy [6].

4.3 Chaboche's Theory

Chaboche's theory [14] is formulated on the basis of a yield surface. Inside the yield surface it is assumed that no inelastic deformation can take place. Different flow laws are thus required for loading and unloading. The use of a yield surface permits isotropic hardening to be modeled by an increase in the size of the yield surface rather than by an increase in the drag stress. Hence, in this theory, K is assumed to be constant. Initially, the isotropic variable Y is assumed to be zero and inelastic deformation occurs only when $3J_2'>K$, where K is a constant. As Y grows with inelastic deformation, the yield surface expands and inelastic deformation takes place only when $3J_2'>K+Y$. Yield surface translation occurs as the equilibrium stress changes with inelastic deformation. The growth law for the equilibrium stress contains a temperature rate term which allows the equilibrium stress to change with temperature during nonisothermal elastic excursions. The model contains 13 constants. All of the material constants are functions of temperature and must be experimentally determined at each temperature of interest.

4.4 Bodner and Partom's Theory

The elastic-viscoplastic theory of Bodner and Partom, (B-P), was probably the first "unified" set of constitutive equations without a yield criterion or loading/unloading conditions to be developed (described in the literature in 1968) [59]. Those equations include certain physical concepts provided by the work on dislocation dynamics during the 1950's and early 1960's. The equations are placed in the context of multi-dimensional continuum mechanics which makes them capable of solving problems by analytical and numerical methods. One of the initial papers, in 1972, considered large deformations [60] and another the same year included isotropic hardening [61]. At the present stage of development, the constitutive theory includes isotropic and directional hardening, thermal recovery of hardening, general temperature dependence of plastic flow, and isotropic and anisotropic damage development [7-9]. In principle, the equations could provide for the pressure dependence of plastic flow and could be expanded to include anelastic effects.

The B-P theory differs from others of the same type in certain details, although most all other proposed theories follow the same general principles. The main points of difference of the B-P theory to others are the following:

1. The basic equation for plastic strain rate as a function of stress and history dependent internal variables is taken to be of exponential form. The initial work [59], before 1970, was based on a power law relation which seems to have been adopted by other investigators. Properties of the exponential function used in the B-P formulation that may be especially useful are its very low value, almost zero, at low stress levels and its limiting value of plastic strain rate. As a consequence, that particular function seems to be suitable to represent material behavior over a wide range of strain rates including the very high rates, i.e. about 10^5 sec^{-1}.

2. The scalar measure for hardening is taken to be the plastic work rate. However, the overall theory is not dependent on this point and other measures, e.g. plastic strain rate or a function of the plastic strain rate history, are admissable within the context of the theory.

3. The treatment of directional hardening by Bodner and his associates has been based on the general anisotropic form of the flow law rather than on the "back stress" concept. An incremental isotropic form of the flow law has been proposed as an approximation which would simplify the numerical computations. In the incremental isotropic equation, the scalar coefficient is a function of both the isotropic and directional hardening variables which depend on the loading history.

4. In the evolution equations for directional hardening, B-P theory uses the direct stress as the directional index of hardening. The plastic strain rate had been used previously for that purpose and most other theories still rely on that variable.

5. Anelastic effects, i.e. reversible deformations with energy loss, are taken to be given by a separate parameter in the B-P theory and are not included in a "back stress" parameter.

Applications of the B-P constitutive equations have been made to problems of steady and variable creep [57, 62], creep crack growth [63,64],

static and dynamic response of metal matrix composites [65,66], dynamic fracture mechanics [67,68], wave propagation [69], and adiabatic shear band formation [70]. The equations have been adopted in various finite element and finite difference computer programs, e.g. ADINA and DEPROSS [71].

4.5 Stouffer and Bodner's Theory

This theory [18,19] is an anisotropic generalization of Bodner and Partom's theory for isotropic materials and is based on an anisotropic version of the Prandtl-Reuss flow law. The inelastic deformation rate is related to the deviatoric stress by a linear transformation (a fourth order tensor) whose components are functions of stress, stress history, and the internal variables. The procedure adopted by Stouffer and Bodner was to transform the anisotropic flow equation into six-dimensional vector form with the matrix of coefficients becoming a 6 x 6 second order tensor. Upon diagonalization of the tensor, the strain rate component equation becomes uncoupled and allows the coefficients to incorporate the hardening variables in a simple manner. The hardening variables which represent both isotropic and directional hardening are obtained from a proposed anisotropic work hardening law written in a hardening/recovery format. The anisotropic formulation, however, does not automatically lead to plastic incompressibility and results in plastic volume changes [18]. The anisotropic theory was subsequently revised to enforce plastic incompressibility by a relatively simple recalculation of the matrix coefficients [19]. The model has been successfully used for the solution of a number of dynamic penetration and impact problems [72].

4.6 Miller's Theory

Miller's model is based on a combination of creep phenomenology and physical mechanisms. Proposed in 1975 [10], the model uses the Garafalo hyperbolic sine relation for steady state creep as a starting point and introduces two internal variables to describe non-steady state inelastic responses. The two structural variables are the drag stress and the rest stress and they represent isotropic and kinematic hardening, respectively. The model has since been modified to include the phenomenon of solute strengthening [11] by adding two solute strengthening internal variables to the drag stress. The more recent version of the Miller's model also takes into account of irradiation

effects [73]. Excluding the solute strengthening variables, the latest version of Miller's model consists of four internal variables [12]. The drag stress and the rest stress are both decomposed into short range and long range components. The two isotropic hardening variables represent the hardening effects of obstacles such as total dislocation density, dislocation cells and subgrain boundaries. On the other hand, the long range and short range rest stress components represent the directional hardening effects due to dislocation interaction with internal stresses with long characteristic wavelength and short characteristic wavelength, respectively.

The evolution rate equations of the internal variables are written in a hardening/recovery format. An Arrhenius expression is used to model the temperature dependence of the activation energy for thermally-activated plastic flow. A dynamic recovery term is later introduced in the four-variable model. Both the two-variable and the four-variable Miller's model have the capabilities to simulate monotonic and cyclic stress-strain behavior. In both models, cyclic deformation behavior and the Bauschinger effect are modeled through the rest stress term. In the two-variable model, a linear hardening term is used and it results in the predictions of overly-square hysteresis loops. This shortcoming has been resolved by using a nonlinear hardening coefficient which varies with the loading direction and becomes very large after a load reversal [74]. The high hardening rate in turn results in rounded and physically-realistic hysteresis loops.

Cyclic hardening is modeled through the increase in both the drag stress K and the rest stress Ω_{ij}. Cyclic saturation is represented by an interaction between rest stress and drag stress in the hardening coefficient in the drag stress equation, and it requires a balance between strain hardening and dynamic recovery. The level of K at cyclic saturation depends upon the average absolute value of Ω_{ij} which in turn is a function of the cyclic strain amplitude.

Steady state inelastic deformation occurs when the evolution rate equations become zero (i.e., $\dot{X}_i = 0$). This condition occurs when the hardening rate is equal to the sum of the dynamic and thermal recovery rates.

The use of four internal variables in Miller's model allows the simulations and predictions of a large variety of inelastic deformation behavior including complex loading histories involving strain rate changes, temperature transients, and hold time. The model is, however, very complex and contains a large number of material constants. Neglecting the constants for irradiation effects and the solute strengthening terms, the latest four-variable model contains 24 material constants. However, excluding the elastic modulus, the material constants are all temperature independent and need not be evaluated as a function of temperature.

4.7 Kagawa and Asada's Modification of Miller's Model

Kagawa and Asada recently extended Miller's two-variable model to multi-axial form [22]. The extension is, however, quite different from Miller's version [73], particularly in the choice of the flow rules for treating kinematic hardening. Kagawa and Asada separate the inelastic strain rate into isotropic and anisotropic components. The isotropic component of the inelastic strain rate is proportional to the deviatoric stress, while the anisotropic component is a linear function of the inner product of the rest stress and the effective stress. The evolution rate equations for the drag stress and the rest stress are essentially identical to Miller's model.

The model has been used successfully to simulate and/or predict monotonic and cyclic stress-strain behavior, creep, biaxial strain ratcheting under cyclic loading, and equi-creep rate surface (flow potentials).

4.8 Krieg, Swearengen, and Rohde's Theory

This theory uses a power-law kinetic relation and is formulated in terms of two internal variables [13]; the drag stress is used to model isotropic hardening, while the back stress is used to model directional (kinematic) hardening. The evolution rate equations are formulated in a hardening/recovery format. However, the hardening function in the drag stress evolution rate equation has not been defined and is assumed to be a constant. Recovery of drag stress is considered a thermally-activated process and is represented using Friedel's climb recovery model [34].

Directional (kinematic) hardening is modeled using a nonlinear hardening function in the back stress evolution rate equation. At large strain, the hardening function saturates to a constant value. The recovery of back stress is, again, by Friedel's climb recovery model.

This theory does not include a dynamic recovery term. The state variables thus saturate at large strain values when the static thermal recovery term is balanced by the strain hardening terms. Recovery always occurs toward an isotropic referenced or "annealed" state. The recovery rate depends upon the magnitude by which the current state differs from the annealed state.

The model contains nine temperature-dependent constant. Krieg et al [13] obtained good results between model and experiment for monotonic, cyclic, and creep loading conditions, but they also pointed out the inadequacy of the model at high strain rates. Walker [6] has evaluated and applied the model for predicting steady state hysteresis loops as well as thermomechanical cyclic loops.

4.9 Hart's Theory

Hart's theory [16] employs an equilibrium stress internal variable Ω_{ij} with a constant drag stress K. Cyclic hardening is assumed to occur only in the equilibrium stress. The equilibrium stress is a function of the parameter σ^* which is referred to as the current "hardness" of the deforming materials by Hart [16] and his colleagues [17]. σ^* which occurs in the evolutionary equations of Ω_{ij} but not in the flow law nor in the kinetic equation serves only to modify the equilibrium stress and may be considered as a secondary internal variable.

Written in a hardening/recovery format, the equilibrium stress grows linearly with inelastic strain in the initial loading phase and reaches a saturation when the static thermal recovery term containing the "hardness" variable balances the linear hardening term. Since dynamic recovery terms are not included, the saturated value of the equilibrium stress depends on the strain rate. The linear hardening growth of the equilibrium stress, together with the rapid growth of the static thermal recovery term at large strain values,

produces the trilinear stress-strain response characteristic shown in in Delph's review paper [75]. Since the drag stress is assumed to be constant, the theory can model only directional (kinematic) hardening.

Jackson et al [17] have recently modified Hart's model by introducing two kinematic hardening varibles Ω_{ij}^1 and Ω_{ij}^2. The hardness variable $\overset{*}{\sigma}$ has also been separated into two components σ_1 and σ_2. The growth rates of Ω_{ij}^1 and Ω_{ij}^2 are governed by two independent evolutionary equations formulated in terms of $\overset{*}{\sigma}_1$ and $\overset{*}{\sigma}_2$. The updated Hart model gives an improved correlation of the monotonic stress-strain behavior as well as cyclic hysteresis behavior at both large and small strain amplitudes. However, the deficiency of allowing cyclic hardening only in the equilibrium stress, and not in the drag stress, still remains.

The introduction of an extra term in the equilibrium stress, together with a new hardening coefficient, $\overset{*}{\sigma}_2$, makes the determination of the material constants more difficult. The updated Hart model contains 19 material constants. The material constants which depend on temperature are not explicitly stated in this formulation.

4.10   Ghosh's Model

Ghosh's model [21] uses only one internal state variable to describe the evolution of microstructures and the microscopic mechanisms of inelastic deformation. The inelastic deformation processes are divided into those occurring within grains, and along grain boundaries. Thus, the total strain rate is the sum of the elastic strain rate, the microplastic strain rate which includes anelasticity, the inelastic strain rate due to slip within grains and, finally, the inelastic strain rate due to grain boundary sliding. Different power laws are used to describe the kinetics of each of the inelastic strain rates. For deformation occurring within grains, the internal variable g describes the internal strength within the grains. The magnitude of the internal strength variable g is assumed to be equal to that of the back stress. The evolution rate of the internal strength variable is formulated in terms of hardening and recovery. Both the hardening function and the recovery function

are dependent on the current value of the internal strength variable. Two modified forms of Friedel's recovery model are used to describe two stages of recovery which are referred to as "dynamic" and "post-dynamic" recoveries.

The Bauschinger effect is incorporated in the model through the micro-oplastic strain rate term. Inelastic loading and elastic unloading are defined through the use of, and depends on whether the current stress exceeds, the maximum value of the internal strength variable g^* obtained in the prior deformation histories. Microplasticity occurs when $|\sigma| < g^*$ and is modeled through the back stress and the microplastic strain, which is allowed to be "stored" and "recovered" in a time-dependent manner. The inelastic strain rate due to grain boundary sliding is taken as a Newtonian viscous type of flow.

The model contains 13 constants and they must be evaluated as a function of temperature. The model has been used to simulate monotonic and cyclic stress-strain behavior, creep, and stress relaxation. The model has been formulated and applied in one-dimensional form only. Extension of this theory to multidimensional form appears to be difficult because of the need to keep tract of g^* to define loading and unloading conditions.

5.0 PREDICTIVE AND SIMULATIVE CAPABILITIES OF UNIFIED CONSTITUTIVE THEORIES

The unique characteristic that distinguishes the unified theories from constitutive theories based on classical plasticity or creep approaches is the ability of the unified theories to predict or simulate material responses under monotonic, cyclic, creep, and stress relaxation loading conditions by using the same set of internal variables and material constants. At present, not all unified theories can perform all the four categories of inelastic behavior. The capacities of some of the models have been demonstrated through numerical exercises, but they have not been severely tested by comparing with experimental data. Four of the more established models which have been successfully applied for simulating and/or predicting monotonic, cyclic, creep, and stress relaxation behavior are those of Robinson [15], Walker [6], Bodner-Partom [7-9], and Miller [10-12]. Robinson's model is based on a yield condition and utilizes loading and unloading criteria, while the latter three do not. The kinetic equations commonly used in unified theories without a yield surface or flow potential are based on the power-law, exponential, and hyperbolic sine functions; these kinetic equations are represented in Walker, Bodner-Partom and Miller theories, respectively. The simulative and predictive capabilities of these four unified theories are illustrated below.

5.1 Monotonic Stress-Strain Behavior

All unified theories are capable of reproducing the monotonic stress-strain curve. Most unified theories use the monotonic stress-strain data as part of the data base from which model constants are evaluated. Figure 9 shows an experimental uniaxial tensile stress-strain curve of Hastelloy-X deformed at a strain rate of 1.3×10^{-4} sec^{-1} at 922°K and model simulation using the Bodner-Partom theory. The computed curve includes contributions from both work hardening and thermal recovery. The use of the exponential function in the kinetic relation allows Bodner-Partom's theory to simulate stress-strain response over a wide range of strain rates including those in the dynamic range. Figure 10 shows the calculated and experimental static, dynamic, and incremental shear stress-strain curves for copper at 298°F [54].
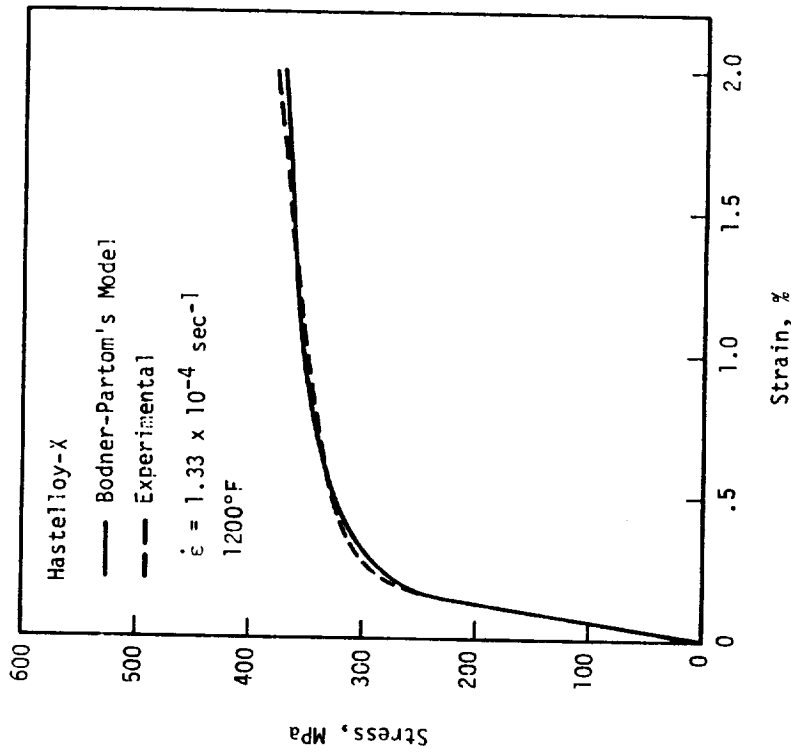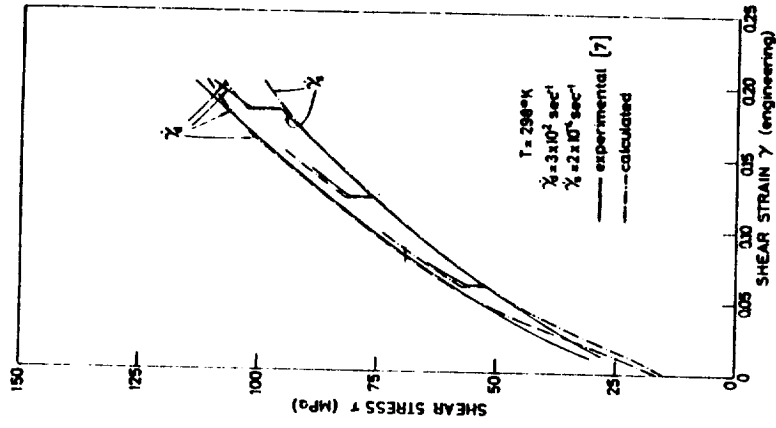
FIGURE 10. CALCULATED AND EXPERIMENTAL STATIC, DYNAMIC, AND INCREMENTAL STRESS-STRAIN CURVES FOR COPPER AT 298°K. Calculation is based on Bodner-Partom's model, from [54].

FIGURE 9. A MONOTONIC STRESS-STRAIN CURVE SIMULATED BY BODNER-PARTOM'S MODEL FOR HASTELLOY-X AT 1200°F

It can be seen in Figure 10 that Bodner-Partom's model duplicates well the stress-strain of copper at both low (2×10^{-4} sec^{-1}) and high (3×10^{2} sec^{-1}) strain rates.

5.2 Cyclic Stress-Strain (Hysteresis) Behavior

The Bauschinger effect is represented in most unified theories by a kinematic or directional hardening internal variable. Cyclic hardening, however, can be represented by increases in the isotropic hardening variable, the kinematic hardening variable, or both. These different types of cyclic hardening behavior are illustrated in Figure 11 for Walker's theory, which uses an equilibrium stress for modeling kinematic hardening, and in Figure 12 for Bodner-Partom's theory which does not use an equilibrium stress. Cyclic hardening depicted in the hysteresis loops of Figures 11a and b are due to the increases of the equilibrium stress and the drag stress, respectively. On the other hand, cyclic hardening in Bodner-Partom theory are the consequences of the increases in (a) the directional component, and (b) both the isotropic and directional components of the internal variable Z, as shown in Figure 12a and b, respectively. Despite the different approaches in treating directional hardening, both the Walker and Bodner-Partom theories yield realistically rounded hysteresis loops. This is demonstrated in Figure 13 which shows comparisons of theoretical calculations of saturated hysteresis loops based on these two theories and experimental data of Hastelloy-X deformed at five different strain rates at 1144°K.

The use of different growth laws of the equilibrium stress in different regions of stress space allows Robinson's model to reproduce rounded hysteresis loops. Examples of cyclic saturated hysteresis loops calculated using Robinson's model are compared with experimental results of 2-1/2Cr-1Mo steel in Figure 14 [55].

5.3 Creep Responses

Most of the unified models can predict or simulate primary and secondary creep responses of material subjected to constant load or stress. Steady state creep rates are predicted by these unified models to occur when the evolutionary rates of the isotropic and/or directional hardening variable vanish
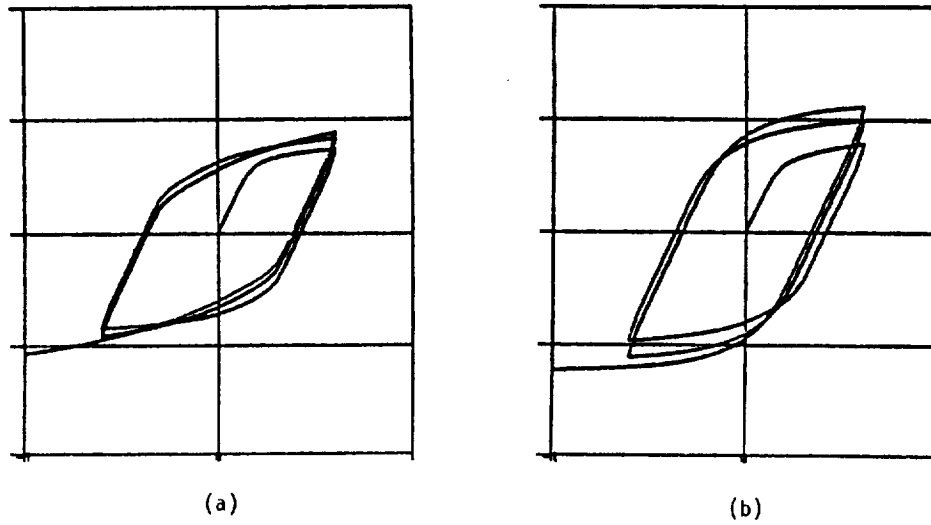
(a)   (b)

FIGURE 11.   HARDENING OF HYSTERESIS LOOP IN WALKER'S MODEL.
             (a) Hardening due to equilibrium stress; (b)
             Hardening due to drag stress, from [6].
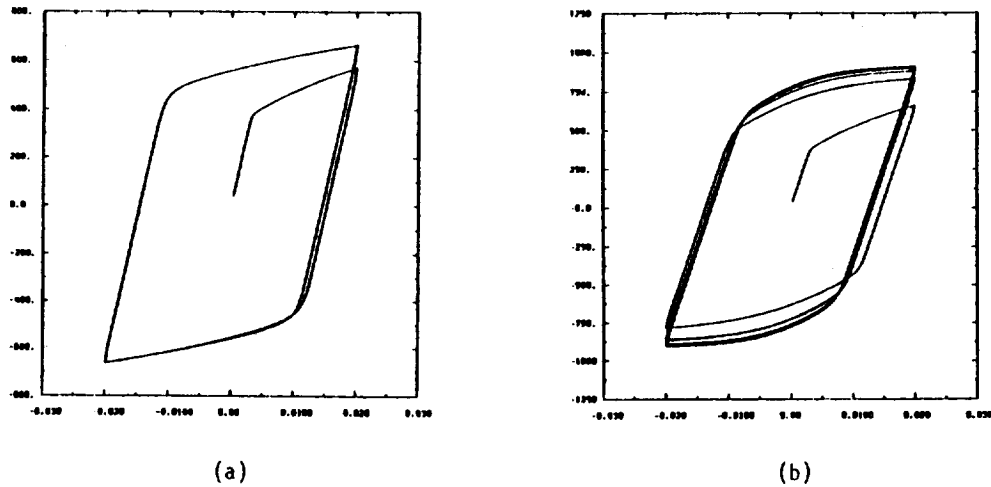

(a)   (b)

FIGURE 12.   HARDENING OF HYSTERESIS LOOP IN BODNER-PARTOM'S MODEL.
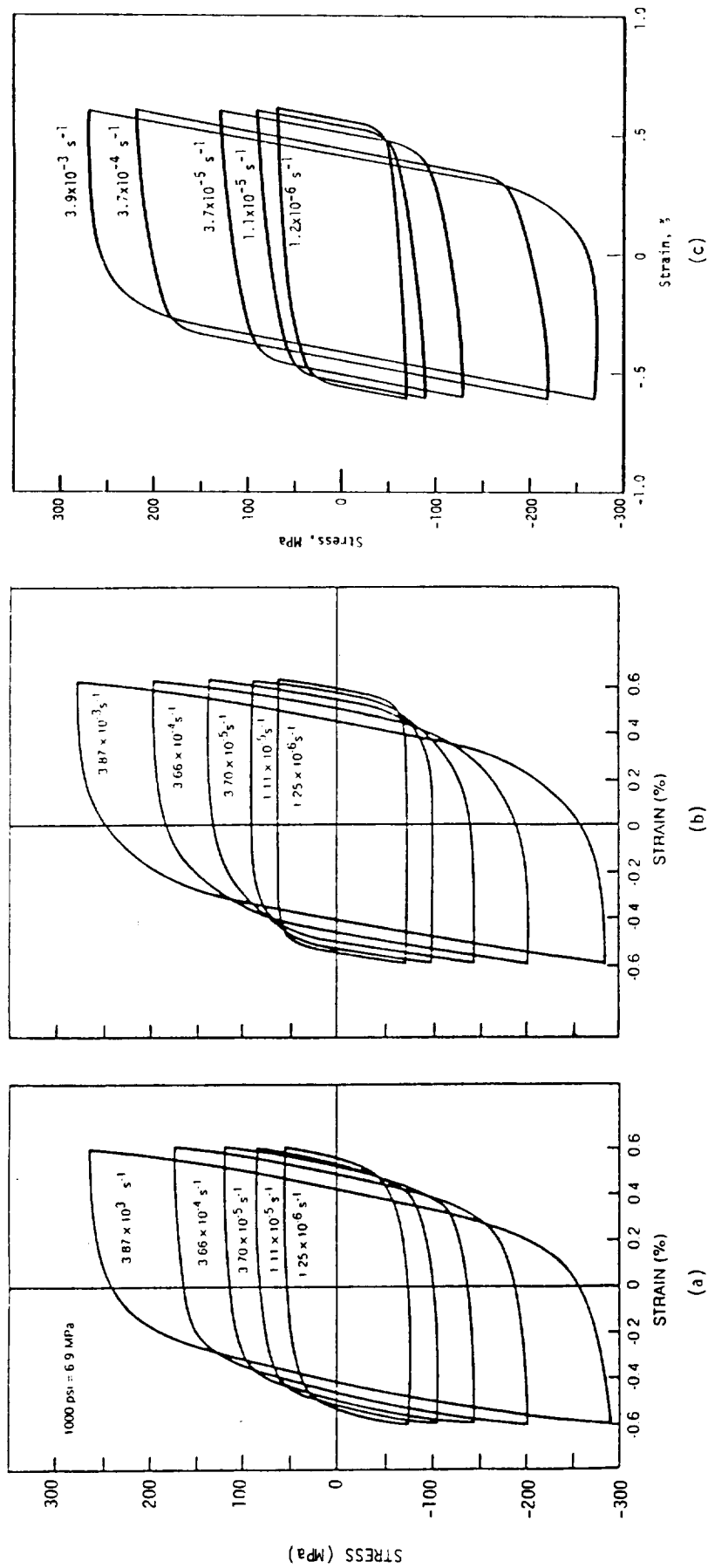   (a) Hardening due to Z^D; (b) Hardening due to Z^I and
             Z^D.

FIGURE 13. COMPARISON OF EXPERIMENTAL AND FUNCTIONAL THEORY PREDICTIONS FOR HASTELLOY-X AT 871°C (1600°F).
(a) Experimental data, (b) Walker's Theory [6], and (c) Bodner-Partom's Theory.
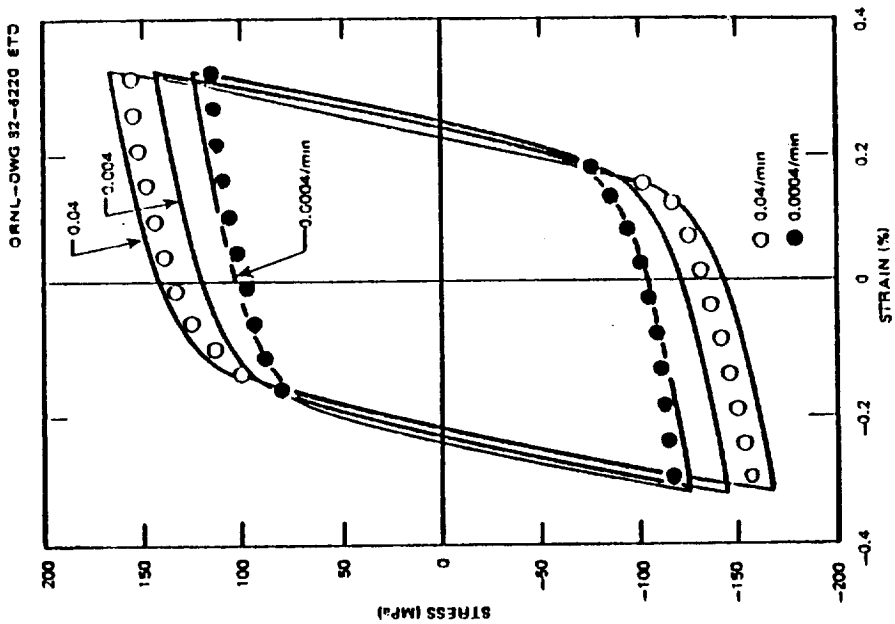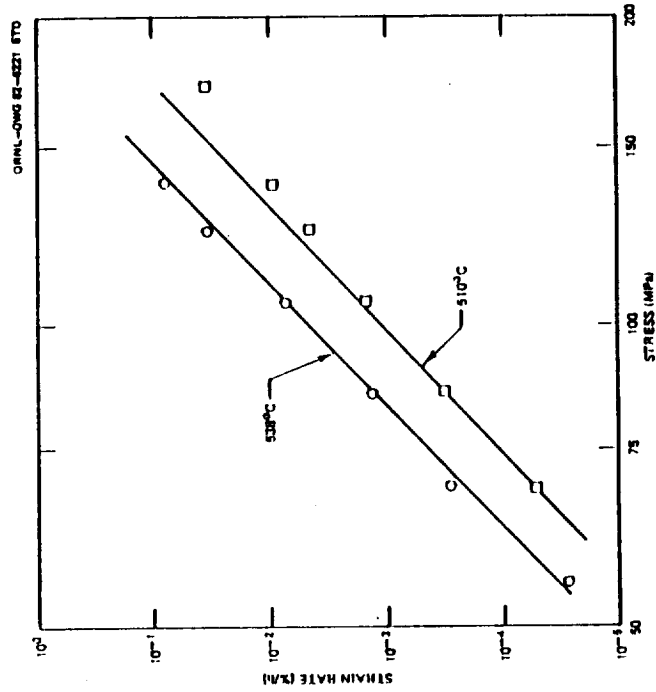
FIGURE 15. STEADY-STATE CREEP RATE VS STRESS FOR 2-1/4Cr-1Mo STEEL AT 538°C AND 510°C. Solid lines, Robinson's model; dots, experiment; from [55].

FIGURE 14. STABLE HYSTERESIS LOOPS OF 2-1/4Cr-1Mo STEEL FOR $\Delta\varepsilon \approx$ ±.32% AT VARIOUS STRAIN RATES AT 538°C. The calculated curves (solid lines) are generated with Robinson's model, from [55].

as the hardening terms are balanced by the thermal recovery. Examples of calculated steady state creep rates under constant stress and comparison with experimental data are shown in Figure 15 and Figure 16 for Robinson's model [53] and Bodner-Partom's model, respectively. According to the unified theories, the steady state creep rate is a function of stress and temperature only; it should not depend on the loading histories. This is demonstrated in both experimental data and predictions by Miller's model in Figure 17 which shows the response of a creep specimen subjected to a sudden decrease in applied stress from 27.6 MPa to 13.8 MPa after a creep strain of 16 percent. Miller's calculation [56] indicates that the 16 percent strain at 27.6 MPa results in an internal variable which is larger than the steady-state one at 13.8 MPa; hence, when the stress is decreased, the creep rate first drops instantaneously but then gradually increases as recovery reduces the value of the internal variable to one which is characteristic of the lower stress.

The instantaneous creep response of material subjected to an arbitrary loading history depends on the current values and the growth laws of the internal variables. For unified theories based on an equilibrium stress and without a flow potential, the creep response would, according to the flow law, depend on the difference between the current stress and the equilibrium stress. Different creep responses would result from the same imposed stress (Points A and D in Figure 18) on the loading and unloading branches of a cyclically-saturated hysteresis loop because of differences in the equilibrium stresses, as demonstrated in Figure 18 which shows both Walker's model prediction and experimental data of Hastelloy-X at 1144°K [6]. Walker's model also predicts that a compressive creep strain can occur under a constant tensile stress if the equilibrium stress is algebraically larger; this reverse creep behavior is characteristic of unified theories which are based on the equilibrium stress and without a yield surface.

5.4. Stress Relaxation Response

The behavior of unified constitutive models under stress relaxation is analogous to the creep behavior. Under a constant strain condition, the relaxation rate would, again, depend on the current values of the internal variables and on the growth laws which describe their changes with time and inelastic deformation. Stress relaxation calculations based on Bodner-Partom's
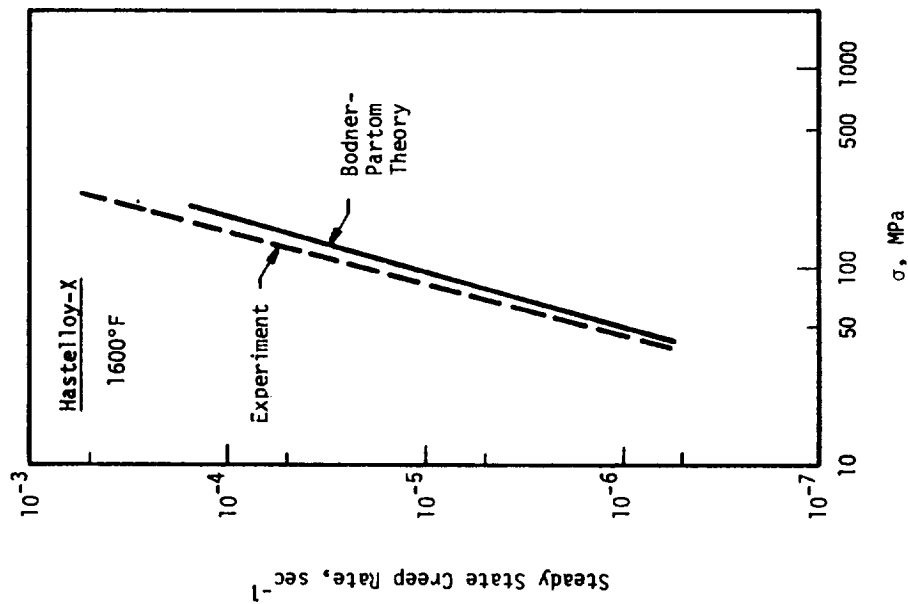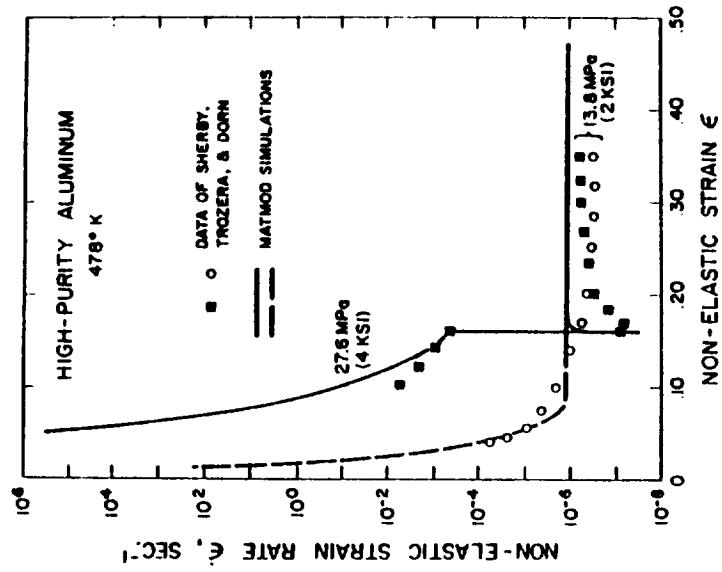
FIGURE 17. MILLER'S MODEL PREDICTION COMPARED WITH EXPERIMENTAL DATA FOR A CREEP TEST WITH A SUDDEN DECREASE IN APPLIED STRESS, FROM [28]

FIGURE 16. STEADY CREEP RATES AS A FUNCTION OF STRESS SIMULATED BY BODNER-PARTOM'S MODEL
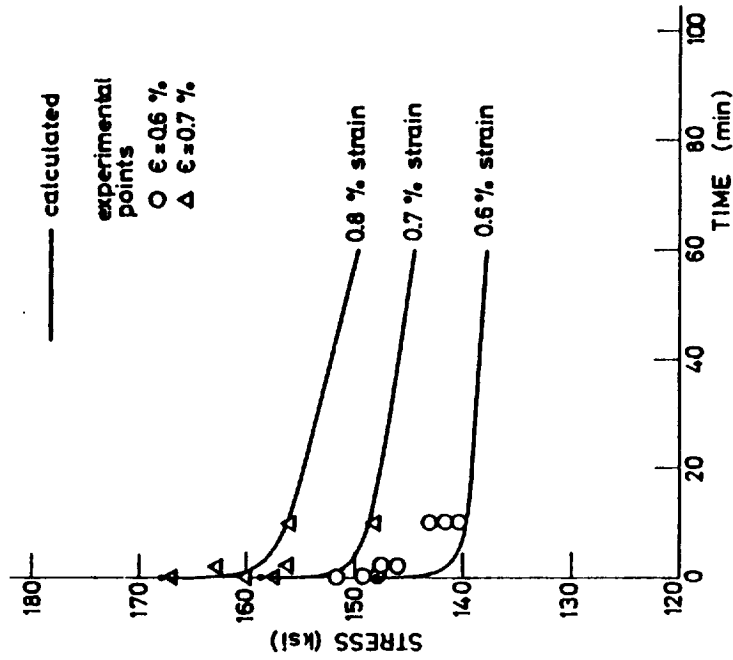
FIGURE 19. CALCULATED AND EXPERIMENTAL STRESS RELAXATION RESPONSE OF RENE' 95 (AT 923°K) FOR VARIOUS CONSTANT STRAIN LEVELS. The calculated curves are generated with Bodner-Partom's theory, from [57].
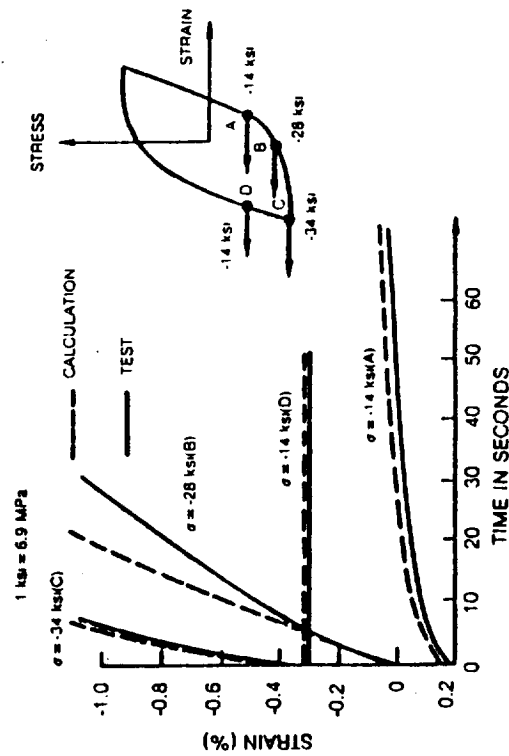

FIGURE 18. COMPARISON OF CREEP RESPONSE OF HASTELLOY-X AT 871°C ON THE LOADING AND UNLOADING BRANCHES OF A STEADY STATE HYSTERESIS LOOP EXECUTED AT A CONSTANT STRAIN RATE OF ± 1.4 x 10-3 SEC-1 WITH A STRAIN AMPLITUDE OF ± .4%. Calculated curves are generated with Walker's theory, from [6].

A-57

model and Walker's theory are compared with experimental data of Rene 95 [57] and Hastelloy-X [6] in Figure 19 and Figure 20, respectively. Figure 20 shows that cyclically saturated Hastelloy-X subjected to compressive strain hold at $1144°K$ relaxes from an initial compressive stress to a tensile one after approximately 3 seconds. This behavior is predicted qualitatively though not quantitatively by Walker's model on the basis of a positive equilibrium stress, as shown in Figure 20.

5.5   Thermomechanical Response

The behavior of unified constitutive theories under thermomechanical cycling depends critically on the change of material constants with temperature. In particular, the shape of the predicted thermomechanical loop is sensitive to the growth of the kinematic hardening variable (the equilibrium stress) with temperature. Walker has also found that it is necessary to include a temperature rate term in the evolutionary equation such that the equilibrium stress can change during nonisothermal "elastic" excursions. Walker's model prediction of thermomechanical loop of Hastelloy-X is shown in Figure 21 [6].

5.6   Multiaxial Behavior

All the unified theories utilize single-valued kinetic equations formulated in terms of either $3J_2/K^2$ or $3J_2'/K^2$. For a constant value of the internal K, these kinetic equations predict a locus of constant inelastic strain rate invariant (D_2^p = constant) in stress space; the shape of the predicted "yield surface" or "flow potential" is identical to von Mises yield function and is described by

$$3J_2 - C^2K^2 = 0 \quad \text{or} \quad 3J_2' - C^2K^2 = 0$$

where C is a constant. This is illustrated in Figure 22 which shows that for proportional loading the "yield surface" predicted by Bodner-Partom's model is identical to the von Mises one, and the inelastic strain rate vectors are all normal to the "yield surface." For unified models formulated based on the equilibrium stress, Equation (10) remains valid. With J_2' given by Equation (8b), the size of the "yield surface" is given by CK, while the center of the "yield surface" is at Ω_{ij} and translates according to the evolution rate of
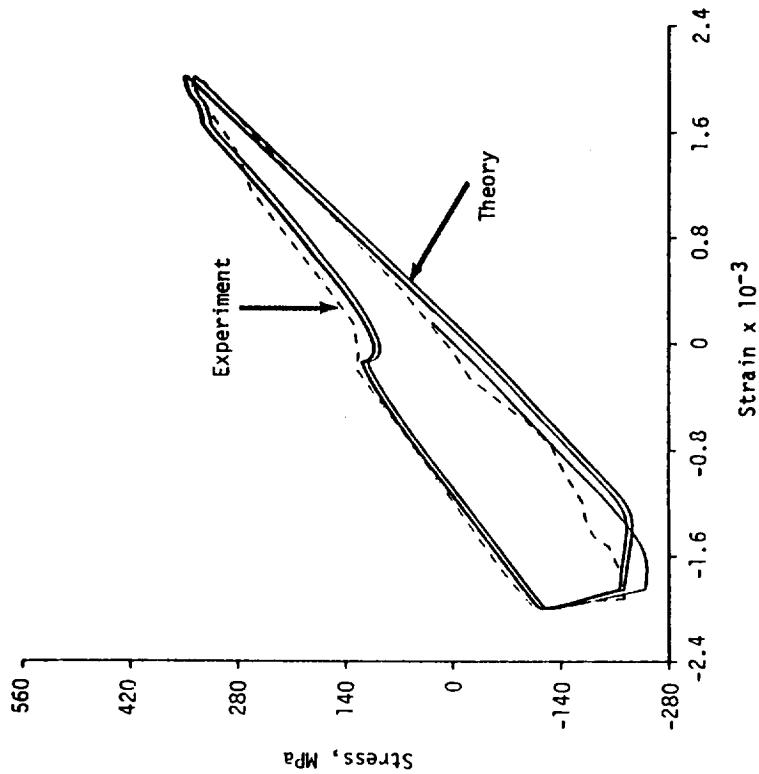
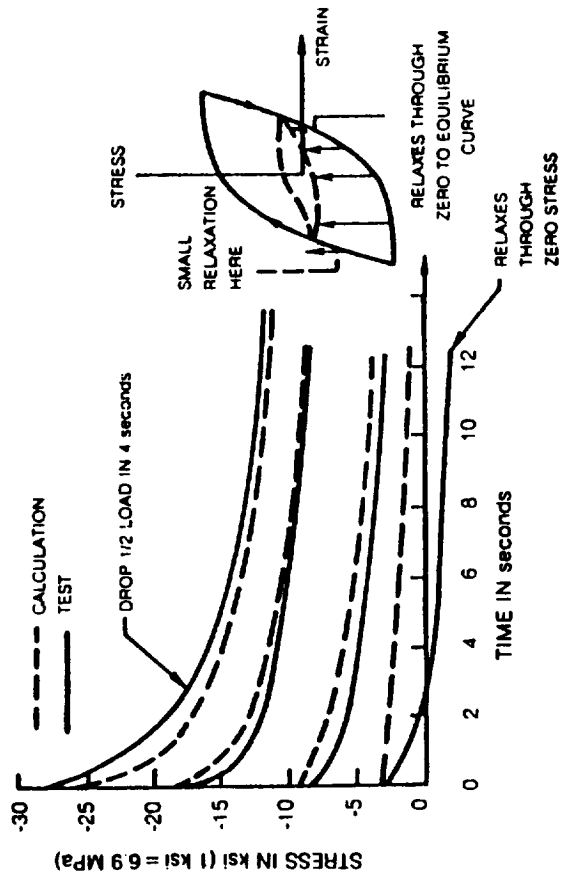FIGURE 21. THERMOMECHANICAL STRESS-STRAIN PREDICTION BY WALKER'S THEORY

FIGURE 20. NEGATIVE STRESS RELAXATION RESPONSE OF HASTELLOY-X AT 871°C (1600°F) INITIATED FROM A STEADY STATE HYSTERESIS LOOP EXECUTED AT A CONSTANT STRAIN RATE OF ± 1.35 × 10⁻³ SEC⁻¹ WITH A STRAIN AMPLITUDE OF ± .4%. The calculated curves are based on Walker's theory, from [6].

A-59

Modified Miller's Model (Kagawa and Asada)

Equi-Creep Rate Surface

$\dot{\bar{\epsilon}} = 1 \times 10^{-5}$ sec^{-1}

● Initial Surface
○ Initial Origin
▲ Subsequent Surface after a 3 x 10^{-2} Prestrain
○' Subsequent Origin

$3J_2' - C^2 K^2 = 0$

$J_2' = \frac{1}{2}(S_{ij} - \Omega_{ij})(S_{ij} - \Omega_{ij})$

FIGURE 23. EQUI-CREEP RATE SURFACE GENERATED BY KAGAWA AND ASADA USING A MODIFIED MILLER'S MODEL. The subsequent surface after a 3 x 10^{-2} axial prestrain is seen to translate in the axial direction from o to o'. Both the initial and the subsequent surfaces can be described by the J$_2$-based von Mises criterion, from [22].

● Bodner-Partom's Theory
$Z^I = 2050$ MPa

Plastic Strain Rate Vector (Bodner-Partom's Theory)
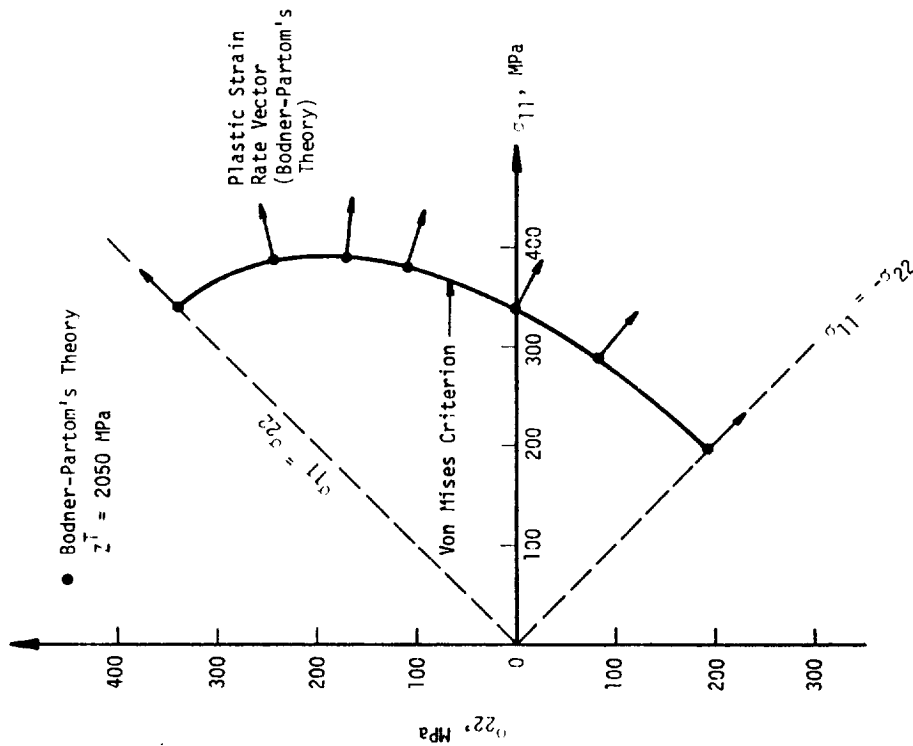
Von Mises Criterion

FIGURE 22. YIELD SURFACE GENERATED BY BODNER-PARTOM'S THEORY IS IDENTICAL TO THE ONE DESCRIBED BY VON MISES CRITERION. The strain rate vectors are normal to the yield surface.
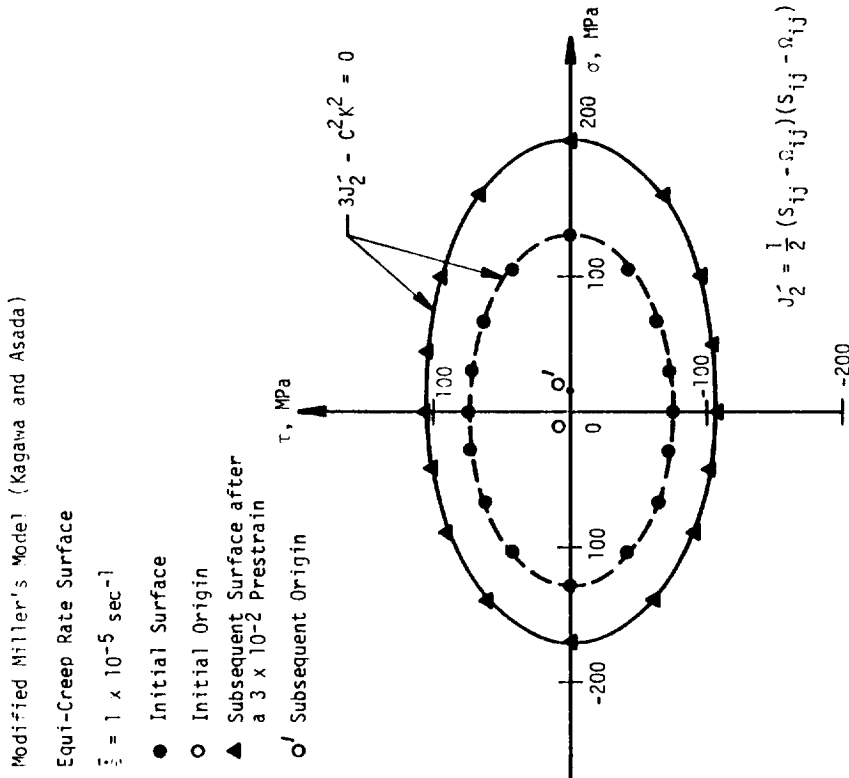
A-60

Ω_{ij}. This is demonstrated in Figure 23 which shows the equi-creep rate
surfaces calculated for proportional loading under combined tension and tor-
sion using a modified Miller theory [22]. The broken line shows the initial
creep surface, and the solid line depicts the subsequent surface after a
3×10^{-1} prestrain in tension. The equivalent creep rate for both surfaces is
1×10^{-5} sec^{-1}. The subsequent creep surface shows both an expansion and a
translation of the origin in the prestrain direction.

6.0 SUMMARY AND CONCLUSIONS

1. A review of more than ten time-dependent elastic-viscoplastic constitutive theories indicates that these theories differ in the choice of flow law, kinetic equation, and evolutionary equation of the internal variables.

2. The unified approach treats all aspects of inelastic deformation including plasticity, creep, and stress relaxation using the same set of flow law, kinetic equation, and internal variables.

3. The unified constitutive theories satisfy the uniqueness and stability criteria imposed by Drucker's postulate for rate independent stable plastic flow and Ponter's inequalities for constitutive theories based on internal variables.

4. The unified theories can be formulated either with or without the use of a yield criterion. Three basic flow laws are identified in theories without a yield criterion. For theories with a yield criterion, the associated flow law is derived from the yield function or the flow potential.

5. Three different formulations of the kinetic equations are identified, and they include the exponential, power law, and hyperbolic sine functions. The exponential formulation gives a limiting inelastic strain rate and appears to give better results for high strain rate applications.

6. All forms of kinetic equations reviewed are functions of $3J_2/K^2$ (or $3J_2'/K^2$) and result in "yield surfaces" and equi-creep rate surfaces which are described by the von Mises criterion.

7. The number of internal variables used in the unified theories range from one to six. Most unified theories use two internal variables, one to represent isotropic hardening and one to present kinematic or directional hardening. The measure of hardening is either the inelastic strain rate or the inelastic work rate.

8.　Directional (kinematic) hardening can be modeled with or without the use of an equilibrium stress. The directional index of kinematic hardening can be based on either the inelastic strain rate or the direct stress.

9.　Material constants in the unified models are necessarily temperature-dependent and required to be evaluated at the temperatures of interest. The change of material constants with temperature has a drastic effect on the shape of the thermomechanical hysteresis loops. There are indications that a temperature rate term is also required in the unified theories.

10.　All of the unified theories which are reviewed do not automatically predict additional cyclic hardening under nonproportional loading paths. Additional terms are needed in the unified theories to include such hardening behavior.

11.　The equilibrium-stress-based unified theories can describe reverse creep and/or reverse stress relaxation behavior without further modifications. Unified models which are not based on the equilibrium stress would require modification by adding an anelastic term in order to take into account these types of behavior.

12.　The unified constitutive equations are stiff but can be integrated using either explicit or implicit methods. The choice of a particular integration scheme in finite element analysis appears to be code and problem dependent.

7.0 REFERENCES

1. C. E. Pugh and D. N. Robinson, Nucl. Eng. and Design, 1978, Vol. 48, No. 1, p. 269.

2. R. W. Swindeman, ORNL Report, TM-6380, 1978.

3. W. G. Johnston and J. J. Gilman, J. Appl. Phys., 30, 1959, p. 129.

4. J. J. Gilman and W. G. Johnston, in "Dislocation and Mechanical Properties of Crystals," ed. by Fisher et al., John Wiley & Sons, Inc., New York, 1957, p. 116.

5. W. G. Johnston, J. Appl. Phys., 33, 1962, p. 2716.

6. K. P. Walker, NASA Contract Report NASA CR 165533, 1981.

7. S. R. Bodner and Y. Partom, ASME J. of Applied Mechanics, Vol. 42, 1975, p. 385.

8. S. R. Bodner, I. Partom, and Y. Partom, ASME J. of Appl. Mech., Vol. 46, 1979, p. 805.

9. S. R. Bodner, "Evolution Equations for Anisotropic Hardening and Damage of Elastic-Viscoplastic Materials," Pro. Conference on Plasticity Today, Udine, Italy, 1983.

10. A. K. Miller, ASME J. of Eng. Mat. & Tech., Vol. 96, 1976, p. 97.

11. C. G. Schmidt and A. K. Miller, Res. Mechanica, Vol. 3, 1981, p. 109.

12. T. C. Lowe and A. K. Miller, to appear in the Proceedings of the ASME Symposium on "Constitutive Equations: Micro and Macro Aspects," New Orleans, Louisiana, 1984.

13. R. D. Krieg, J. C. Swearengen, and R. W. Rohde, in "Elastic Behavior of Pressure Vessel and Piping Components," PVP-PB-028, 1978, p. 15.

14. J. L. Chaboche, Bulletin de L'Academie des Sciences, Serie des Science Techniques, Vol. XXV, No. 1, 1977, p. 33.

15. D. N. Robinson, ORNL Report/TM-5969, 1978.

16. E. W. Hart, ASME J. of Eng. Mat. and Tech., Vol. 98, 1976, p. 193.

17. M. S. Jackson, et al, ASME J. Eng. Mat. & Tech., Vol. 103, 1981, p. 314.

18. D. C. Stouffer and S. R. Bodner, Int. J. Engng. Sci., Vol. 17, 1979, pp. 757-764.

19. S. R. Bodner and D. C. Stouffer, Int. J. Engng. Sci., Vol. 21, 1983, pp. 211-215.

20. D. Lee and F. Zaverl, Jr., Acta Met., Vol. 26, No. 11, 1975, p. 385.

21. A. K. Ghosh, Acta Metallurgica, Vol. 28, 1980, p. 1443.

22. H. Kagawa and Y. Asada, Proceedings of the ASME Int. Conf. on Advances in Life Prediction Methods, Albany, New York, 1983, p. 33.

23. E. H. Lee, Int. J. Solids Structures, Vol. 17, 1981, pp. 859-872. See also "Finite Deformation Theory with Nonlinear Kinematics," Proc. Workshop on Plasticity of Metals at Finite Strain, Stanford University, ed. by E. H. Lee and R. L. Mallett, 1981, pp. 107-120.

24. D. C. Drucker, Discussion on paper of E. H. Lee in Proceedings of Workshop, Stanford University (see Reference 23 above), pp. 121-129.

25. P. Perzyna, Advances in Applied Mechanics, Vol. 9, 1966, pp. 243-377.

26. W. Prager, Proc. Inst. Mech. Engrs., Vol. 169, 1955, p. 41.

27. E. H. Lee and T. B. Wertheimer, Proceedings of ASME Applied Mechanics for Nonlinear Solid and Structural Mechanics, Houston, TX, June 1983. See also E. H. Lee, R. L. Mallett, and T. B. Wertheimer, to appear in ASME J. of Appl. Mechanics, 1984.

28. A.R.S. Ponter and F. A. Leckie, ASME J. of Eng. Mat. & Tech., Vol. 98, 1976, p. 47.

29. U. S. Lindholm and S. R. Bodner, unpublished research, 1983.

30. E. P. Cernocky and E. Krempl, Int. J. of Nonlinear Mechanics, Vol. 14, pp. 183-203, 1979.

31. R. W. Bailey, J. of Institute of Metals, Vol. 35, 1926, p. 27.

32. E. Orowan, J. West. Scot. Iron & Steel Inst., Vol. 54, 1946, p. 45.

33. H. Ghoneim, S. Matsouka, and Y. Chen, J. Appl. Mech., Vol. 50, 1983, pp. 465-468.

34. J. Friedel, "Dislocations," Addison Wesley Pub. Co., 1967, pp. 277-279.

35. H. Ziegler, Quart. Appl. Math., Vol. 17, 1959, p. 55.

36. U. S. Lindholm, K. S. Chan, S. R. Bodner, and K. P. Walker, unpublished research, 1983.

37. R. W. Rhode, Acta Metall., Vol. 17, 1969, p. 353.

38. A.R.S. Ponter, Int. J. Solids Structure, Vol. 16, 1980, p. 793.

39. D. C. Drucker, J. de Mechanigue, Vol. 3, 1964, p. 235.

40. H. S. Lamba and O. M. Sidebotton, ASME J. of Eng. Mats. and Technology, 1978, Vol. 100, p. 96.

41. K. Kanazawa, K. J. Miller and M. W. Brown, Fat. of Eng. Mat. and Structures, 1979, Vol. 2, p. 217.

42. N. Nouailhas, H. Policella, and H. Kaczmarek, Proceedings of Int. Conf. on Constitutive Laws for Eng. Materials, edited by C. S. Desai and R. H. Gallagher, 1983, Tucson, Arizona, p. 45.

43. Y. Ohashi and K. Kawashima, J. Mech. Phys. Solids, 1971, Vol. 25, p. 409.

44. Y. Ohashi, E. Tanaka, and Y. Gotoh, Mech. of Materials, 1982, Vol. 1, p. 297.

45. Y. Ohashi and N. Ohno, J. Mech. Phys. $ Solids, 1982, Vol. 30, No. 5, p. 287.

46. S. A. Meguid, Proceedings of Int. Conf. on Constitutive Laws for Eng. Materials, edited by C. S. Desai and R. H. Gallagher, 1983, Tucson, Arizona, p. 133.

47. V. Kumar, M. Morjaria and S. Mukerjee, ASME J. of Eng. Mat. and Tech., 1980, Vol. 102, p. 92.

48. R. D. Krieg, Proceedings of the 4th Int. Conf. on Structure Mech. in Reactor Tech., San Francisco, 1977, Paper No. M6/4.

49. T. G. Tanaka, "Deformation of Metals and Alloys," Ph.D. Thesis, Stanford University, 1983.

50. K. Bathe, Finite Element Procedures in Eng. Analysis, Prentice-Hall, Inc., Englewood Cliffs, New Jersey, 1982, p. 395.

51. B. N. Cassenti, Proceedings of AIAA/SAE/ASME 19th Joint Propulsion Conference, Seattle, WA, 1983.

52. D. Lee, C. F. Shih, F. Zaverl, Jr., and M. D. German, EPRI NP-500 RP 452-2, Final Report, May 1977.

53. K. P. Walker, "Constitutive Modeling of Engine Materials," Final Report FR-17911 to AFML Contract F33615-81-C-5040, November 1983.

54. S. R. Bodner and A. Merzer, ASME Journal of Engineering Materials and Technology, Vol. 100, 1978, pp. 388-394.

55. D. N. Robinson and R. W. Swindeman, ORNL Report TM-8444, 1982.

56. O. D. Sherby and A. K. Miller, ASME J. of Eng. Mat. and Tech., 1979, Vol. 101, p. 387.

57. S. R. Bodner, Technical Report AFML-TR-79-4114, Air Force Materials Laboratory, Wright-Patterson AFB, OH, 1979.

58. L. Anand, ASME J. of Eng. Mat. and Tech., 1976, Vol. 98, p. 193.

59. S. R. Bodner, Mechanical Behavior of Materials Under Dynamic Loads, ed. by U. S. Lindholm, Springer-Verlag, New York, 1968, pp. 176-190.

60. S. R. Bodner and Y. Partom, ASME Journal of Applied Mechanics, Vol. 39, 1972, pp. 741-757.

61. S. R. Bodner and Y. Partom, Proc. Eighth Congress of the International Council of the Aeronautical Sciences, (ICAS), Amsterdam, 1972.

62. A. M. Merzer, ASME Journal of Engineering Materials and Technology, Vol. 104, 1982, pp. 18-25.

63. T. Hinnerichs, T. Nicholas, and A. N. Palazotto, Engineering Fracture Mechanics, Vol. 16(2), 1982, pp. 265-277.

64. J. Smail and A. N. Palazotto, Engineering Fracture Mechanics, (in press).

65. J. Aboudi, International Journal of Engineering Science, Vol. 19, 1981, pp. 1269-1281.

66. J. Aboudi, International Journal of Engineering Sciences, Vol. 20, 1982, pp. 605-621.

67. J. Aboudi and J. D. Achenbach, International Journal of Solids and Structures, Vol. 17, 1981, pp. 879-890.

68. J. Aboudi and J. D. Achenbach, ASME Journal of Applied Mechanics, (in press).

69. S. R. Bodner and J. Aboudi, International Journal of Solids and Structures, (in press).

70. A. M. Merzer, J. of the Mech. and Phys. of Solids, Vol. 30, 1982, p. 323.

71. M. Newman, Z. Zaphir, and S. R. Bodner, Journal of Computers and Structures, Vol. 6, 1976, pp. 157-162.

72. J. Aboudi and S. R. Bodner, Int. J. Eng. Sci., Vol. 18, 1980, p. 801.

73.   S. Oldberg, A. K. Miller, and G. E. Lucas, ASTM STP 681, 1979, p. 370.

74.   A. K. Miller, ASME J. Eng. Mat. & Tech., Vol. 102, 1980, p. 215.

75.   T. J. Delph, ASME J. Eng. Mat. & Technology, Vol. 102, 1980, p. 327.